

ABSTRACT

Title of Thesis: DISSECTION AND MODELING OF AEDC WIND
TUNNEL 9 CONTROL LAW AND
FACILITY DURING BLOW PHASE

Samuel George Gigioli,
Master of Science in Mechanical Engineering,
2023

Thesis Directed By: Professor Ashwani K. Gupta,
Department of Mechanical Engineering

This work presents the progress towards a mathematical modeling of the Arnold Engineering Development Complex (AEDC) Wind Tunnel 9 control law during the blow phase of a given tunnel run, composing of electrical analog physics, ideal gas control volume physics, incompressible fluid mechanics, and force balance kinematics. This work is unique to Tunnel 9 and unique in respect to other works, as no other existing models of the current control law exist. The primary goal of this work is to provide enhanced support to the Tunnel 9 engineers with the ability to model different run conditions. Key facility measurements can be estimated, aiding in the determination if proposed non-standard run conditions will meet or maintain the facility capabilities, and if the facility can be operated under safe operating limits. The secondary goal of this model is to progress toward a digitally controlled valve system to replace the current analog system. Such will help provide advantages in the facility (1) performance, (2) health monitoring, (3) maintainability, and (4) sustainment.

DISSECTION AND MODELING OF AEDC WIND TUNNEL 9 CONTROL LAW AND
FACILITY DURING BLOW PHASE

by

Samuel George Gigioli

Thesis submitted to the Faculty of the Graduate School of the
University of Maryland, College Park, in partial fulfillment
of the requirements for the degree of
Master of Science
2023

Advisory Committee:
Professor Ashwani K. Gupta, Chair
Professor Bao Yang
Professor Kenneth H. Yu

© Copyright by
Samuel George Gigioli
2023

Department of Defense
United States Air Force – Arnold Engineering Development Complex
Distribution Statement A. Approved for public release; distribution is unlimited.
AEDC IRA # 7124

Dedication

This work is dedicated to my wife for her constant support and encouragement throughout my graduate career and beyond.

Acknowledgements

I would like to thank my thesis advisor Professor Ashwani K. Gupta for his support and patience throughout my research and time at UMD. I would also like to thank the other thesis defense committee board members, Professor Bao Yang and Professor Kenneth Yu, for their time and patience.

I would like to thank a handful of incredible personnel, both past and present, from the Arnold Engineering Development Complex (AEDC) Wind Tunnel 9 as their support has been is gratefully acknowledged; Nicholas Fredrick, Andy Askew, Calvin Dunn, Jason McDonald, Ray Schlegel, Alex Parker, and all the other site personnel for their support and guidance throughout my research and writing of this work.

This work is funded through the PALACE ACQUIRE Air Force Program, residing at Arnold Engineering Development Complex Hypervelocity Wind Tunnel No. 9 in White Oak, Maryland. All images used with permission from Arnold Engineering Development Complex Hypervelocity Wind Tunnel No. 9

Table of Contents

| | |
|---|------|
| Dedication..... | iii |
| Acknowledgements | iv |
| Table of Contents | v |
| List of Figures | vii |
| List of Tables..... | viii |
| Chapter 1: Introduction | 1 |
| Tunnel 9 Background..... | 1 |
| Design of Tunnel 9 | 3 |
| Tunnel 9 Control Law Inception | 5 |
| Problem Statement..... | 5 |
| Chapter 2: Literature Review..... | 7 |
| Summary of Blowdown Facility Literature..... | 7 |
| Critical Facility Hardware Configuration..... | 7 |
| Driver Vessels and Gas Control Valves..... | 7 |
| Heater Vessel..... | 9 |
| Diaphragm Section..... | 9 |
| Historical Modeling of Tunnel 9 Control System and Gas Dynamics | 11 |
| M15 Shakedown Tests..... | 12 |
| HIRE Control System Digital Modeling..... | 12 |
| CTA Inc Model and Johns Hopkins APL Work | 13 |
| Chapter 3: Mathematical Model and Numerical Methods | 15 |
| Control System Modeling..... | 15 |
| Fundamental Electrical Engineering Analysis..... | 15 |
| Control Law and Command Voltage Terminology | 18 |
| Sequencing for Control System | 19 |
| Derivation of Control Law | 21 |
| Servo Amplifier-Controller Card Transfer Function Derivation | 25 |
| Data System Command Voltage | 29 |
| Sequencer Relays and Trips..... | 31 |
| Guidelines for Design of Experiments..... | 31 |
| Background..... | 31 |
| Response Parameter Determination..... | 32 |
| PHE Slope Calculation..... | 33 |
| Control Valve Start Time | 37 |
| Electro-Hydraulic Servo Valve and Actuator Modeling of Tunnel 9..... | 39 |
| AEDC Servo Valve Model..... | 39 |
| Servo Valve Internal Flow Modeling | 40 |
| Actuator Physics..... | 41 |
| System Delays and Slew Rates | 43 |
| Gas Dynamics Modeling of Tunnel 9..... | 45 |
| AEDC Standard Simulink Block Library..... | 45 |
| Nitrogen Equation of State | 46 |
| Ideal Gas Finite Control Volume Approach..... | 47 |
| Control Volume Equations | 47 |
| Flow Device Mass and Energy Flow Rate Equations..... | 48 |
| Intermediate State Computations | 49 |
| Implication to Tunnel 9 Modeling..... | 52 |

| | |
|---|-----|
| Chapter 4: Design Expert and Historical Data Analysis | 55 |
| Tabular Input..... | 55 |
| ANOVA for Reduced 2FI model | 59 |
| Implementation to Simulink | 71 |
| Chapter 5: Simulink Model Architecture and Plots..... | 72 |
| Model Construction and Top View | 72 |
| Controller..... | 74 |
| Control Law..... | 74 |
| Servo Amplifier Controller Card..... | 74 |
| Plant..... | 77 |
| Gas Control Valves..... | 80 |
| Heater vessel..... | 83 |
| Flow Restrictor, Diaphragm Area, Nozzle Throat, and Vacuum..... | 83 |
| Results..... | 84 |
| Chapter 6: Conclusions and Recommendations for Future Research..... | 95 |
| Simulink Model Conclusions..... | 95 |
| Recommendations for Future Research and Modeling..... | 96 |
| Appendices | 99 |
| Appendix A: Control Valve Run Faults; Slew Rate Observations..... | 99 |
| Bibliography | 104 |

List of Figures

| | |
|---|-----|
| Figure 1: Tunnel 9 Top View Schematic | 2 |
| Figure 2: Tunnel 9 Facility High Pressure Schematic | 4 |
| Figure 3: Basic OpAmp Schematic | 16 |
| Figure 4: Amplifier Schematic..... | 16 |
| Figure 5: Summing Amplifier Schematic..... | 17 |
| Figure 6: Differentiating Amplifier Schematic..... | 17 |
| Figure 7: Integrating Amplifier Schematic..... | 18 |
| Figure 8: Control Law Schematic..... | 23 |
| Figure 9: Servo Amplifier Card Schematic | 28 |
| Figure 10: Facility CVCMD Input Schematic | 30 |
| Figure 11: T9 Data Comparison App – PHE Slope Calculation Range Selection.... | 34 |
| Figure 12: T9 Data Comparison App – PHE Slope Calculation Scatter..... | 36 |
| Figure 13: T9 Data Comparison App – CV Start Time Function Outputs..... | 38 |
| Figure 14: Theoretical vs Observed Normalized Heater Pressure Slope | 58 |
| Figure 15: Normal Plot of Residuals | 65 |
| Figure 16: Box-Cox Plot for Power Transforms..... | 66 |
| Figure 17: ANOVA 2FI Coded Equation Predicted vs Actual Response..... | 67 |
| Figure 18: ANOVA 2FI Coded Equation Residual vs Prediction..... | 68 |
| Figure 19: ANOVA 2FI Coded Equation Residual vs Run..... | 69 |
| Figure 20: Simulink Model Top Level | 73 |
| Figure 21: Control Law Block Architecture..... | 75 |
| Figure 22: Servo Amplifier Controller Card Transfer Function Block Architecture | 76 |
| Figure 23: Single-Heater Model Plant – Block Architecture (Drivers to Heater).... | 78 |
| Figure 24: Single-Heater Model Plant – Block Architecture (FR to Vacuum)..... | 79 |
| Figure 25: Control Valve Upper Level Block Architecture | 81 |
| Figure 26: Servo Valve and Actuator Block Architecture | 82 |
| Figure 27: Control Valve Position vs Time..... | 85 |
| Figure 28: Stand Alone Control Law Voltage vs Time | 86 |
| Figure 29: Driver Pressure vs Time..... | 87 |
| Figure 30: Driver Temperature vs Time | 88 |
| Figure 31: Heater Pressure (Single-Volume Heater Model) vs Time..... | 89 |
| Figure 32: Heater Temperature (Single-Volume Heater Model) vs Time | 90 |
| Figure 33: Heater Exit Pressure (Two-Volume Heater Model) vs Time | 91 |
| Figure 34: Heater Exit Temperature (Two-Volume Heater Model) vs Time..... | 92 |
| Figure 35: Nozzle Supply Pressure vs Time..... | 93 |
| Figure 36: Nozzle Supply Temperature vs Time | 94 |
| Figure 37: Normalized Control Valve Position vs Time, Run A | 100 |
| Figure 38: Normalized Control Valve Position vs Time, Run B | 102 |

List of Tables

| | |
|---|----|
| Table 1: Control Law Constants and Gain Formula..... | 24 |
| Table 2: Nominal Run Conditions Control Law Parameters and Observed Metrics. | 56 |
| Table 3: ANOVA Table for 2FI Model | 60 |
| Table 4: Coefficients in Terms of Actual Factors | 62 |
| Table 5: ANOVA 2FI Coded Equation Summary Report..... | 70 |

Chapter 1: Introduction

Tunnel 9 Background

Hypervelocity Wind Tunnel No. 9 (Tunnel 9) is located in White Oak, Maryland and is part of Arnold Engineering Development Complex (AEDC). It is a unique world class ground-test facility that operates as a blowdown facility with gaseous nitrogen as the working fluid, with two separate test cell and nozzles that provide different flight characteristics for the test article. The facility is capable of simulating flight conditions at Reynolds numbers of $0.05E6/\text{ft}$ up to $48E6/\text{ft}$ and at Mach numbers of 8, 10, 14, and 18 in the North Leg. In addition, the facility is capable of duplicating flight conditions at Reynolds numbers of $2E6/\text{ft}$ up to $8E6/\text{ft}$ at Mach 7 in the Center Leg. As one of the few leading hypersonic facilities in the country, Tunnel 9 provides unmatched hypersonic ground testing for various customer-driven purposes such as computational fluid dynamics (CFD) simulation validation. Figure 1 displays the schematic of the Tunnel 9 facility from the top-level view, labeled with the core systems and components [1].

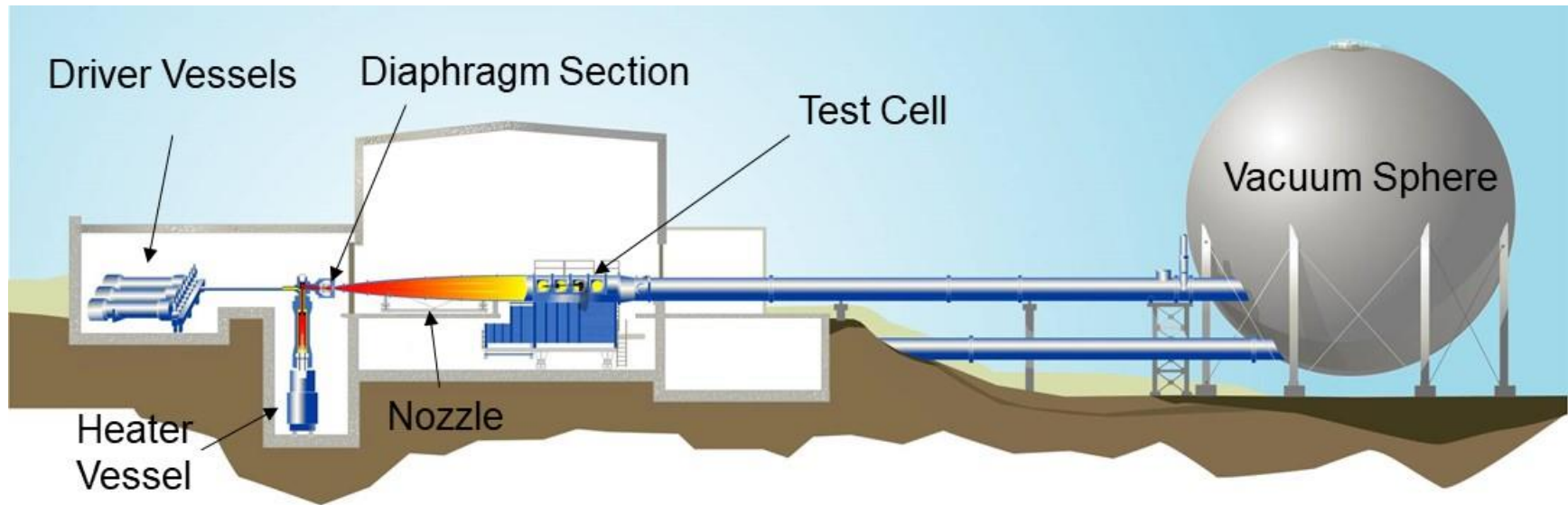


Figure 1: Tunnel 9 Top View Schematic

Design of Tunnel 9

The facility was constructed of large, steel assemblies and unique geometries that enabled such scale of temperatures and pressures. The high-pressure side consist of three thick-walled cylinder “driver vessels” and the low-pressure side consists of a singular, large volume, spherical vacuum chamber. For any given run, the driver vessels are pressurized, a vertical heater vessel is pressurized and charged to contain hot gas, and the vacuum sphere is brought to near vacuum to achieve a targeted pressure ratio from the heater vessel pressure to vacuum. The tunnel blow phase is initiated by tunnel operators by which the diaphragm cavity, the midpoint volume between the high pressure and low pressure sides, is over pressurized. The diaphragm cavity is a hollow cylindrical body that with two burst diaphragms on either side that are designed to burst at a specific pressure differential, thus creating a high speed and disposable valve action. Once blown, cold GN2 flows from the drivers and *drives* the hot heater gas out to the diaphragm and nozzle section, acting as a pneumatic piston. The rate at which gas flows is dependent on the system pressures, control valve control law, and the effective cross-section area at the valve openings [1]. The simplified top level schematic of the facility is shown in Figure 2 [1].

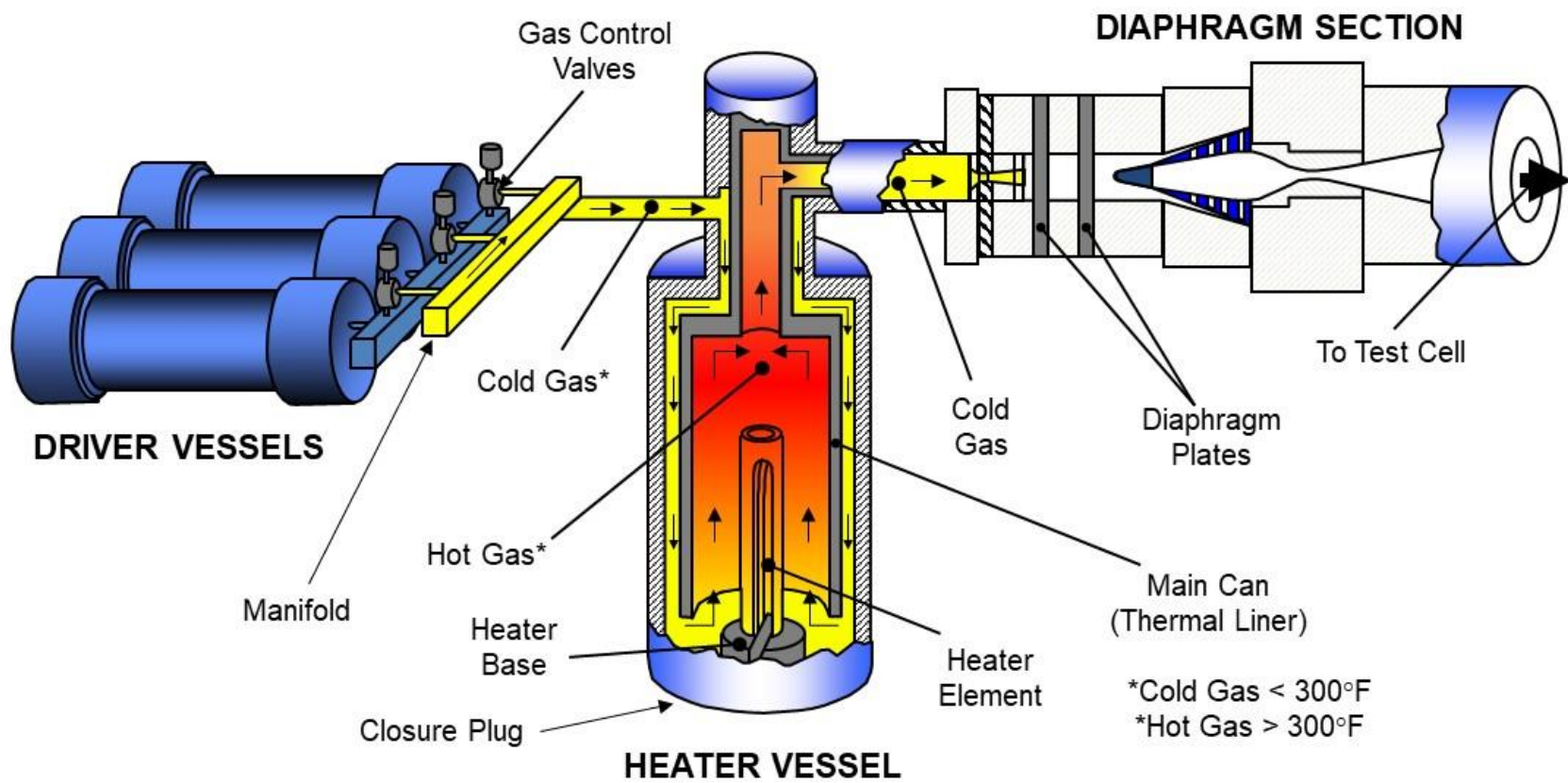


Figure 2: Tunnel 9 Facility High Pressure Schematic

Tunnel 9 Control Law Inception

The first published report of Tunnel 9 control system design came in the AIAA 6th Edition Aviation and Aerodynamics Conference, in an article discussing some of the design challenges of the Naval Ordnance Lab (NOL) Tunnel 9. The report detailed important concepts that were realized in the design and construction of the facility; however, the relevant discussion was the concept of the control valve control law. Upon initial conception, the idea of the control of the tunnel would base off a set point pressure in the nozzle supply location. Contrary to this, a setpoint nozzle supply pressure was near unobtainable as the time constant derived from control valve to nozzle supply was almost equivalent to the total run time. This meant that the desired nozzle supply pressure was near impossible to maintain during extended run times. Instead, the solution was to forgo a setpoint pressure and instead target a desired pressure slope in the nozzle supply pressure and control the gas control valves to produce the target slope. This meant the time constant was effectively diminished since the slope of pressure could ideally be achieved instantaneously. Further into design, the target pressure slope was shifted to the heater pressure slope due to the fact that the heater pressure and flow restrictor control the nozzle supply pressure. This became the standardized model for the control law moving forward, though there was no true modeling involved, simply the proof of concept [2] [3].

Problem Statement

Tunnel 9 does not have a robust or reliable tool to develop run condition pressures, temperatures, and other metrics on the high-pressure side of the facility. Furthermore, a tool does not exist to train tunnel operators with accurate, real-time feedback from a simulator of the facility. There are various models developed in the past by former and current engineers, though some are strictly elementary gas dynamics to calculate pressure drop from the drivers

to the diaphragm, some are empirical from historical runs, or some are approximated through other means. A comprehensive, physics-based model that is repeatable and experimental does not exist for Tunnel 9. Such a model would need to incorporate various subsystem physics models in a coupled fashion, gas thermodynamic processes but more importantly an accurate representation of the control system interaction. Modern simulation packages such as MATLAB Simulink can help replicate analog system controllers and circuitry, as well as ideal gas dynamics processes that operate in closed or semi-closed form.

In recent times, new run conditions were developed to operate the tunnel outside the envelope of current, existing standard conditions, meaning the resulting supply conditions were outside the domain of pre-existing standard conditions. Correlational models and empirical data were implemented to attempt to provide the desired facility behavior, however the control system inputs were noticeably out of tolerance, resulting in multiple revisions to the run condition parameters. In response to this unwarranted discrepancy, the problem extends further in that the control law does not behave as expected in either case of empirical or theoretical [1].

This thesis will present (1) the modeling of the electrical, analog control system, (2) the electrical-hydraulic-pneumatic interaction at the gas control valve and pilot servo valves (3) a design of experiments analysis through Design Expert to further diagnose the control system discrepancies, and finally (4) a preliminary gas dynamics model based on ideal gas effects modeled through a control volume approach will be demonstrated with the accompanying analog electrical and hydraulic models. The end goal is to provide a comprehensive blow down model that incorporates the control system inputs and complex servo valve behavior.

Chapter 2: Literature Review

Summary of Blowdown Facility Literature

Tunnel 9 is a one-of-a-kind facility, which inherently assigns the modeling of the facility a unique solution to the problem. The physical “blowdown” type of facility is not necessarily unique to Tunnel 9, rather it is practiced in other facilities in various industries but predominantly for wind tunnel ground testing operations. In general, blowdown simply is represented by a large delta pressure where the source and sink volumes are generally stable/steady throughout the core process with characterized geometries in between to achieve a desired flow; a conventional control volume approach. The fluid mechanics of control volume analyses and related topics are widely studied and discussed in Tunnel 9 documentation, external source research text, and in traditional fluid mechanics theory text. The control system design, control valve design, hydraulic system interface, and other minor components of the facility, however, are original to Tunnel 9 by which conventional theories may be applied as fit.

Critical Facility Hardware Configuration

Driver Vessels and Gas Control Valves

The driver vessels are large, high-pressure vessels which supply the ‘cold’ GN2 into the heater vessel, which in turn *drives* hot GN2 from the heater to the nozzle throat section. The volume of the driver vessels is relatively large compared to the other components of the facility, excluding the vacuum sphere. Both prior to and after a set of nine gas control valves are a pair of manifolds, traditionally labeled as the inlet and exit manifold. The inlet manifold connects to each of the three driver vessels and has a central bore that then feeds to the nine

gas control valves. On the exit side, the exit manifold connects the outlet of all nine gas control valves to a central bore, which then feeds to the singular heater inlet pipe.

The control valves regulate the flow rate of GN2 from the driver vessels to the heater vessel through a large hydraulic-driven piston valve and stem actuator assembly. The control valves are piloted by electrohydraulic servo valves (ESVs) that modulate the positioning of the actuator through hydraulic force commanded by an electrical signal. The physical valving acts somewhat like a check valve in which a sufficient positive pressure differential between the drivers and heater will seal the gas control valve due to the valve design. The required pressure differential is of course driven by the forces present acting on the assembly, including pressure forces, gravitational forces, and frictional forces. When the valve is opened, there is a tapered portion on the valve stem that gradually increases the cross-sectional area with the movement of the valve. The relationship of valve position to cross-sectional area is not entirely a pure quadratic expression over the full span of vertical travel, rather there are separate geometries of the stem. A direct relationship of valve position to area is obtained and used in modeling. In some instances, the direct geometric relationship is not entirely accurate due to various factors or complex geometries. For these non-traditional relationships, typically a flow-to-area curve is generated by measuring the flowrate through the valve at increments of commanding position. This is of course near impossible given the architecture of the facility where extremely high pressures are observed.

The pilot ESVs are traditional two-stage, 4-way mechanical-feedback servo valves that take in an electrical voltage signal to move their internal servo motor, directing flow of hydraulic fluid to two actuation ports at the actuator assembly, which equate to the valve opening or closing. This voltage is determined by a control law, consisting of amplification, summation, integrals, derivatives, and other signal routing functions. The control law voltage

output to the ESVs is aimed to maintain or ramp the supply pressure, P_0 , at a constant, prescribed slope throughout the run.

Heater Vessel

The heater vessel consists of a large vertical vessel with an internal heating element and a horizontal portion that ports from the upper section of the vertical vessel to the diaphragm section. The gas is heated to high temperatures to account for the significant expansion cooling further downstream at the nozzle and test cell. Such temperatures require unique materials and insulation to protect the vessel walls. During construction of the tunnel, a horizontal heater had been experimented with in the past, however the nature of gas densities at different temperatures resulted in unintended mixture of hot and cold gas. With this in mind, the heater vessel acts as a piston cavity where the cold gas from the driver vessels *drives* the hot gas upwards. There is relatively no mixture of the hot and cold gas which results in a unique interaction that presents a challenge for modeling.

Diaphragm Section

The diaphragm section consists of a few critical components that endure high pressures and temperatures. A simplified diagram of the diaphragm section can be seen in the above Figure 2 downstream of the heater vessel. The flow restrictor is the first component downstream of the heater vessel. The flow restrictor is intended to give more control over the volume of hot gas flowing through the nozzle throat section. The flow restrictor, depending on the tunnel configuration, can have several holes plugged in order to reduce the area through the diaphragm section. In some conditions, the flow area across the flow restrictor is less than that of the nozzle throat, which plays an important role in the flow between respective control volumes. To initiate the blowing of the tunnel, the facility high and low pressure sides are separated with a pair of burst diaphragms which burst at a specific pressure difference across

either diaphragm. There is a set of two identical diaphragms downstream of the flow restrictor to bridge between the low pressure and high-pressure sides. The intermediate volume is pressurized at exactly half the pressure differential until the run is initiated where intermediate volume is pressurized to rupture the downstream diaphragm. When ruptured, the diaphragms fold out into 4 triangular petals that form a square cross-sectional area. This component does not serve any true effects for modeling purposes, rather defines at which point the run data is considered for comparison. Next, a particle separator simply combs out any particles that are expelled from the upstream system components, notably from the burst diaphragms, that travel through the diaphragm section. Lastly, the nozzle throat is the last orifice between high pressure and low pressure during the run, therein defining the expected Mach number derived from geometry. This component is often times the smallest cross-sectional area of the tunnel, but as stated above, there are some conditions that differ.

Historical Modeling of Tunnel 9 Control System and Gas Dynamics

For reference, the *Tunnel 9 control system* refers to the entirety of the system hardware and software used for operating, sensing, measuring, controlling, or otherwise sending and receiving an electrical signal to and from other facility components. Within the control system, there exist a dedicated *control valve control system* that is isolated to only those components that interact or influence the behavior of the supply gas control valves.

The Tunnel 9 control valve control system has been partially modeled for various applications, for example the Mach 10 High Reynolds (M10 HIRE) operations, Mach 15 shakedown operations, or contracted work through CTA and Johns Hopkins APL. Much of the modeling has been done for previous control system architectures by former physicist of Tunnel 9, Jacques A. F. Hill. Hill [1] [2] [3] has modeled much of the control system in tandem with the gas control valves, as the control system interfaces with the control valves directly. We can use much of this material to obtain information about the system and preliminarily start modeling, however deeper fluid mechanical theory of the hydraulics is omitted and instead modeled with empirical constants to simulate valve movement. Often, the models Hill developed did not have any coupling of the electrical to gas dynamics interaction. Instead, empirical constants were used to correct the modeled behavior to get the data to agree more accurately. In addition, any modeling that was performed prior to ~1982 used the first-generation MOOG hydraulic servo valves, vastly different in flowrate than the current Parker and Rexroth servo valves. It was not until some years after the success of Tunnel 9 installation that engineers would start to mathematically derive gas dynamics associated with the high-pressure side of the facility. Most significantly, Hill was the lead physicist and engineer to create these models. Hill and company at the time developed many different models to describe

the gas behavior of various specific run programs. These models will be briefly discussed below and partially used to assist in the new model.

M15 Shakedown Tests

In the early 70's, Tunnel 9 was planning to perform a shakedown test, in which the storage vessels are pressurized, and a test orifice was put in place of a nozzle throat. The goal was to exercise the driver vessel and control valves portion of the facility to get a baseline set of data and generate an empirically driven model of the tunnel. This would allow partial development of test programs and control valve programs. While it is almost entirely experimental, Hill developed estimates of the volume flow and expansion in the Mach 15 heater during cold and hot shakedown tests with the test orifice installed. The volume flow rates could be used to estimate the required flow rates and thus the required control valves to produce various conditions. [1]

HIRE Control System Digital Modeling

In the early 1980's, Tunnel 9 was ramping up the testing and began to explore higher Reynolds number conditions for the existing nozzles. The program M10 High Reynolds (HIRE) program was aimed to give Tunnel 9 higher Reynolds number capabilities with the existing M10 nozzle. Once testing began, it was quickly discovered that the control valves would open and close too fast, leading to forceful pressure waves oscillating into the heater vessel and damaging components as a result. To remedy this issue, Tunnel 9 switched to new Rexroth servo valves that had a much lower nominal flow rate, inherently preventing such harsh pressure waves from forming. With the new servo valves, Tunnel 9 investigated the possibility of digitally controlling the servo valves during a tunnel run. This contrasted the analog components that drove the servo valve operation, and it would open for more flexibility in the control law programming. While this digital control was never fulfilled, many reports

were generated discussing the requirements and computer models to replicate what a digital control system would achieve. These computer models would prove to be obsolete for today's control system architecture. [1]

CTA Inc Model and Johns Hopkins APL Work

In 1989, Tunnel 9 contracted out a work instruction to essentially dissect the operation of tunnel 9 and develop a new control system for the control valves. Part of this contracted work done by CTA Incorporated was a gas dynamics analysis to estimate the pressure and temperature at various points in the high-pressure side, most importantly the driver vessels and heater vessel. As such, CTA Inc. provided a preliminary report to detail the estimated mass flow, pressure, and temperature at various points under the following assumptions: isentropic flow, perfect gas, steady state. The general approach to the CTA Model was to construct a gas dynamics model with the necessary facility geometry, system supply pressures and temperatures, and the current control law. Prior tunnel run data would be used to validate the developed model. As the secondary goal, CTA aimed to revise the current control law and enhance the effective performance of the gas control valves. The overall benefit to the new control law would potentially bring longer run times and faster valve response times. Lastly, the final goal was to write a program such that the control system could run the program for the control law during a tunnel run. No such code was ever written or thoroughly detailed and only the gas dynamics portion was developed. [1]

To piggyback this work from CTA, in 2011 Tunnel 9 contracted out to Johns Hopkins Applied Physics Lab to piggyback the work of CTA and the overall aim was to digitalize the control law that CTA had developed. The model was developed in MATLAB Simulink, but the overall accuracy of the model was inconsistent and there was not enough substantial evidence that the model was viable given the MATLAB results. In addition, between 1989 and

2011, the control system and control law had been modified, rendering the 1989 model obsolete and invalid. As such, the model was scrapped, and all facility modeling has since ceased. [1]

Chapter 3: Mathematical Model and Numerical Methods

Control System Modeling

Fundamental Electrical Engineering Analysis

Tunnel 9's control system uses entirely analog devices to control the behavior of the control valves. This behavior is determined by a 'control law' that is derived from the control system circuitry and user inputs prior to the tunnel run. Like any electrical circuit analysis, there are key formulae to utilize to generate transfer functions of the electrical components. The entirety of the control system is considered direct current voltage (VDC), and thus most alternating current voltage (VAC) formulae will be omitted. Of course, Ohm's Law and Kirchhoff's Law apply to all electrical circuits. Ohm's Law states that the current through a conductor between 2 points is directly proportional to the voltage across those 2 points. More simply, Voltage (V) is equal to the Current (I) multiplied by the resistance (R). Kirchhoff's Law deals with circuitry loops, stating that the total current entering a node is equal to the total current exiting the node. These equations can be used to describe basic electrical circuits. [4]

Operational Amplifiers (OpAmp) are modeled by using these core formulae. An OpAmp is an analog component that can provide very large 'open loop' gains to an incoming voltage source. This component is especially useful in control system circuitry. There are many different combinations and configurations can create very specific functions to be applied to the incoming voltage source(s). The OpAmp component schematic is shown below.

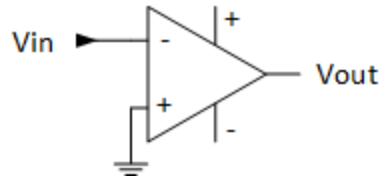


Figure 3: Basic OpAmp Schematic

This is known as an inverting amplifier because the positive voltage is input to the negative terminal of the OpAmp. An *ideal* inverting OpAmp will have infinite open loop gain; V_{out} would effectively be infinite. However, when a resistor (R_F) is connected from the output to the negative input of the OpAmp, this creates negative feedback. This will send some of the output voltage back to the inverting input and create a closed-loop gain. Another resistor (R_1) can then be added in series with the voltage source to dictate the gain (K) of the OpAmp. This is the most common configuration of an OpAmp and is shown below.

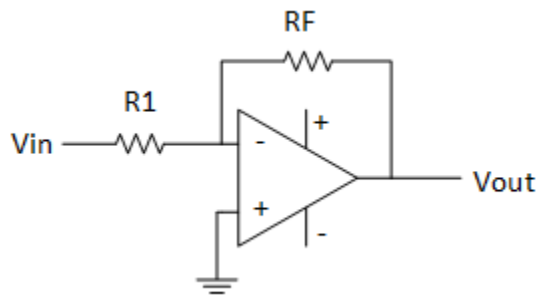


Figure 4: Amplifier Schematic

The effective gain of the OpAmp then becomes a function of the resistors.

$$V_{out} = -KV_{in} = -\frac{R_F}{R_1}V_{in}$$

Voltages can be summed and individually amplified by adding a voltage source and resistor to the negative input as shown below.

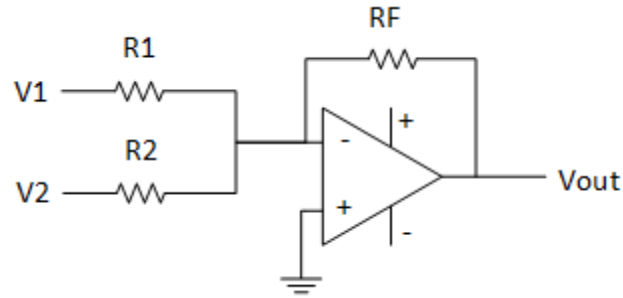


Figure 5: Summing Amplifier Schematic

Where the effective gain is given:

$$V_{out} = -K_1 V_1 + -K_2 V_2 = -\frac{R_F}{R_1} V_1 - \frac{R_F}{R_2} V_2$$

Adding a capacitor to an OpAmp circuit can create a differentiating or integrating OpAmp, depending on where the capacitor is placed. Both the differentiator and integrator OpAmp are opposite of each other in their capacitor and resistor placement. Both OpAmps and their corresponding transfer functions are shown below.

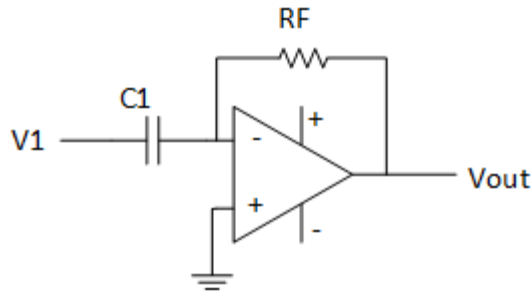


Figure 6: Differentiating Amplifier Schematic

$$V_{out} = -C_1 R_F \frac{dV_{in}}{dt}$$

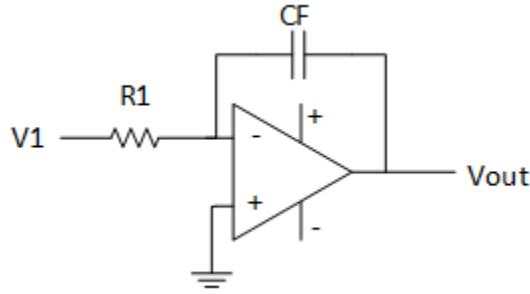


Figure 7: Integrating Amplifier Schematic

$$V_{out} = -\frac{1}{C_F R_1} \int_0^t V_{in} dt$$

Analog signaling is effectively instantaneous, however capacitors and OpAmps provide some transient behavior that can stack to create a minor but significant impact to the model. Capacitors charge/discharge at an exponentially changing rate based on the capacitance and coupled circuitry components. Most OpAmps have a slew rate associated with them; the maximum rate at which gained voltage can change. In other words, if an input voltage is stepped instantaneously from 0 to 1 VDC, the OpAmp will bottleneck the output voltage to a rate of change in Volts per second. For the most part, these slew rates do not have an effect on signals such as that of the control law. Effects for large gains and high frequency input voltages are more apparent. [4]

Control Law and Command Voltage Terminology

When referencing to the following information there are several steps/voltages between the control system, the gas control valves, and the data system in which valve command and position are recorded. The command ramp voltage is a constant voltage that is summed into the control law prior to integration to act as a ramp function to the final command voltage for the pilot servo valves. The initial opening voltage is also a constant voltage summed into the control law to actuate the control valves to a soft-closed position just prior to the blow

phase initiating. Both the command ramp and initial opening voltages are variable in each tunnel run, hand-dialed by tunnel operators. The output voltage of the control law is referenced as the command voltage, and it is input into the servo amplifier controller card which also takes the feedback voltage as the second input. The feedback voltage is the voltage received from the linear potentiometer mounted on the gas control valve actuator. The servo amplifier controller card outputs an error voltage between the command voltage and the feedback voltage. The error is then amplified and output to the servo valve. The command voltage that is used in control system facility data measurement is the command voltage with further signal processing and amplification. It is unknown as to why the command voltage from the control law is further amplified and biased before entering the data system. In addition, the amplification and bias is determined from two manual potentiometers by which knowing the exact values is difficult to replicate in modeling.

Sequencing for Control System

When the tunnel blow phase begins at the burst diaphragm rupture, there is a pressure transducer at the nozzle supply location that will sense an increase in pressure. At a predetermined threshold pressure, the control system will trip a comparator which feeds into a sequencer module that facilitates the timing of further equipment such as the test cell pitching system or the hard closing of the control valves to end the run. Some conditions use multiple comparators to time out different events in different portions of the tunnel run. For simplicity, it is assumed that only one comparator is used for all conditions. Once tripped, there are five events that elapse in the control valve control system, each of which have associated delays.

[1]

1. At time zero after trip, the pilot servo valve supply voltage is transferred from an idle power supply to the command voltage. The control valves are actuated to a

soft-closed or limited-area position by the initial opening voltage. If the valve is hard closed on diaphragm rupture, the transient response of the control valves opening may initially lag due to the mechanical de-stretching of the valve stem and hydraulic flow. With the initial opening, the control valves are given a form of a 'head-start' to overcome the de-stretching of the valve stem, the delay in hydraulic pressure loading, or the delay or mismatch in command voltage from the control system.

2. At the first sequencer event after trip, the command ramp comparator is then switched from off to on. More specifically, an open/close switch exist in the integrating OpAmp that results in the integrating function becoming activated/deactivated. In most run conditions, this switch is activated simultaneously with the comparator trip, therefore there is no delay to the command ramp activating. For modeling, it is assumed that there is no time associated with this event delay, thus the command ramp is activated at time zero.
3. The next sequencer event after trip is the command ramp deactivation. This is simply removing the integration function within the respective OpAmp and causing the command voltage to return to 'initial opening' state. This is generally considered the end of the good flow portion of the run. This time delay is generally derived from trial and error but can be approximated through correlational equations involving the mass flow rate and heater vessel hot gas volume.
4. The fourth sequencer event after trip is the return of idle power supply to the servo valve. As mentioned in the first event, the servo valves' commanding signal is transferred to the command voltage, thus this event is simply the reversal. This event is delayed by a quarter of a second after the command ramp is deactivated.

5. The final sequencer event is the tunnel stop event, which deactivates the command voltage circuit, and the run is terminated.

Derivation of Control Law

A pressure transducer located at the exit port of the heater vessel will feed the heater pressure PHE into the control law. It is important to note that this transducer reads the heater exit pressure, rather than the vessel's pressure in the center. This will be discussed in depth later on. This transducer voltage is amplified, processed through a differentiator amplifier, and then subsequently processed through an integrator amplifier. During this process, the command ramp voltage C_r and the initial opening voltage V_0 are summed into the final command voltage V_c . Historical modeling memorandums and reports such as those published [2] [3] have indicated that the open-loop command law follows the governing equation shown below:

$$V_c = V_0 + C_r(t - t_c) + K \frac{V_{max}}{PHE} \int_{t_c}^t \frac{dPHE}{dt} dt$$

Where $t - t_c$ is the time elapsed after the tunnel start comparator is satisfied. The command ramp voltage C_r is a constant voltage varied by a potentiometer. This voltage is applied after the differentiator and prior to the integrator, thus the constant voltage then becomes a ramped voltage of constant slope that increases with time after integration. The maximum voltage V_{max} is the voltage differential that drives the servo valves to 100% open. The non-dimensional gain K is a function of the heater pressure transducer sensitivity, the transducer excitation voltage, and other control system gains. Therefore, this equation only governs the true blow phase portion of the tunnel run when the command ramp relay is satisfied. This equation, however, is not mathematically coincident with our current control system configuration, per electrical schematics. It is believed the control system circuitry has changed since the equation was initially derived.

The schematic shown below is a simplified electrical schematic of the current control law for the gas control valves. The signal input in the top left corner is the heater pressure transducer voltage which is proportional to the pressure inside the heater vessel. The signal is further processed through a low-pass filter to remove high frequency noise in the signal. Then the signal goes through a handful of Operational Amplifiers that differentiate, integrate, and sum voltages to generate the final command voltage. In addition, there are relays, comparators, and a sequencer that sequence the control valve events after the blow phase begins. For example, if the transfer relay at the end of the control law is not satisfied, the control valves are in idle position from the supply voltage that actuates the pilot servo valves hard closed.

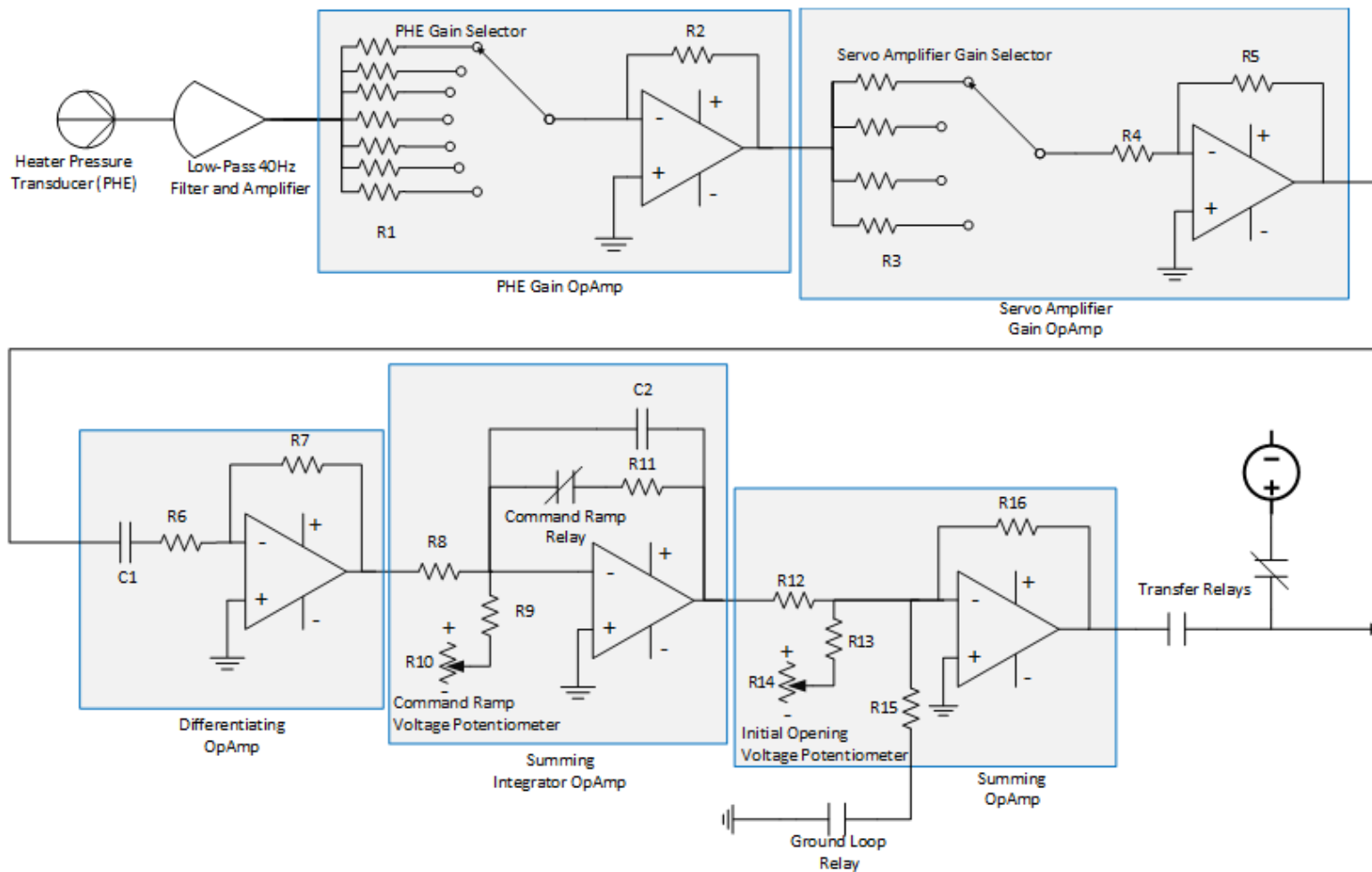


Figure 8: Control Law Schematic

There are several gains associated with each process in the control law, and therefore the gains cannot be simply combined into one effective non-dimensional gain such as that in the historical AEDC equation. Instead, the control law gains can be shown below:

| Constant/Gain Formula | General Description |
|------------------------------------|--|
| S_{HE} | Heater Pressure Transducer Sensitivity (mv/v/psig) |
| B_{HE} | Heater Pressure Transducer Slope Intercept |
| $K_{HE} = \frac{R_2}{R_1}$ | Heater Pressure Input Gain Selector |
| $K_{SA} = \frac{R_5}{(R_3 + R_4)}$ | Servo Amplifier Gain Selector |
| $K_{dif} = C_1 R_7$ | Differential OpAmp Gain |
| V_r | Command Ramp Input Voltage |
| $K_r = 1/R_9$ | Command Ramp Input Voltage Gain (Closed Relay) |
| $K_a = \frac{R_{11}}{R_8}$ | Command Ramp Input Voltage Gain (Open Relay) |
| V_i | Initial Opening Input Voltage |
| $K_i = \frac{R_{16}}{R_{13}}$ | Initial Opening Input Voltage Gain |
| $K_n = \frac{R_{16}}{R_{12}}$ | Summing Amplifier Input Gain |
| $K_c = 1/C_2$ | Ground Loop Closed Resulting Gain |
| $K_o = 0$ | Ground Loop Open Resulting Gain |

Table 1: Control Law Constants and Gain Formula

Resistor R_6 does not contribute any gain to the system, rather it is used for stability of the signal transmission. Resistor R_{10} and R_{14} are voltage dividers to tune the voltage input for the command ramp and initial opening. The transducer slope intercept for most transducers is on the order of $10E-5$ times that of the full voltage range of the transducer. Given the ambient

electrical noise of the control system and the size of the heater vessel, the slope intercept will not have any significant effect on the downstream simulation components.

The variable gains, PHE gain selector and the servo amplifier gain selector, are selected based on historical data or rough equations. To say the least, the conditions Tunnel 9 uses today are based on historical trial and error and formed into empirical models. If the transfer function of the existing control system circuitry and the control law is derived using OpAmp transfer functions, the true command voltage is given by the equation below:

$$V_c = K_c \left\{ K_i V_i + K_n \int_{t_c}^t \left(S_{HE} K_{HE} K_{SA} K_{dif} \frac{dP_{HE}}{dt} + K_r C_r \right) dt \right\}$$

Which can be simplified to the equation,

$$V_c = \left\{ K_1 V_i + \int_{t_c}^t \left(K_2 \frac{dP_{HE}}{dt} + K_3 C_r \right) dt \right\}$$

where

$$K_1 = K_c K_i$$

$$K_2 = K_c K_n S_{HE} K_{HE} K_{SA} K_{dif}$$

$$K_3 = K_c K_n K_r$$

This equation defines how the control valves actuate in response to the heater exit pressure PHE.

Servo Amplifier-Controller Card Transfer Function Derivation

The servo amplifier controller card is a custom component that regulates the final command voltage based on the feedback voltage received from the control valve itself. The feedback voltage is supplied from a linear position transducer coupled to the control valve piston. The simplified purpose of this card is to balance the command voltage with the actual position of the control valve. There are 2 inputs to the controller card: the control law

‘command’ voltage, and the feedback voltage. The control law voltage, or command voltage, ranges from +0.1 to -3.1 VDC, where +0.1 VDC hard closes the control valve shut and -3.1 VDC fully opens the control valve to 100% open. The feedback voltage ranges from 0 to 3 VDC, where 0 VDC measures a fully closed valve, and 3.0 VDC measures a fully open valve. The buffer of ± 0.1 VDC for the command voltage ensures the control law command voltage is always greater in absolute value than the feedback voltage at either fully closed or fully open. Especially for fully hard-closed valves, the offset must ensure the valves are not “soft-closed” to prevent a Nitrogen leak.

The card sums the command voltage and the feedback voltage together to create an effective error between the control system signal input and the control valve position output. The error is then amplified and inverted to generate an output voltage inversely proportional to the error. In the first stage on the left-hand side, there are potentiometers to help balance the input voltage spans, offset the voltages up or down, or modify the gain produced by the summing amplifier. In the second stage on the right-hand side, there is another amplifier along with a couple transistors that act as a saturation limiter, or also termed a CMOS. The output voltage is saturated at some voltage to prevent overloading the servo coils with excessive voltage. The approximate transfer function is built up from the following equations and simplified schematic with each variable location is given in Figure 9.

$$V_{error} = K_{SA} \left(V_{fb} \frac{R6}{R1} \left(\frac{RGAIN}{R6} + \frac{RGAIN}{R7} + 1 \right) + \frac{VBIAS}{R5} + V_{cmd} \frac{R6}{\left(\frac{1}{R3} + \frac{1}{R4} \right)^{-1} + R2} \right)$$

$$\text{if } V_{error} \geq V_{sat} \quad \text{then } V_{out} = V_{sat}$$

$$\text{if } V_{error} \leq -V_{sat} \quad \text{then } V_{out} = -V_{sat}$$

$$V_1 = V_{error} * \left(\frac{R15}{R15 + R_{servo}} - 1 \right)$$

$$V_2 = -V_1 \left(1 + \frac{R_{servo}}{R15} \right) - V_z \left(\frac{R_{servo}}{R15} \right)$$

$$V_{dif} = V_2 - V_1$$

$$i_{servo} = \frac{V_{dif}}{R_{servo}}$$

The output voltage differential, V_{dif} , and feeds to the input connector to the servo valve. The resistance of the servo valve, R_{servo} , is given by the manufacturer, thus the current across the servo valve coils is given by the voltage differential over the servo resistance. The constant gain, K_{SA} , is the gain associated with the ‘Output OpAmp’ as a function of resistors $R8$ through $R14$. Both ‘sides’ of the circuit have a pair of reverse-direction diodes which act as a voltage limiter.

The servo valves operate on this voltage differential which induces the current across two parallel coil resistors that act as an electromagnetic motor when coupled with a permanent magnet. The current drives the servo coils to actuate an armature inside the servo 1st stage. The 1st stage then translates to movement of the control spool 2nd stage. The 2nd stage control spool directs hydraulic fluid to the actuator valve ‘3rd stage’ which controls the flow of GN2 from the driver vessels to the heater vessel. Unfortunately, due to the nature of analog components, POTs, and human input, the exact resistances of these POTs are not known, therefore deviation from the nominal value output current can vary based on the POT location and respective gain.

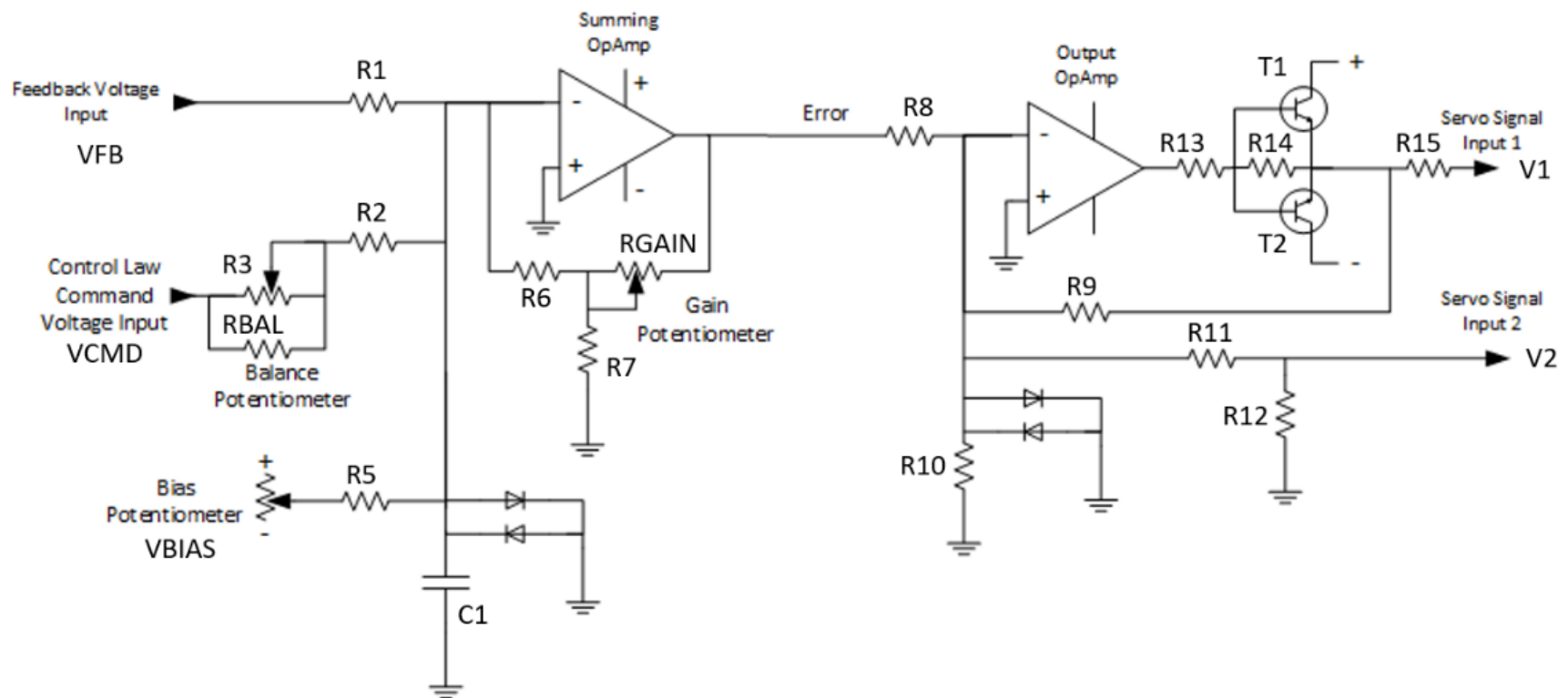


Figure 9: Servo Amplifier Card Schematic

Data System Command Voltage

The control system records the command voltage in a non-intuitive way; the output voltage of the control law is further processed through another circuit before eventually becoming the facility data command voltage. This auxiliary circuit does not feed into the rest of the system and is solely in place to modulate the control law voltage to the data system. The transfer function of this analog circuitry and a simplified schematic of this circuit is shown in Figure 10.

$$V_{CVCMD} = \left(\frac{R6 + R5}{R4} \right) * \left(V_{CL} \left(\frac{R3}{R1} \right) + V_{zero} \left(\frac{R3}{R2} \right) \right)$$

The voltages V_{CVCMD} is the output voltage that is received by the data system. The voltages V_{CL} and V_{zero} are the control law output voltage and the zero point voltage, respectively. This circuit, like the other analog circuits, has a pair of potentiometers in which are hand-adjusted. The output voltage will be modeled only for verification or comparison purposes.

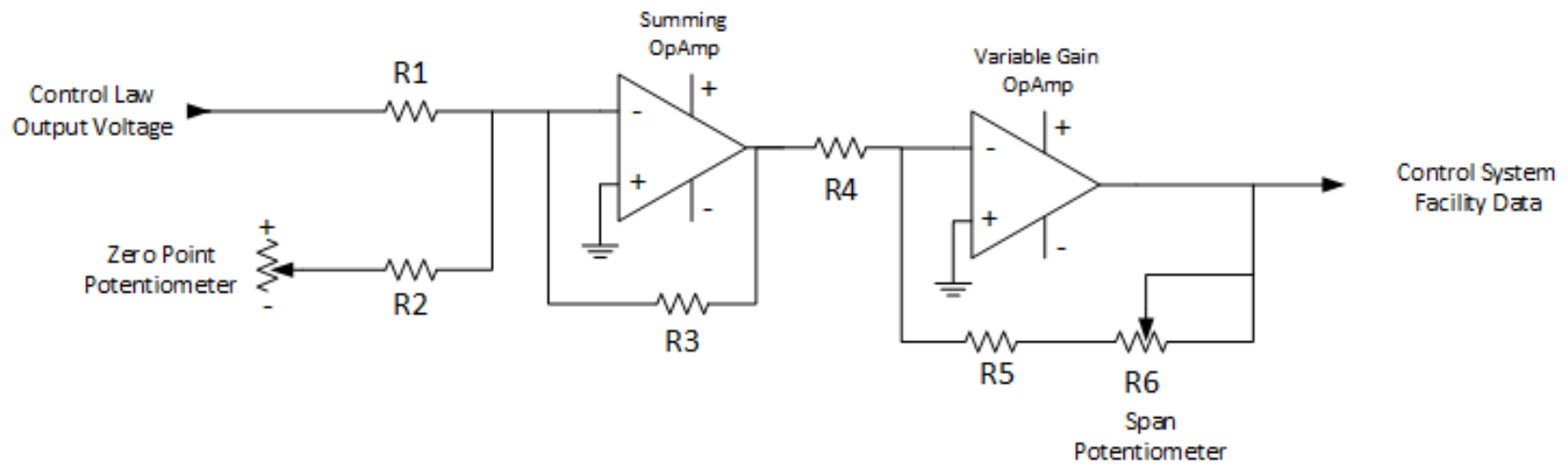


Figure 10: Facility CVCMD Input Schematic

Sequencer Relays and Trips

Finally, there needs to be some mathematical logic for the comparator trips and sequencer events. These are simply relay switches, but for mathematical purposes, this can mean a step function applied/removed at certain time steps. Step functions are modeled as function of time shown below:

$$u(t - 10)$$

This step function would indicate the function u will step from 0 to 1 once 10 units of time t has passed. Therefore, when multiplied by another function, step inputs can be applied to activate/suppress the function. In our case, this will be used to trip comparator relays and sequencer delays. In MATLAB and Simulink, there are blocks that can delay the transmission of a signal. When combined with logical true/false statement blocks, the transmission of the respective sequencer events can be timed out exactly as defined in the run configuration.

Guidelines for Design of Experiments

Background

A more rudimentary way of ‘modeling’ the tunnel is through what is generally termed empirical. As stated in prior sections, the tunnel standard conditions were developed and standardized predominantly through trial and error. These conditions input parameters were then formed into empirical formulas which future conditions could be designed by. However, these empirical relationships quickly became obsolete once tunnel configurations changed. The same concept can be employed to the current historical data set and potentially provide insight into the control law. One method to expediting an empirical model is to utilize a design of experiments analysis that incorporates statistical analysis. The program DesignExpert is a design of experiments program that allows the user to input large amounts of data and quickly process the data to derive relationship, surface maps, mathematical fitting equations, residual

plots, etc. typically used to provide statistical analysis for experimental work. In this case, the program can be used to take in standard conditions run at tunnel 9 with relevant facility configuration and control system input parameters and the resulting facility measurements such as heater pressure and nozzle supply pressure. Many input parameters shall be categorical values such as the Mach and Reynolds number, thus they are not necessarily discrete data points. These parameters in theory do not have any effect on the tunnel performance and are used as condition identifiers. Other parameters such as command ramp voltage and heater run pressure are nominal parameters but can be treated continuous response parameters that can take any continuous value. Lastly, parameters such as PHE gain and flow restrictor area are discrete values that only have a finite number of settings or values. The distinction of each type of parameter is important to provide meaningful results from the analysis.

Response Parameter Determination

To potentially get a better understanding of what is happening inside the control law, historical data from various run condition were examined. Each condition has the respective nominal control system configuration that is relevant to the control law; Nominal Mach, Nominal Reynolds, Heater Run Pressure (PHE), Heater Run Temperature (THG), Nominal Flow Restrictor Area, Nozzle Throat Area, and Mass Flow Rate, Run Times (total and good flow), PHE Gain, Command Ramp Voltage (CR), Initial Opening Voltage (IO), Servo Amplifier Gain (SA Gain), Number of control valves, PHE Transducer Sensitivity (SHE), the observed rate of change in heater pressure ($dPHE/dt$), and the observed initial actuation time of the average valve position (CV Start Time). All factors excluding the observed rate of change in heater pressure and the observed CV start time are nominal values and are generally the same for any given run at the condition. Some parameters are discrete settings while others are continuous.

PHE Slope Calculation

The observed rate of change in heater pressure is measured through averaging slope of heater pressure for the past ~15 historical runs at the condition. This is achieved through a MATLAB program that allows the user to access historical runs from the specified condition and compare facility data channels. The historical run analysis program was initially created to observe control valve behavior with respect to historical runs, but eventually grew to incorporate all facility metrics. To summarize, the program prompts the user to enter what condition, run(s), and phase the user would like to compare to historical runs, then the program imports run that were ran at the same condition and phase and computes the average and 95% confidence interval for each data channel.

Perhaps the largest factor to observe the average and confidence intervals in regard to the control law is the heater pressure (PHE). A function was built to further quantify the heater pressure historical data by calculating a simple linear regression of the heater pressure. The function prompts the user to specify the start and end points to calculate the rate of change in heater pressure, with the assumption that the slope is linear throughout the specified range. This

graphic can be shown in

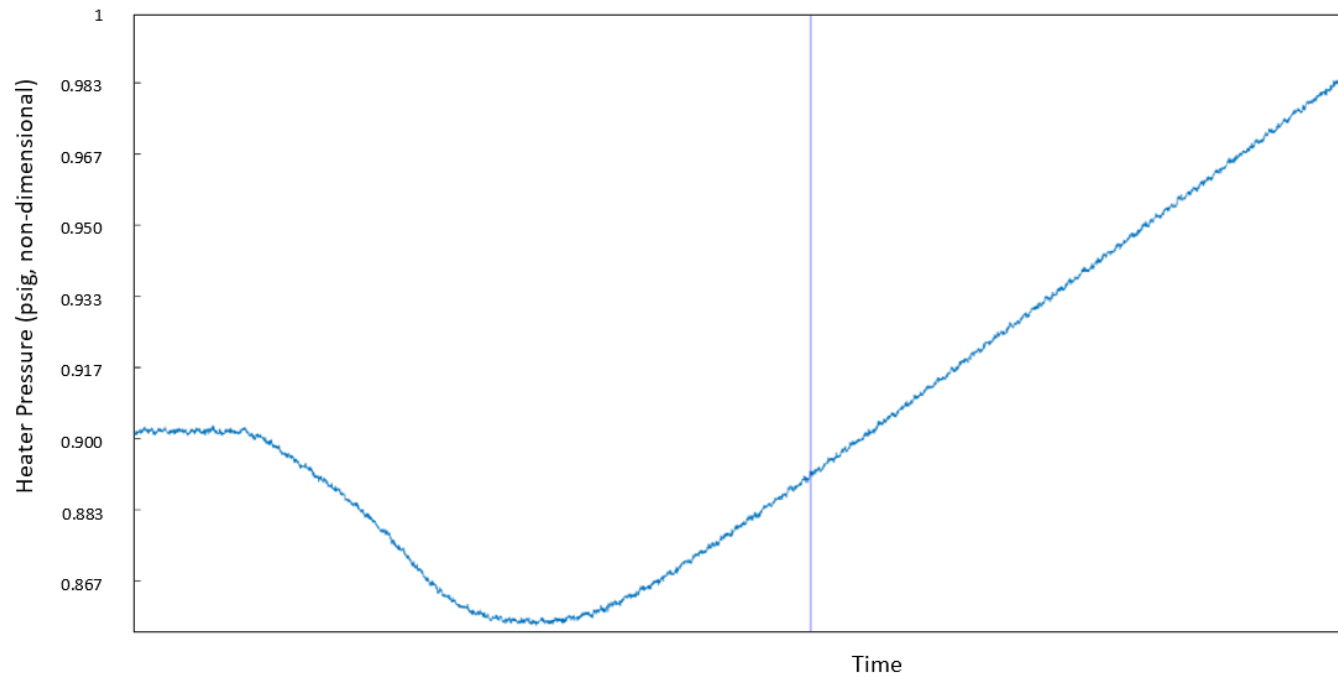


Figure 11, where the time elapsed during the run is plotted on the x axis and the heater pressure is plotted on the y axis.

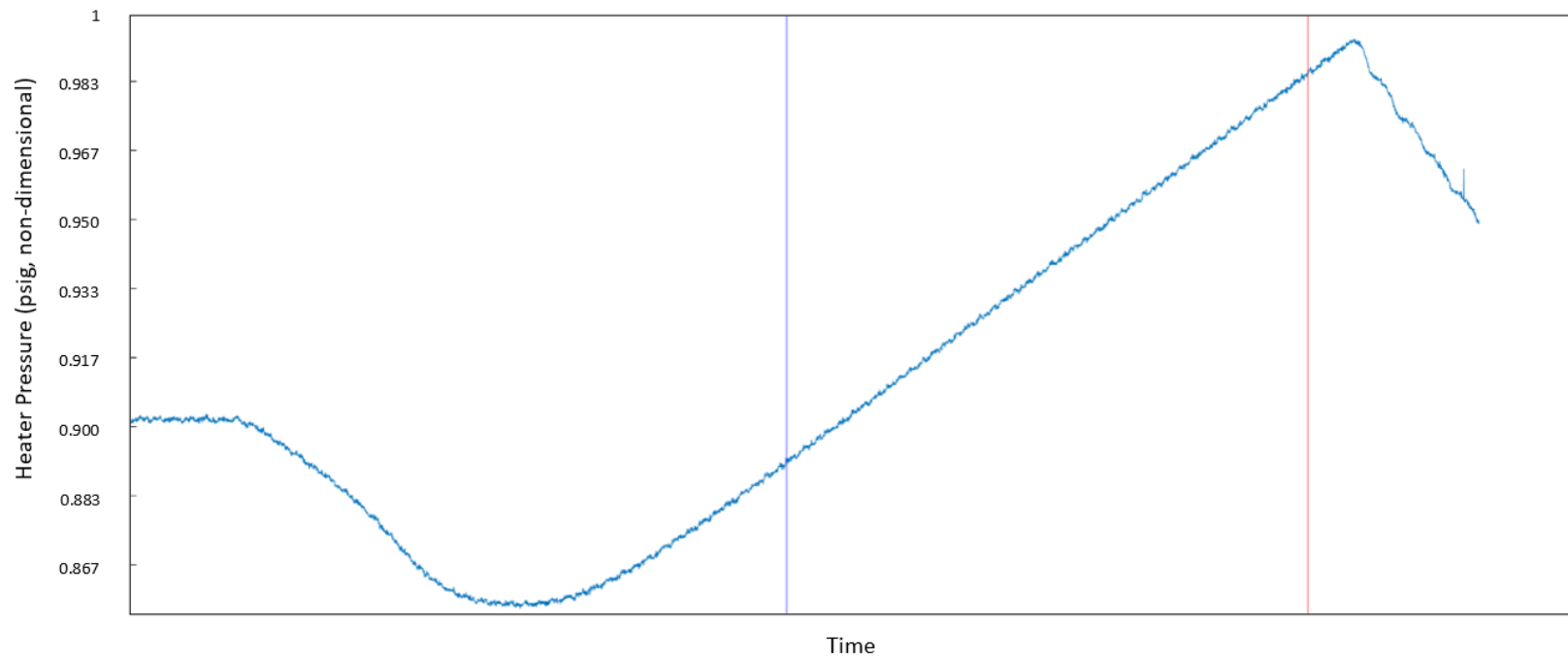


Figure 11: T9 Data Comparison App – PHE Slope Calculation Range Selection

The user selects the start and end to the range of data to consider in the slope calculation, after which the next run(s) are also prompted to the user until all runs have been iterated through. Most conditions are able to produce very linear heater pressure slopes, however there are some shorter runs that don't quite steady out to a distinct slope. The R-squared value is output from the linear regression computation and a simple if-statement was written such that if the R-squared value is below a certain threshold (ie. 0.95), a warning message would be output. Once done, a resulting plot shows a spread of all calculated PHE slopes in addition to the average and 95% confidence interval, shown in Figure 12. If the R-squared criteria is unsatisfied, the code will still execute and produce results, but this condition is then omitted from the resulting DesignExpert analysis. Other attempts were made to use a cubic spline regression or similar in attempts to further automate the code, however, heater run pressure trends vary significantly between conditions, resulting in case by case results that may not be valid.

This slope approximation was conducted for a range of conditions across different Mach numbers such that the population of response factors is large enough to generate meaningful results in the DoE program. To reiterate, only conditions that satisfy the regression criteria are fed into the DesignExpert analysis.

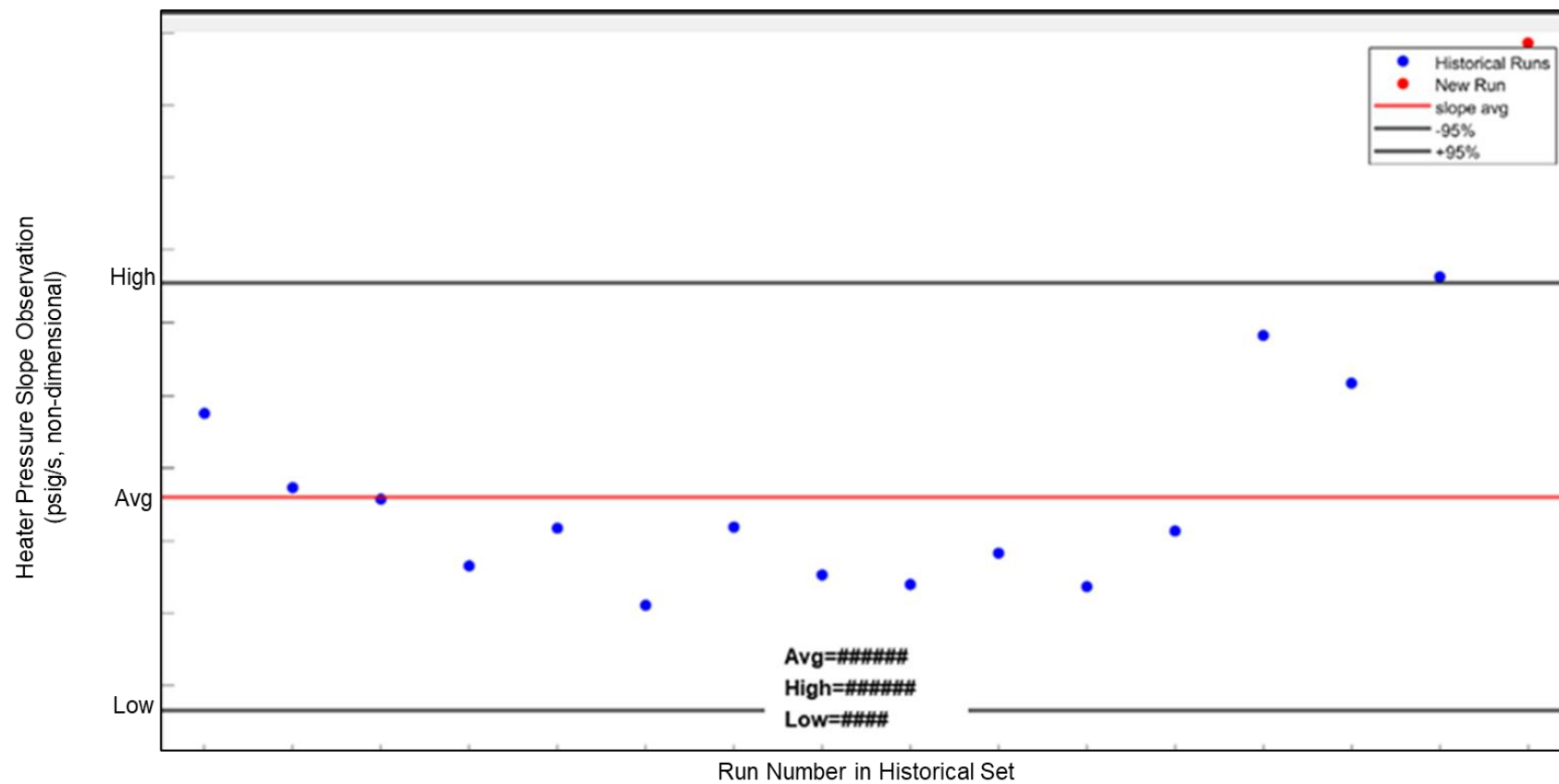


Figure 12: T9 Data Comparison App – PHE Slope Calculation Scatter

Control Valve Start Time

Another function was written to detect the time at which the average valve position. The function simply scans for the average control valve position rising above a pre-determined threshold. To provide context, each control valve idles at some arbitrary positive voltage between 0 and 1 volts. This is due to the general system design and calibration of the control valves. To correct for this, each valve position channel is offset to a starting point of 0 volts at the time of blow. Then the control valve start time function simply indexes the time at which the average control valve position for each run surpasses the set threshold. The output of the function displays the plot of the average control valve positions in addition to the set threshold, average and 95% confidence intervals, and the average time at which the threshold is surpassed. The command window is populated with a list of time delays in respect to the average for each run. The plot for the control valve start time function is shown below, where the left is the plot of all historical run data and the right is the run data of the 'new' run of interest.

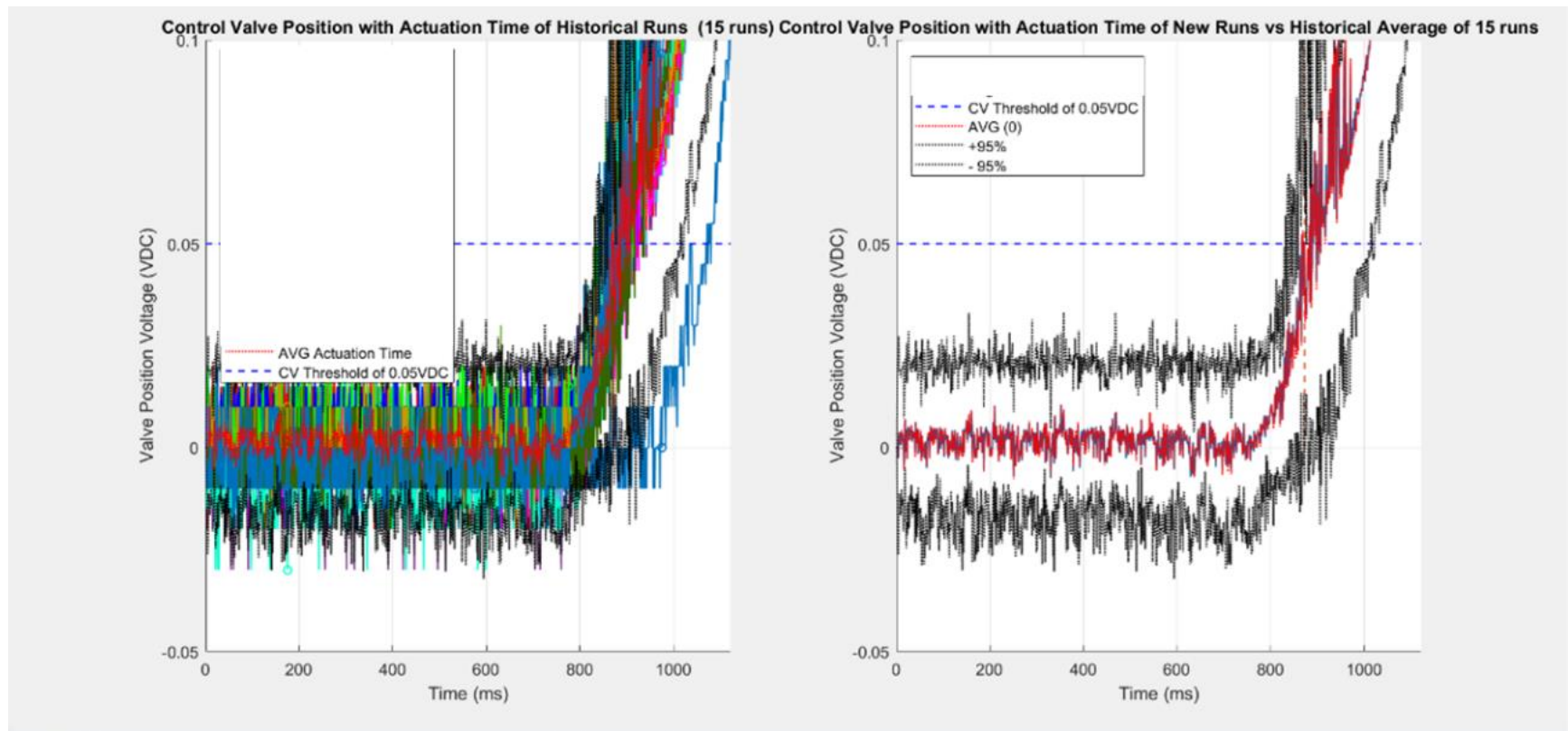


Figure 13: T9 Data Comparison App – CV Start Time Function Outputs

Various existing standard conditions' nominal control system inputs and the respective average PHE slope and average CV start times are tabulated, later shown in Table 2. It is important to note that certain Mach 8, 10, and 14 runs use ablators which significantly reduce the time to actuation. These ablators are inserted in the flow restrictor and upon initial blow, the ablators significantly reduce the flow until they are eventually burned out. The purpose is to allow the diaphragm components to reach bulk temperature and provide more consistent nozzle supply conditions. As a result, the control valves are actuated to the initial opening during this ablator burnout period, thus the valves do not suffer from the inherent lag that is experienced without ablators.

Electro-Hydraulic Servo Valve and Actuator Modeling of Tunnel 9

AEDC Servo Valve Model

Internal servo valve characteristics are given by the servo valve manufacturers, but the coupled control valve assembly must be modeled as well. In a 2013 AEDC Technical Report, AEDC TN system engineers discussed the continued development of a Simulink model to simulate the performance of electro-hydraulic servo valves in efforts to better monitor the health of their on-site electro-hydraulic servo valves. This extensive model incorporated all relevant flow and inertial equations to simulate a hydraulic servo valve piloting a larger actuator valve. In fact, the report details even minute details such as the torque motor and feedback rod spring mechanics. The 94 page report will not be fully incorporated, however the basic equations and assumptions needed specifically for Tunnel 9 application will be discussed [1]. In addition, there is older text that described the basic transfer functions of servo valves, which can aid in the modeling of certain servo valve mechanics [5].

Servo Valve Internal Flow Modeling

There are various computations to the electro-hydraulic servo valve, including nominal fluid flow rate, force balance, and electromechanical torque generation. To start, the model assumes the generic flow Q given by the servo valve datasheets [6] [7],

$$Q = constant * A * \sqrt{|\Delta P|}$$

Where the constant is a function of the servo valve flow rating, A is the servo valve nominal flow area, and the ΔP is the differential in input and exit pressure. Given that the valve is driven by an electrical current and the open area is generally linear with the current, the flow is also dependent on a function of the current, i .

$$Q = constant * i * \sqrt{|\Delta P|}$$

There is a step response delay time and associated slew rate that is given by the valve data sheet that is later specified and incorporated into the model, but for initial modeling, the response time and slew rate are omitted. The nominal flow given by the manufacturer is generally assuming a uniform, constant pressure supply and reservoir. Likewise, the facility hydraulic supply and reservoir have been observed as relatively constant pressures throughout a given run (ie. $\pm \sim 1\%$ psig). In addition, this nominal flow rate is assuming the nominal current is applied. As such, the flow can be adjusted to account for these nominal values, where the subscript *nom* indicates the nominal constants of that variable.

$$Q = sign(\Delta P) * Q_{nom} * \left(\frac{i}{i_{nom}}\right) * \sqrt{\frac{|\Delta P|}{|\Delta P_{nom}|}}$$

At Tunnel 9, the servo valves are operated by a direct current i within the nominal max current, $\pm 15\text{mA}$. The current is then normalized so the resulting flow is based on a 0 to 1 scale of the nominal flow. Similarly, the pressure differential is also normalized. Lastly, the nominal

flow is multiplied by these normalized values to give the actual flow rate. Further dynamics of the internal spool can be modeled; however this will not be modeled in this preliminary model.

Actuator Physics

The actuator is composed of two volumes on either side of a piston with a large actuation area. The piston translates vertically, or normal with respect to the piston actuation faces, thus the actuation volumes change inversely to one another. This concept is synonymous with the volumetric flow in and out. With incompressibility, the continuity condition simply states that volumetric flow in and flow out are equal, however there are significant forces that oppose the flow of hydraulic fluid, causing non-linear effects. The bulk modulus β is given as,

$$\beta = -\frac{dP_{act}}{\frac{dV}{V}}$$

Where P_{act} is the pressure within the actuator volumes, and V is the actuator volumes.

Which can be rewritten for the differential volume dV .

$$dV = -\frac{VdP}{\beta}$$

Now, volumetric flow in and out of the actuator volumes can be written,

$$Q_{act} = \frac{dV}{dt} + \left(\frac{V}{\beta}\right)\left(\frac{dP_{act}}{dt}\right)$$

Where both the actuation and bulk effects are present. It is important to note that minute changes in the metal components containing the hydraulic fluid do not experience significant deformation due to fluid pressure. In addition, we will assume there is no significant leakage of the hydraulic system, therefore there is no loss of mass throughout the process. This flow can then be rearranged to solve for the change in pressure, and then integrated to obtain the resulting pressure.

$$\frac{dP_{act}}{dt} = \left(\frac{\beta}{V_{act}} \right) \left(Q_{act} - \frac{dV_{act}}{dt} \right)$$

$$P_{act} = \left(\frac{\beta}{V_{act}} \right) \int \left(Q_{act} - \frac{dV_{act}}{dt} \right) dt$$

Next, the force balance can be expressed with the actuation forces, frictional, countering, and gravitational forces.

$$F_{tot} = A_p P_{act_{up}} - A_p P_{act_{low}} - F_f - F_c + F_{mass}$$

Where F_{tot} is the total force acting on the piston, A_p is the area of either piston actuation surface, P_{act_*} is the upper or lower pressure within the actuator volumes, F_f is the frictional force opposing the motion of the piston, F_c is the countering force due to external loading, and F_{mass} is the force due to gravity acting on the actuator assembly. It is important to note the positive direction is the downward, as the Tunnel 9 gas control valves operate as such.

The frictional force F_f is simply countering the positive direction of motion, however the actual force created is highly variable to internal component geometry, such as the stem packing components and the internal hydraulic fluid cavity components. For simplicity, this force is estimated for initial testing and iteratively changed to produce more accurate modeling.

$$F_f = k \text{ (estimated constant)}$$

The countering force is a combination of the opposing supply pressure acting on the valve stem.

$$F_c = PDR * A_{stem}$$

Where PDR is the driver pressure and A_{stem} is the area of the valve stem in which nitrogen gas is acting upon.

The force of gravity acting on the mass of the assembly is further given by the following.

$$F_{mass} = M_{act} * g$$

Where M is the total mass of the actuator assembly and g is the acceleration due to gravity.

Given the total force exerted on the piston, the acceleration, a_{act} , velocity, v_{act} , and position, x_{act} , can be extracted through rearranging and integration.

$$a_{act} = \frac{F_{tot}}{M_{act}}$$

$$v_{act} = \int a_{act} dt$$

$$x_{act} = \int v_{act} dt$$

Therefore, the volumetric flow in and out of the actuator volumes can be computed with the following.

$$\frac{dV_{act}}{dt} = A_{act} * v_{act}$$

As stated earlier, the model in the AEDC report is comprehensive and overwhelmingly too large to discuss and incorporate all parts within the timeframe of developing this model. Such work will be accomplished in future work. These topics have also been omitted from the discussion in this thesis.

System Delays and Slew Rates

Typically, two-stage servo valves in tandem with actuator blocks exhibit some finite slew rate that limits the rate of change in position or flow of said actuator. The model by Steinle and Sells should properly incorporate this delay and slew, however in modeling, there is still inherent delay and slew that is not accounted for. The following delays, slew rates, and offsets are exhibited in the tunnel 9 control valve system.

1. From start to end of the control law, there is assumed no delay as common OpAmps have a significantly large slew rate and analog electronics do not typically exhibit signal delaying unless other components induce such delays.
2. The servo amplifier controller card has a saturation set point in which the voltage may be limited if excessive, as discussed in prior sections.
3. From the servo amplifier card to servo valve, there will be an assumed voltage drop between the control system equipment room to the field servo valve. In reality, there is approximately 50-100 feet of cabling that connects the gas control valve electronic components to the control system. Historically, there have been voltage drops recorded as high as 1.2 VDC in rare, faulty instances. Under normal conditions, the voltage drop is recorded to an average of 0.05 VDC.
4. The response time of the Parker servo valves is listed as less than 15 milliseconds, to which it is assumed the full 15 milliseconds is the delay.
5. The slew rate of the servo valve is a function of the hydraulic pump, servo valve characteristics, and other factors.
6. The slew rate of the actuator is defined by the hydraulic pressure and the max flow rate of hydraulic fluid in and out of the actuator volumes, similar to the slew rate of the servo valve. Both the servo valve and actuator valve slew rates can be accounted for in the former section.
7. The resulting position recorded by the potentiometer experiences a voltage drop from the potentiometer to the data system. It is assumed to be an identical voltage drop to (1).

Each voltage offset or drop, slew rate, and response time delay can be modeled from the theoretical equations or system configuration and then input to the MATLAB model

through the respective modeling blocks. Alternatively, or to reinforce a hard-bound slew rate, the system can be modeled to have a specific slew rate determined by historical data, where the control valve position shows a relatively constant second derivative, indicating the entirety of the system cannot surpass not just a first order slope, but also a second order concavity/convexity. The first-order linear slew rate and the second order quadratic slew rate of the control valves can be determined and described in Appendix A.

Gas Dynamics Modeling of Tunnel 9

The gas dynamics modeling of Tunnel 9 can be approached in different manners where assumptions vary. For instance, the working fluid can be assumed as a perfect, ideal gas where the specific heats are constant, allowing for a simpler modeling process. On the other hand, the working fluid can be assumed as a real gas where the specific gas in question has certain properties that result in the variance of specific heats with change in temperature and density (or pressure). Typically, compressible gas models require real gas computations, however in some instances, ideal gas modeling will suffice. There are several relevant thermodynamic concepts that are critical to understand prior to modeling the gas dynamics of the wind tunnel. These include the equation of state for the gas medium, the method to computing gas properties given few input properties, the control volume analysis method, and other important concepts.

AEDC Standard Simulink Block Library

AEDC has a system modeling group of engineers which typically develop physical models through MATLAB Simulink that are used to implement control system architectures. Former attempts have been made to create a heat phase model of the tunnel such that tunnel operator training programs can be developed and the most critical operation phase of the tunnel is executed correctly by trained individuals. However, no model has been formally developed to simulate the gas dynamics model of the tunnel during the blow phase, that is with control

valve physics. At the start of the summer in 2023, Tunnel 9 employed the system modeling group to begin development of the heat phase and blow phase through gas dynamics. The system modeling group employs their standard Simulink block library which has various blocks for simpler and more efficient modeling. Most notably, the library includes an ideal gas control volume blocks and control orifice blocks by which these can be employed to create a preliminary model of the gas dynamics of the tunnel. The ideal gas control volume block library was utilized to model the gas dynamics portion of the blow phase model. The model equations will be discussed in the below sections.

Aside from gas dynamics modeling, the system modeling group is not equipped to model the analog control system and the control law to its true form. That is, the standard block library does not include blocks to explicitly model analog components and instead typical control laws are integrated via PID controllers. The AEDC standard block library will be utilized to model the gas dynamics though the control law, hydraulic servo valve, and actuator physics will be modeled through the other techniques described.

Nitrogen Equation of State

The equation of state refers to the governing, empirical equations that have been developed for calculating nitrogen gas and fluid properties. In particular, NIST Applied Chemicals and Materials Division and the NIST Standard Reference Data Program have developed an extensive empirical model of nitrogen properties, sourcing from hundreds of independent sources and thousands of experimental data and stretching as far back as the late 1800s. This model of Nitrogen properties and the equation of state are valid for nearly all of Tunnel 9 working temperatures and pressures. Further, NIST has ported the Nitrogen Equation of State model to a larger computer program known as NIST RefProps (Reference Properties),

of which there are several other fluids or gases with equation of state models. This will allow for integration of Nitrogen properties into the Tunnel 9 Blow Phase Simulink Model. [8]

Ideal Gas Finite Control Volume Approach

The fundamental analysis of the facility gas dynamics will be under the approach of finite control volume analysis through ideal gas convention. That is, the facility components, driver vessels, heater, etc., can more or less be modeled as independent, finite control volumes through which an ideal, Nitrogen gas flows in and out of the specified boundaries. The boundaries of which are the respective orifices at the inlet or exit of the control volume [9]. Prior to discussing the formulae and theory, there are several assumptions associated with the AEDC Simulink Library: (1) momentum is not conserved, (2) volumes are lumped, as one uniform volume (typically cylindrical), deeming the volume conditions to be bulk, or average across the volumes, and (3) the system is isentropic. The assumption of cylindricity of the control volume works to the favor of Tunnel 9 considering most, if not all pressure vessels and volumes are axisymmetric and cylindrical volumes. There are few cases where this is not the case, in which flow devices can be set in place to account for non-bulk desired conditions.

Control Volume Equations

To start the modeling, the conservation of mass in a system is assumed, where no mass enters or exits the overarching boundaries of the control volume(s) in the entire scope of the problem. In other words, from the driver vessels to the vacuum sphere, there is no mass lost in the process. The mathematic description of the mass in a system can be given as the following.

$$\frac{DM_{sys}}{Dt} = 0$$

Where the system mass is given by M_{sys} . This may also be given by the general expression.

$$M_{sys} = \int_{sys} \rho d\mathcal{V}$$

Where ρ is the gas density and \mathcal{V} is the volume. When viewing a control volume in a system, the time rate of change of mass entering or exiting the control volume, subscripted cv , can be further expressed as the following.

$$\frac{DM_{sys}}{Dt} = \frac{D}{Dt} \int_{sys} \rho d\mathcal{V} = \frac{\partial}{\partial t} \int_{cv} \rho d\mathcal{V} + \int_{cs} \rho \mathbf{V} \cdot \hat{\mathbf{n}} dA$$

Where $\hat{\mathbf{n}}$ is the normal direction of the control volume surface, subscripted cs , and dA is the differential area of the control volume surface. When assuming the entire system has no loss in mass, the continuity equation is derived, setting the right hand side to zero.

$$\frac{\partial}{\partial t} \int_{cv} \rho d\mathcal{V} + \int_{cs} \rho \mathbf{V} \cdot \hat{\mathbf{n}} dA = 0$$

Flow Device Mass and Energy Flow Rate Equations

Hinted earlier in the section, a *flow device* in regard to the Simulink model is simply a device that bridges two control volumes such that the mass flow rate or energy flow rate can be computed. The flow device can be a valve, orifice, piping elbow, etc. where in any case, the flow is altered from bulk, control volume flow. Without a flow device, the control volumes would simply assume bulk, average properties and no transportation is observed. From the mass continuity equation, mass flow rate within the control volume can be extracted and expressed as the common formula below.

$$\dot{m} = \rho VA$$

Where ρ is the density of the fluid, V is the velocity of the fluid, and A is the cross-sectional area of the geometry at the specified location. This formula satisfies for steady, one-dimensional flow through a duct where the specified point is a cross-section of infinitesimally small width. For a duct with an axially varying cross section (ie. nozzle), this equation can be

used to equate two different points in the control volume, given that the fluid is treated as an ideal gas. Both mass flow rate and velocity are unknown, which requires further calculations based on other system metrics (ie. pressure and temperature), orifice geometry, pressure differential, etc. Within the AEDC Simulink Block Library, this is accomplished by using intermediate state variables and conditions.

Intermediate State Computations

The “intermediate state” conditions are the conditions associated with the control volume to bridge the input and output variables. More specifically, variables are input to a control volume or flow device and fed into intermediate state equations to produce an intermediate state variable where then the new output equations then depend on the intermediate state variables. This is rather unconventional, but the AEDC Simulink Library has been designed around older coded equations from former system modelers, of which the intermediate state equations were utilized [1].

These intermediate state conditions can be determined by the formulae below, which are dependent on control volume values.

$$T_{int} = \frac{E}{M_{tot} C_v}$$

$$P_{int} = \frac{M_{tot} R T_{int}}{144 * \Psi}$$

Where E is the total energy, M_{tot} is the total mass, C_v is the specific heat with respect to constant volume, R is the gas constant for pure N_2 , and Ψ is the volume, all with respect to the upstream control volume. These intermediate state variables then influence the total and static temperature and pressure output from the control volume block.

$$T_0 = T_p - (\gamma - 1) * \left(\frac{(|\dot{m}_{avg}| R T_{int})^2}{2 C_p g} \right)$$

$$T_s = T_0 - \left(\frac{(|\dot{m}_{avg}| RT_{int})^2}{2C_p g} \right)$$

$$P_s = P_{int} \left(\frac{T_s}{T_{int}} \right)$$

$$P_0 = P_s \left(\frac{T_0}{T_s} \right)^{\frac{\gamma}{\gamma-1}}$$

Where T_0 and T_s are the total and static temperatures, and P_0 and P_s are the total and static pressures, respectively. In addition, γ is the ratio of specific heats, \dot{m}_{avg} is the average mass flow rate, C_p is the specific heat with respect to constant pressure, and g is the acceleration due to gravity. Once again, these are the properties with respect to the upstream control volume. The velocity of the fluid within the control volume is computed as the Mach number.

$$Mach = \sqrt{\left(\frac{(|\dot{m}_{avg}| * RT_{int})^2}{2C_p g} \right) * \frac{\left(\frac{2}{\gamma-1} \right)}{T_s}}$$

The Mach number can then be employed to determine the volumetric flow in and out of a control volume, a critical point that will be important in later discussion.

$$\dot{V}_{cv} = Mach * a * A_{cv}$$

Where A_{cv} is the control volume cross-sectional area, and a_{sound} is the local speed of sound, computed with the following.

$$a_{sound} = \sqrt{\frac{\gamma RT_0}{M_{gas}}}$$

Where M_{gas} is the molecular weight of pure N_2 .

Upon computing these variables, the actual implications of the flow device are then considered. In the AEDC standard block library, the mass flow rate is determined through an

alternative equation stemming from the geometry (area), pressure ratio, and gas characteristics (specific heats and gas constants).

$$\dot{m} = 144 * constant * C_f * A_{fd} * CSN * \frac{P_{up}}{\sqrt{T_{up}}}$$

Where the *constant* is an empirical constant for pure N_2 , A_{fd} is the restriction area of the flow device, or commonly termed the orifice or valve area, C_f is a flow coefficient used to better approximate field devices, and P_{up} & T_{up} are the upstream pressure and temperatures. The constant *CSN* is termed the ‘Chester-Smith Number’ within the AEDC Simulink Block library, and it stems from the regime of flow downstream of the flow device restriction area. The regime of flow is dependent on the pressure ratio of upstream and downstream volumes, PR . If the pressure ratio is above a threshold, termed the critical pressure ratio, PR_{crit} , then the flow may become sonic at the minimum area of the flow device, hence throttling the mass flow rate through the flow device. If the critical pressure ration is surpassed, further increase in pressure ratio will not result in more mass flow rates [9] [10]. In the AEDC Simulink Block Library, this effect is captured and the *CSN* is computed with the following equations.

$$PR_{crit} = \left(\frac{2}{\gamma + 1} \right)^{\frac{\gamma}{\gamma - 1}}$$

$$PR = \frac{P_{down}}{P_{up}}$$

$$constant = \gamma * \left(\frac{2}{\gamma + 1} \right)^{\frac{\gamma + 1}{2 * (\gamma - 1)}} * \sqrt{\frac{g}{R * \gamma}}$$

$$if \ PR > PR_{crit}, CSN = \frac{\left(PR^{\frac{2}{\gamma}} \right) - \left(PR^{\frac{\gamma + 1}{\gamma}} \right)}{\sqrt{\frac{\gamma - 1}{2} * \left(\frac{2}{\gamma + 1} \right)^{\frac{\gamma + 1}{\gamma - 1}}}}$$

$$if PR \leq PR_{crit}, CSN = 1$$

Calculating this mass flow rate for any given orifice or converging-diverging nozzle starts with these pressure ratios because the correct or proper flow regime is required. The flow restrictor can in fact have the smallest cross sectional area, however because the pressure differential across the flow restrictor is not significantly large, the flow restrictor will not meet the critical pressure ratio, thus the flow remains subsonic downstream of the flow restrictor. Under this assumption, the nozzle throat remains as the key component to determine critical pressure ratio and therefore the resulting downstream test cell conditions where supersonic and hypersonic flows exist.

The energy flow rate is dependent on the mass flow rate computation and is simply given by the following.

$$mh = C_p \dot{m} T_{up}$$

While these equations allow for simply modeling, there are limitations to what scope of modeling can be done. In some cases, an excessive number of flow devices can cause semi-divergent oscillations in pressures.

Implication to Tunnel 9 Modeling

For modeling the facility, the following control volumes exist; driver vessels (3), heater vessel, diaphragm area and nozzle inlet, vacuum sphere. The following flow devices exist to bridge the four control volumes; main gas control valves, heater exit flow restrictor, and nozzle throat. Each volume and orifice may vary between Mach and/or Reynolds number changes.

The challenge with the control volume approach is the vertical heater vessel being partitioned between cold gas and hot gas, effectively creating two control volumes that change in volume throughout the run. As stated earlier, the standard block library assumes a bulk or average temperature of each control volume, which renders the heater vessel invalid due to the

separation of hot and cold gas. A potential idealized solution to this is to create separate control volume blocks in the model that dynamically change such that the geometrical volume of the control volume changes with time. The blocks are not connected in the same manner as for example the driver vessels to the heater vessel lower portion through conventional flow device such as an orifice or valve, rather only by the change in volume due to mass flow and the change in pressure. The pressures must remain the same between both volumes while the temperatures must be separate due to the nature of the heater vessel and driving action. This scope of modeling requires an extension to the former mentioned control volume equations, and now the control volume surfaces have a relative velocity given by the equation below.

$$\frac{DM_{sys}}{Dt} = \frac{\partial}{\partial t} \int_{cv} \rho dV + \int_{cs} \rho \mathbf{W} \cdot \hat{\mathbf{n}} dA = 0$$

Where \mathbf{W} is the relative velocity of the control volume fluid with respect to the observer. In this case, the ‘observer’ is the fixed reference frame. The time rate of change variable, the first integral term, is not zero in this case because the respective hot and cold gas volumes change in density with change in volume and pressure, both of which then are variable over time. The assumption is that the cold gas control volume only changes in volume by movement of the upper control surface upward, and conversely, the hot gas control volume changes in volume by movement of the lower control surface upward. The two control surfaces of each volume are assumed to be intersecting, creating an infinitesimal temperature gradient between volumes and no reduction in the summed volumes. However, the boundary surfaces have no relative position since each control volume is assumed as a bulk volume, therefore there is no boundary or surface to account for. Simply the volume of each control volume shall be controlled. This can be employed with the volumetric flow in and out of each control volume such that the following is true.

$$V_{tot} = V_{cold} + V_{hot} = constant$$

Recall earlier the volumetric flow rate in and out of the control volume was derived, given by the following.

$$\dot{V}_{cv} = v_{cv} * A_{cv}$$

The integration of the volumetric flow rate with initial value of the initial volume will generate the dynamically changing volume of each heater control volume. The two control volumes change inversely to one another, and the two pressures, P_{up} and P_{low} , shall remain identical throughout the process. The temperatures, T_{up} and T_{low} , will vary only due to expansion and contraction of the volumes and the respective mass flow in and out.

$$P_{low} = P_{up}$$

$$T_{low} \neq T_{up}$$

This solution is explored and preliminarily modeled, however the results, as later shown, are not as refined and do not necessarily model the facility as accurately as the single heater control volume model.

Chapter 4: Design Expert and Historical Data Analysis

Tabular Input

The import data function in design expert simply takes the user clipboard, and as such the template table below is imported directly into design expert. Each condition at Tunnel 9 has a variety of factors that need to be specified in Design Expert such that the analysis is properly evaluated. For example, the Mach number is simply a categoric factor, meaning the actual discrete value has no true value and is simply a nominal value used to categorize the nozzle selected in the tunnel. There are several run conditions at each Mach number listed in the introduction, though the table is shortened for brevity. Exact values of the respective condition parameters are omitted, though the response parameter of the heater pressure slope has been non-dimensionalized by the run heater pressure for presentation purposes.

| Nominal Mach | Nominal Re # | Run PHE | PHE Gain | Command Ramp Voltage (CR) | Initial Opening Voltage (IO) | Servo Amplifier (SA) Gain | Heater Pressure Transducer Sensitivity (SHE) | Normalized dPHE/dt Calculated | Normalized dPHE/dt Observed | Control Valve Start Time |
|-----------------|-----------------|------------|-------------|------------------------------------|---------------------------------------|---------------------------------|--|-------------------------------------|-----------------------------------|-----------------------------------|
| (-) | (10e6/ft) | (psi) | (-) | (vdc) | (vdc) | (-) | (mvdc/vdc/psig) | (% PHE/sec) | (% PHE/sec) | (ms) |
| 7 | 1.9 | ### | ### | ### | ### | ### | ### | 9.01 | 11.35 | #### |
| 7 | 4 | ### | ### | ### | ### | ### | ### | 29.32 | 6.26 | #### |
| ⋮ | ⋮ | ⋮ | ⋮ | ⋮ | ⋮ | ⋮ | ⋮ | ⋮ | ⋮ | ⋮ |
| 18 | 1.1 | ### | ### | ### | ### | ### | ### | 7.03 | 7.24 | #### |
| 18 | 1.56 | ### | ### | ### | ### | ### | ### | 3.34 | 3.67 | #### |

Table 2: Nominal Run Conditions Control Law Parameters and Observed Metrics

Every single condition is different for obvious reasons, however there are similarities in certain conditions that can provide insight as to what the effects of the control system inputs are. Prior to completing the analysis, the theoretical, normalized heater pressure slope is calculated for each condition from the equation discussed in the earlier control law section. This is then plotted with the observed, normalized heater pressure slope, shown below. The color of each point represents the order within the dataset, not relevant to the study.

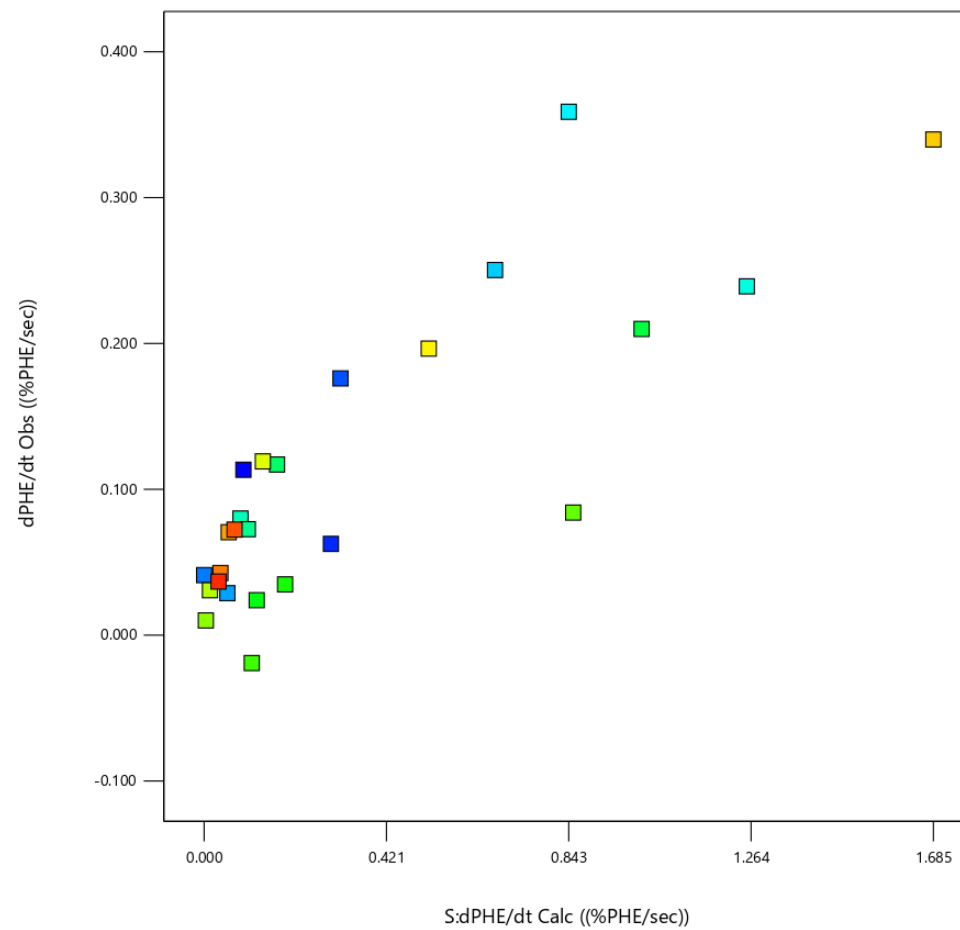


Figure 14: Theoretical vs Observed Normalized Heater Pressure Slope

The correlational coefficient $R^2 = 0.7797$ which means the calculated and observed heater pressure slopes are somewhat correlated, but not ideal in terms of predicting the expected heater pressure slope. This especially becomes problematic when trying to model the heater pressure with respect to the historical run condition.

With the factor table above, a simple 2 factor interaction (2FI) analysis is executed, however the terms considered in the analysis are trimmed only to terms that influence a change in behavior in the control law. That is, the control law gains, voltages, transducer metrics, and other control law parameters are only considered in the analysis. The 2FI model is the regression by which each factor or pair of factors (ie. PHE gain multiplied by command ramp) may have a constant coefficient that produces a weighted correlation. Depending on the factor magnitude and the coefficient magnitude, each factor-coefficient pair has an associated f-value and p-value, both indicating which factors provide a greater influence on the response factor, which in this case is the observed, normalized heater pressure slope.

ANOVA for Reduced 2FI model

The analysis of variance (ANOVA) provides these factor-coefficient P-values to show which factors have the greatest significance.

| Source | Sum of Squares | df | Mean Square | F-value | p-value | |
|-------------------|----------------|----|-------------|---------|---------|-------------|
| Model | 0.2484 | 21 | 0.0118 | 370.35 | 0.0002 | significant |
| L-PHE Gain | 0.0000 | 1 | 0.0000 | 0.4044 | 0.5700 | |
| M-IO | 0.0002 | 1 | 0.0002 | 6.43 | 0.0850 | |
| N-CR | 0.0003 | 1 | 0.0003 | 8.72 | 0.0599 | |
| O-SA Gain | 0.0018 | 1 | 0.0018 | 55.75 | 0.0050 | |
| Q-SHE | 0.0052 | 1 | 0.0052 | 162.82 | 0.0010 | |
| LM | 0.0001 | 1 | 0.0001 | 2.28 | 0.2283 | |
| LN | 0.0002 | 1 | 0.0002 | 4.74 | 0.1177 | |
| LO | 0.0052 | 1 | 0.0052 | 162.76 | 0.0010 | |
| LQ | 0.0043 | 1 | 0.0043 | 133.36 | 0.0014 | |
| MN | 0.0014 | 1 | 0.0014 | 43.55 | 0.0071 | |
| MQ | 0.0053 | 1 | 0.0053 | 165.20 | 0.0010 | |
| NO | 0.0017 | 1 | 0.0017 | 53.23 | 0.0053 | |

| | | | | | | |
|-----------------------|--------|----|--------|--------|--------|--|
| NQ | 0.0046 | 1 | 0.0046 | 144.21 | 0.0012 | |
| OQ | 0.0024 | 1 | 0.0024 | 76.00 | 0.0032 | |
| N² | 0.0020 | 1 | 0.0020 | 63.14 | 0.0042 | |
| O² | 0.0019 | 1 | 0.0019 | 60.16 | 0.0045 | |
| Q² | 0.0051 | 1 | 0.0051 | 160.19 | 0.0011 | |
| LNO | 0.0023 | 1 | 0.0023 | 72.69 | 0.0034 | |
| LNQ | 0.0045 | 1 | 0.0045 | 139.88 | 0.0013 | |
| LN² | 0.0023 | 1 | 0.0023 | 70.56 | 0.0035 | |
| N²O | 0.0014 | 1 | 0.0014 | 42.72 | 0.0073 | |
| Residual | 0.0001 | 3 | 0.0000 | | | |
| Cor Total | 0.2484 | 24 | | | | |

Table 3 shows that several terms have significant p-values (highlighted grey rows), thus indicating the greatest factor in observing change in the heater pressure slope. Lastly, the overall model is considered significant by DesignExpert, as indicated by the second row which generates the cumulative or average values and gives a statement to signify the status of significance.

| Source | Sum Squares | of df | Mean Square | F-value | p-value | |
|-----------------------|----------------|----------|-------------|---------|---------|-------------|
| Model | 0.2484 | 21 | 0.0118 | 370.35 | 0.0002 | significant |
| L-PHE | 0.0000 | 1 | 0.0000 | 0.4044 | 0.5700 | |
| Gain | | | | | | |
| M-IO | 0.0002 | 1 | 0.0002 | 6.43 | 0.0850 | |
| N-CR | 0.0003 | 1 | 0.0003 | 8.72 | 0.0599 | |
| O-SA Gain | 0.0018 | 1 | 0.0018 | 55.75 | 0.0050 | |
| Q-SHE | 0.0052 | 1 | 0.0052 | 162.82 | 0.0010 | |
| LM | 0.0001 | 1 | 0.0001 | 2.28 | 0.2283 | |
| LN | 0.0002 | 1 | 0.0002 | 4.74 | 0.1177 | |
| LO | 0.0052 | 1 | 0.0052 | 162.76 | 0.0010 | |
| LQ | 0.0043 | 1 | 0.0043 | 133.36 | 0.0014 | |
| MN | 0.0014 | 1 | 0.0014 | 43.55 | 0.0071 | |
| MQ | 0.0053 | 1 | 0.0053 | 165.20 | 0.0010 | |
| NO | 0.0017 | 1 | 0.0017 | 53.23 | 0.0053 | |
| NQ | 0.0046 | 1 | 0.0046 | 144.21 | 0.0012 | |
| OQ | 0.0024 | 1 | 0.0024 | 76.00 | 0.0032 | |
| N² | 0.0020 | 1 | 0.0020 | 63.14 | 0.0042 | |
| O² | 0.0019 | 1 | 0.0019 | 60.16 | 0.0045 | |
| Q² | 0.0051 | 1 | 0.0051 | 160.19 | 0.0011 | |
| LNO | 0.0023 | 1 | 0.0023 | 72.69 | 0.0034 | |
| LNQ | 0.0045 | 1 | 0.0045 | 139.88 | 0.0013 | |
| LN² | 0.0023 | 1 | 0.0023 | 70.56 | 0.0035 | |
| N²O | 0.0014 | 1 | 0.0014 | 42.72 | 0.0073 | |
| Residual | 0.0001 | 3 | 0.0000 | | | |
| Cor Total | 0.2484 | 24 | | | | |

Table 3: ANOVA Table for 2FI Model

The 2FI ANOVA was computed using the actual coding equation, which is the algorithm based on the actual term factors rather than normalized factors. The coding equation in terms of actual factors can be used to make predictions about the response for the levels of each factor. In the above

| Source | Sum of Squares | df | Mean Square | F-value | p-value | |
|-----------------------|----------------|----|-------------|---------|---------|-------------|
| Model | 0.2484 | 21 | 0.0118 | 370.35 | 0.0002 | significant |
| L-PHE Gain | 0.0000 | 1 | 0.0000 | 0.4044 | 0.5700 | |
| M-IO | 0.0002 | 1 | 0.0002 | 6.43 | 0.0850 | |
| N-CR | 0.0003 | 1 | 0.0003 | 8.72 | 0.0599 | |
| O-SA Gain | 0.0018 | 1 | 0.0018 | 55.75 | 0.0050 | |
| Q-SHE | 0.0052 | 1 | 0.0052 | 162.82 | 0.0010 | |
| LM | 0.0001 | 1 | 0.0001 | 2.28 | 0.2283 | |
| LN | 0.0002 | 1 | 0.0002 | 4.74 | 0.1177 | |
| LO | 0.0052 | 1 | 0.0052 | 162.76 | 0.0010 | |
| LQ | 0.0043 | 1 | 0.0043 | 133.36 | 0.0014 | |
| MN | 0.0014 | 1 | 0.0014 | 43.55 | 0.0071 | |
| MQ | 0.0053 | 1 | 0.0053 | 165.20 | 0.0010 | |
| NO | 0.0017 | 1 | 0.0017 | 53.23 | 0.0053 | |
| NQ | 0.0046 | 1 | 0.0046 | 144.21 | 0.0012 | |
| OQ | 0.0024 | 1 | 0.0024 | 76.00 | 0.0032 | |
| N² | 0.0020 | 1 | 0.0020 | 63.14 | 0.0042 | |
| O² | 0.0019 | 1 | 0.0019 | 60.16 | 0.0045 | |
| Q² | 0.0051 | 1 | 0.0051 | 160.19 | 0.0011 | |
| LNO | 0.0023 | 1 | 0.0023 | 72.69 | 0.0034 | |
| LNQ | 0.0045 | 1 | 0.0045 | 139.88 | 0.0013 | |
| LN² | 0.0023 | 1 | 0.0023 | 70.56 | 0.0035 | |
| N²O | 0.0014 | 1 | 0.0014 | 42.72 | 0.0073 | |
| Residual | 0.0001 | 3 | 0.0000 | | | |
| Cor Total | 0.2484 | 24 | | | | |

Table 3, the F-value is a term to quantify the significance of the model overall, where the value of 370.35 implies the model is significant, with less than a 0.02% chance that an F-value this large could occur due to noise, where this percentage is the p-value. The coefficients generated from the ANOVA results can be output and displayed in

| Factor | Coefficient Estimate | df | Standard Error | 95% Low | CI | 95% High | CI | VIF |
|------------------|----------------------|----|----------------|---------|----|----------|----|-----|
| Intercept | 0.9345 | 1 | 0.3630 | -0.2206 | | 2.09 | | |

| | | | | | | |
|-----------------------|------------|---|-----------|------------|------------|-----------|
| L-PHE Gain | 0.0019 | 1 | 0.0030 | -0.0076 | 0.0114 | 1371.06 |
| M-IO | 9.34 | 1 | 3.69 | -2.39 | 21.07 | 13778.04 |
| N-CR | -12.29 | 1 | 4.16 | -25.53 | 0.9574 | 31814.83 |
| O-SA Gain | 0.0421 | 1 | 0.0056 | 0.0242 | 0.0600 | 1.350E+05 |
| Q-SHE | -87104.43 | 1 | 6826.24 | -1.088E+05 | -65380.29 | 3.553E+05 |
| LM | 0.0371 | 1 | 0.0246 | -0.0411 | 0.1154 | 697.65 |
| LN | 0.4355 | 1 | 0.2000 | -0.2011 | 1.07 | 1.009E+05 |
| LO | 0.0004 | 1 | 0.0000 | 0.0003 | 0.0005 | 1741.60 |
| LQ | -608.62 | 1 | 52.70 | -776.34 | -440.89 | 10778.10 |
| MN | -178.93 | 1 | 27.12 | -265.22 | -92.64 | 10017.52 |
| MQ | -5.226E+05 | 1 | 40657.34 | -6.520E+05 | -3.932E+05 | 3019.82 |
| NO | -0.2281 | 1 | 0.0313 | -0.3276 | -0.1286 | 26042.39 |
| NQ | 7.157E+05 | 1 | 59597.29 | 5.260E+05 | 9.054E+05 | 28968.45 |
| OQ | -3.71 | 1 | 0.4255 | -5.06 | -2.36 | 34.28 |
| N² | 351.06 | 1 | 44.18 | 210.47 | 491.66 | 87649.73 |
| O² | -0.0001 | 1 | 0.0000 | -0.0002 | -0.0001 | 1.325E+05 |
| Q² | 2.811E+08 | 1 | 2.221E+07 | 2.104E+08 | 3.517E+08 | 4.482E+05 |
| LNO | 0.0124 | 1 | 0.0015 | 0.0078 | 0.0170 | 37921.88 |
| LNQ | -34804.77 | 1 | 2942.80 | -44170.08 | -25439.46 | 62016.75 |
| LN² | -8.24 | 1 | 0.9813 | -11.37 | -5.12 | 56469.45 |
| N²O | -0.6713 | 1 | 0.1027 | -0.9981 | -0.3444 | 4493.80 |

Table 4. These coefficients can be utilized to create a full equation that can reproduce the regression line of best fit based on each input factor. In addition to the coefficients, each column thereafter; the standard error, confidence intervals (CI), and variance inflation factor (VIF) for each term are given. The standard error represents the standard deviation of the coefficient, while the confidence intervals represent the 95% plus or minus bound on the coefficient such that 95% of trials fall within the bound. The variance inflation factor (VIF) measures how much the variance around the coefficient estimate is inflated by the lack of orthogonality in the design.

| Factor | Coefficient Estimate | df | Standard Error | 95% Low | CI High | VIF |
|-----------------------|----------------------|----|----------------|------------|------------|-----------|
| Intercept | 0.9345 | 1 | 0.3630 | -0.2206 | 2.09 | |
| L-PHE Gain | 0.0019 | 1 | 0.0030 | -0.0076 | 0.0114 | 1371.06 |
| M-IO | 9.34 | 1 | 3.69 | -2.39 | 21.07 | 13778.04 |
| N-CR | -12.29 | 1 | 4.16 | -25.53 | 0.9574 | 31814.83 |
| O-SA Gain | 0.0421 | 1 | 0.0056 | 0.0242 | 0.0600 | 1.350E+05 |
| Q-SHE | -87104.43 | 1 | 6826.24 | -1.088E+05 | -65380.29 | 3.553E+05 |
| LM | 0.0371 | 1 | 0.0246 | -0.0411 | 0.1154 | 697.65 |
| LN | 0.4355 | 1 | 0.2000 | -0.2011 | 1.07 | 1.009E+05 |
| LO | 0.0004 | 1 | 0.0000 | 0.0003 | 0.0005 | 1741.60 |
| LQ | -608.62 | 1 | 52.70 | -776.34 | -440.89 | 10778.10 |
| MN | -178.93 | 1 | 27.12 | -265.22 | -92.64 | 10017.52 |
| MQ | -5.226E+05 | 1 | 40657.34 | -6.520E+05 | -3.932E+05 | 3019.82 |
| NO | -0.2281 | 1 | 0.0313 | -0.3276 | -0.1286 | 26042.39 |
| NQ | 7.157E+05 | 1 | 59597.29 | 5.260E+05 | 9.054E+05 | 28968.45 |
| OQ | -3.71 | 1 | 0.4255 | -5.06 | -2.36 | 34.28 |
| N² | 351.06 | 1 | 44.18 | 210.47 | 491.66 | 87649.73 |
| O² | -0.0001 | 1 | 0.0000 | -0.0002 | -0.0001 | 1.325E+05 |
| Q² | 2.811E+08 | 1 | 2.221E+07 | 2.104E+08 | 3.517E+08 | 4.482E+05 |
| LNO | 0.0124 | 1 | 0.0015 | 0.0078 | 0.0170 | 37921.88 |
| LNQ | -34804.77 | 1 | 2942.80 | -44170.08 | -25439.46 | 62016.75 |
| LN² | -8.24 | 1 | 0.9813 | -11.37 | -5.12 | 56469.45 |
| N²O | -0.6713 | 1 | 0.1027 | -0.9981 | -0.3444 | 4493.80 |

Table 4: Coefficients in Terms of Actual Factors

To give some form of visual agreeance in the coded equation, there are various measures that are output by DesignExpert, such as the normalized residuals, Cox-Box lambda value, and others that are shown below, accompanied by a brief discussion of the plot.

In Figure 15, the normalized residuals are the normalized *disagreements* between the predicted value and the coded equation value, where the x axis is the externalized studentized residuals and the y axis is the normal probability. The normal probability plot indicates whether the residuals follow a normal distribution, in which case the points will follow a straight line. Moderate scatter across the data is expected and patterns such as an “S-shaped” curve in the data would indicate that a transformation of the response may provide a better analysis.

In Figure 16, The Cox-Box plot is a plot that aids in the decision for model transformation, similar to the normal residual plot above. Some analyses benefit from transformations such as square root or logarithmic transformation. A recommended transformation is indicated in DesignExpert based on the lambda value in relation to the minimum point of the curve generated by the scaled natural log of the sum of squares of the residuals. It is desirable to have a lambda value of 1 as close to the minimum point of the curve. In this case, the model is not recommended for any transformation as the lambda value is very close to a value of 1, verifying no transformation has indeed generated the best results.

In Figure 17, this plot simply shows the actual response parameter vs the predicted response parameter based on the coded equation. In accordance with the high correlation value, $R^2 = 0.9976$, the prediction and actual heater pressure slope are very closely aligned in linear fashion.

In Figure 18, this plot shows the externally studentized residuals with respect to the predicted response parameter, along with upper and lower bounds. The upper and lower bounds

are significantly beyond the domain of the actual residuals, indicating the predicted coded equation is a good fit to the data.

In Figure 19, this plot shows the same residuals, but across each run number, where Mach 7 starts at run number one, and Mach 18 ends at run number 25.

Lastly, DesignExpert also generates a table to show these residuals and other metrics aside from the coded equation coefficients, shown in Table 5.

dPHE/dt Obs

Color points by value of
dPHE/dt Obs:

-0.0191 0.3588

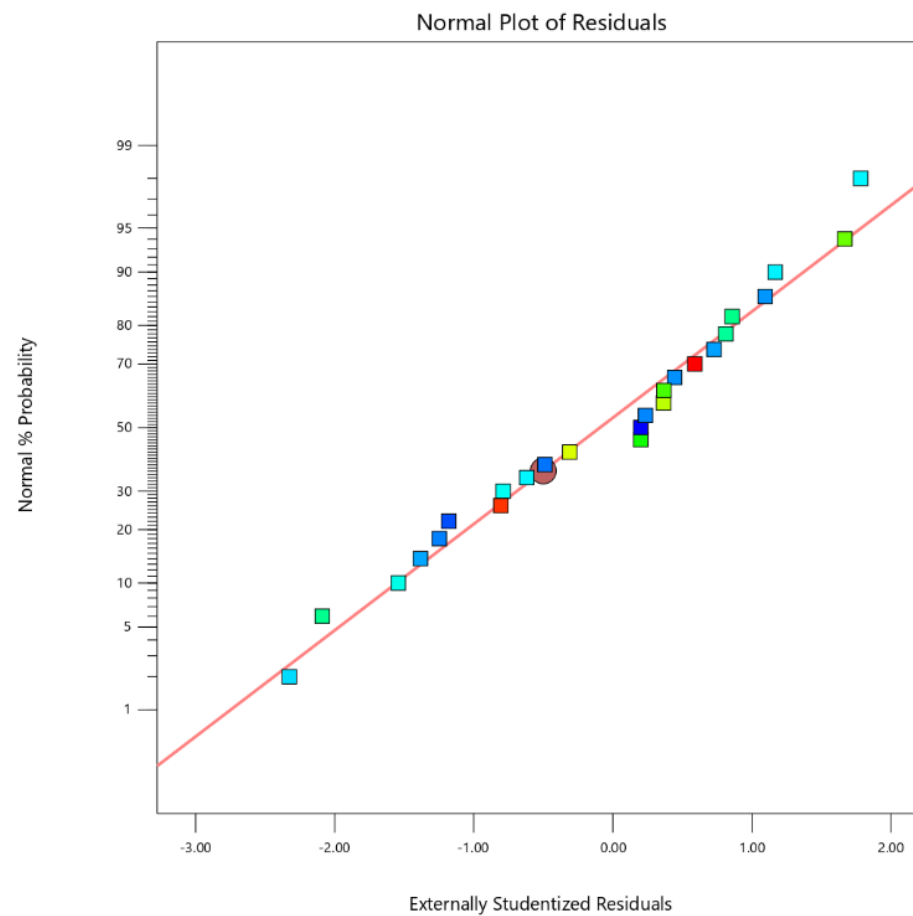


Figure 15: Normal Plot of Residuals

dPHE/dt Obs

Current transform:

None

Current Lambda = 1

Best Lambda = 0.94

CI for Lambda: (0.53, 1.32)

Recommended transform:

None

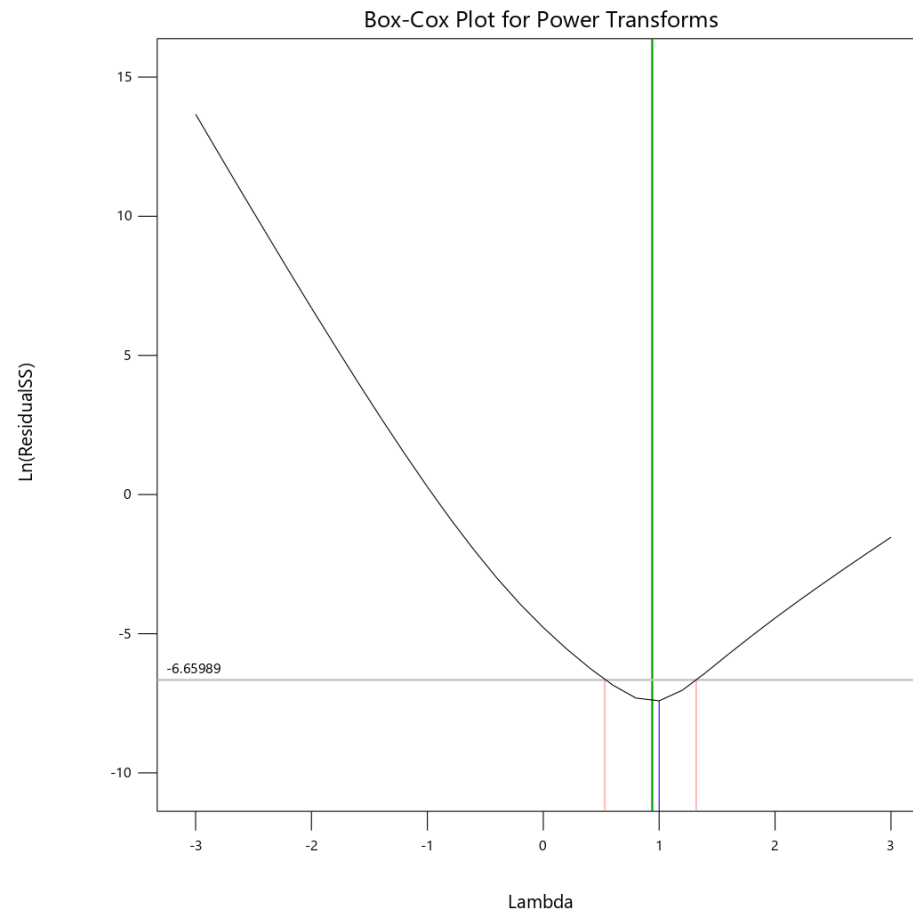


Figure 16: Box-Cox Plot for Power Transforms

dPHE/dt Obs

Color points by value of
dPHE/dt Obs:

-0.0191  0.3588

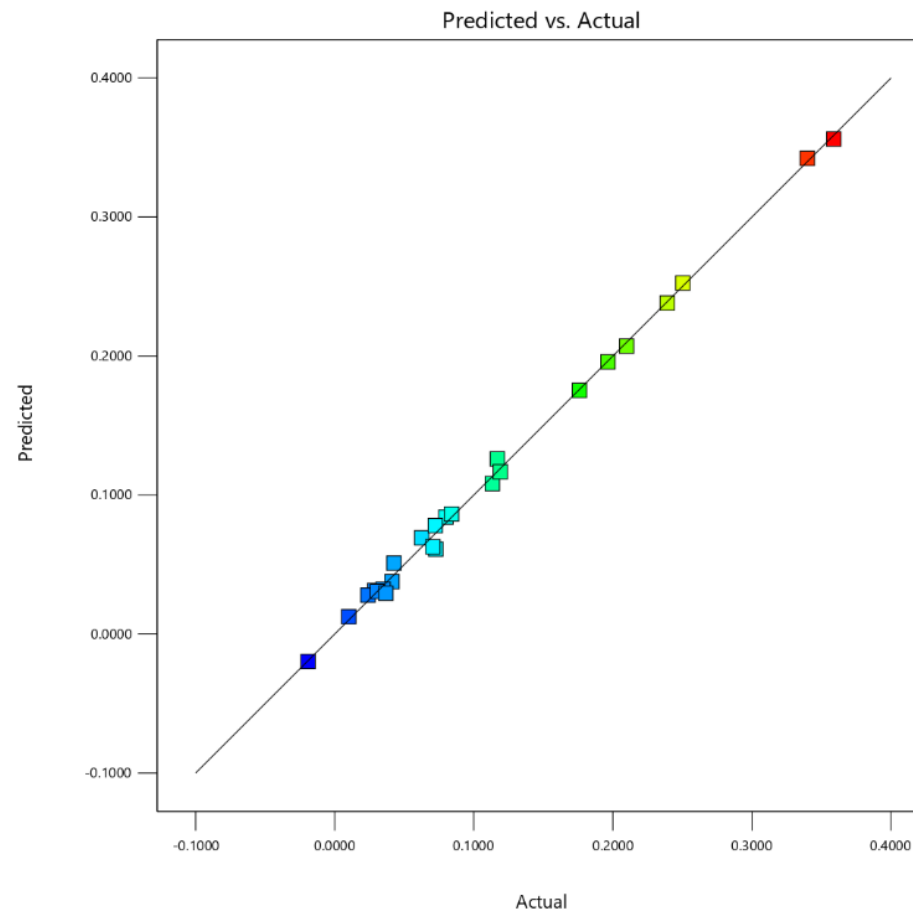


Figure 17: ANOVA 2FI Coded Equation Predicted vs Actual Response

dPHE/dt Obs

Color points by value of
dPHE/dt Obs:

-0.0191  0.3588

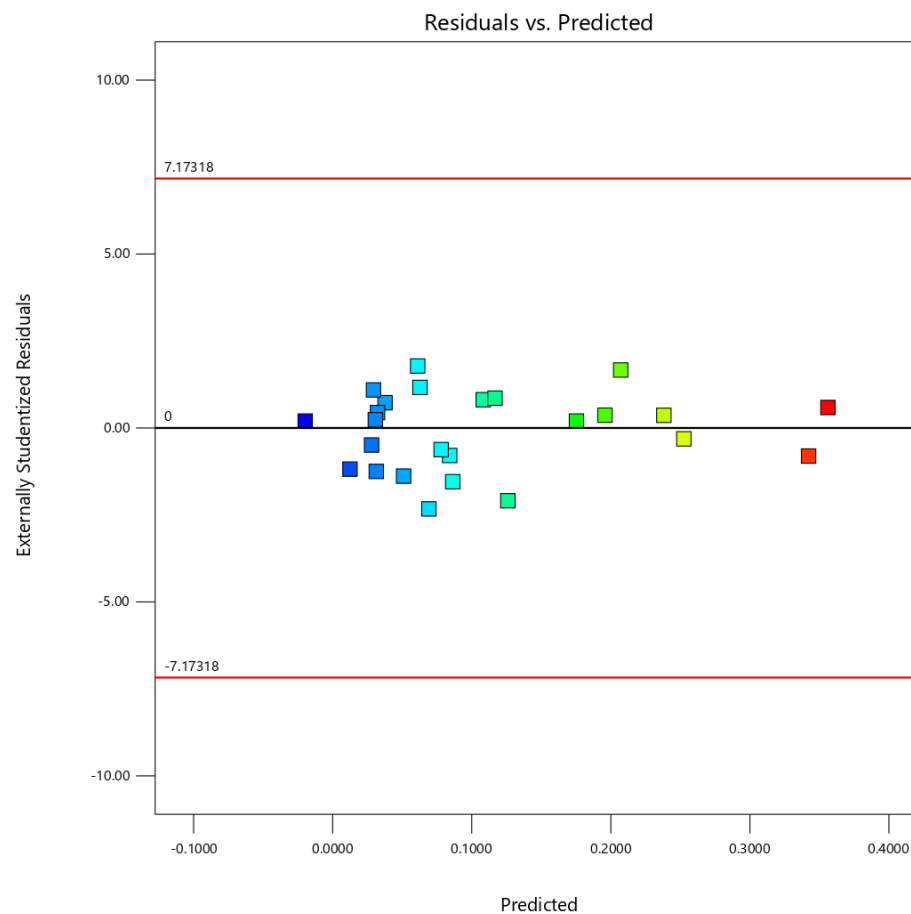


Figure 18: ANOVA 2FI Coded Equation Residual vs Prediction

dPHE/dt Obs

Color points by value of
dPHE/dt Obs:

-0.0191  0.3588

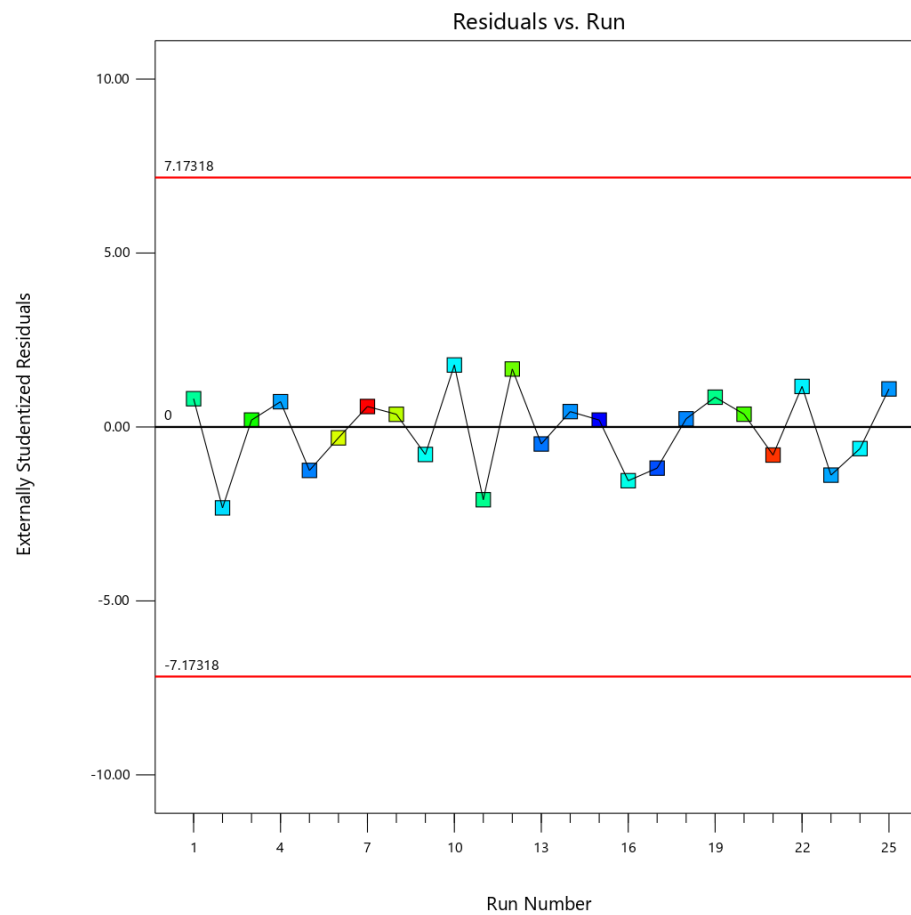


Figure 19: ANOVA 2FI Coded Equation Residual vs Run

| Run Order | Actual Value | Predicted Value | Residual | Leverage | Internally Studentized Residuals | Externally Studentized Residuals | Cook's Distance | Influence on Fitted Value DFFITS | Standard Order |
|-----------|--------------|-----------------|------------|----------------------|----------------------------------|----------------------------------|------------------------|----------------------------------|----------------|
| 1 | 0.1135 | 0.1133 | 0.0002 | 0.956 | 0.152 | 0.124 | 0.023 | 0.578 | 1 |
| 2 | 0.0626 | 0.0631 | -0.0005 | 0.798 | -0.196 | -0.161 | 0.007 | -0.319 | 2 |
| 3 | 0.1761 | 0.1758 | 0.0003 | 0.934 | 0.221 | 0.182 | 0.032 | 0.687 | 3 |
| 4 | 0.0412 | 0.0412 | 0.0001 | 0.886 | 0.037 | 0.031 | 0.000 | 0.085 | 4 |
| 5 | 0.0288 | 0.0288 | 3.447E-06 | 1.000 | | | | | 5 |
| 6 | 0.2504 | 0.2504 | -0.0001 | 1.000 | -0.571 | -0.494 | 46.388 ⁽¹⁾ | -27.627 ⁽¹⁾ | 6 |
| 7 | 0.3588 | 0.3588 | 0.0000 | 1.000 ⁽²⁾ | | | | | 7 |
| 8 | 0.2392 | 0.2391 | 0.0001 | 0.998 | 0.571 | 0.494 | 8.842 ⁽¹⁾ | 12.062 ⁽¹⁾ | 8 |
| 9 | 0.0800 | 0.0848 | -0.0048 | 0.724 | -1.627 | -3.870 | 0.315 | -6.264 ⁽¹⁾ | 9 |
| 10 | 0.0727 | 0.0656 | 0.0071 | 0.403 | 1.629 | 3.920 | 0.082 | 3.223 ⁽¹⁾ | 10 |
| 11 | 0.1170 | 0.1164 | 0.0006 | 0.969 | 0.576 | 0.498 | 0.469 | 2.782 | 11 |
| 12 | 0.2100 | 0.2100 | -0.0000 | 1.000 | -0.571 | -0.494 | 215.813 ⁽¹⁾ | -59.588 ⁽¹⁾ | 12 |
| 13 | 0.0240 | 0.0272 | -0.0032 | 0.882 | -1.653 | -4.522 | 0.928 | -12.361 ⁽¹⁾ | 13 |
| 14 | 0.0348 | 0.0339 | 0.0009 | 0.991 | 1.691 | 6.379 | 13.595 ⁽¹⁾ | 65.235 ⁽¹⁾ | 14 |
| 15 | -0.0191 | -0.0191 | 0.0000 | 1.000 ⁽²⁾ | | | | | 15 |
| 16 | 0.0841 | 0.0842 | -0.0001 | 0.999 | -0.571 | -0.494 | 27.918 ⁽¹⁾ | -21.432 ⁽¹⁾ | 16 |
| 17 | 0.0101 | 0.0101 | -2.826E-06 | 1.000 | | | | | 17 |
| 18 | 0.0308 | 0.0299 | 0.0009 | 0.725 | 0.298 | 0.247 | 0.011 | 0.401 | 18 |
| 19 | 0.1192 | 0.1189 | 0.0002 | 0.983 | 0.299 | 0.248 | 0.232 | 1.873 | 19 |
| 20 | 0.1965 | 0.1965 | 3.106E-07 | 1.000 | 0.032 | 0.026 | 15.342 ⁽¹⁾ | 15.003 ⁽¹⁾ | 20 |
| 21 | 0.3399 | 0.3400 | -0.0000 | 1.000 | -0.571 | -0.494 | 68.128 ⁽¹⁾ | -33.480 ⁽¹⁾ | 21 |
| 22 | 0.0706 | 0.0706 | 4.726E-06 | 1.000 | 0.216 | 0.178 | 142.235 ⁽¹⁾ | 46.034 ⁽¹⁾ | 22 |
| 23 | 0.0427 | 0.0438 | -0.0011 | 0.569 | -0.297 | -0.246 | 0.005 | -0.283 | 23 |
| 24 | 0.0724 | 0.0747 | -0.0023 | 0.491 | -0.561 | -0.484 | 0.014 | -0.475 | 24 |
| 25 | 0.0368 | 0.0351 | 0.0017 | 0.693 | 0.536 | 0.460 | 0.029 | 0.691 | 25 |

⁽¹⁾ Exceeds limits., ⁽²⁾ Case(s) with leverage of 1.0000: Student Residuals, Cooks Distance & External Stud. Residuals undefined.

Table 5: ANOVA 2FI Coded Equation Summary Report

Implementation to Simulink

The coded equation can be input into the model as an alternative control law. That is, the control law Simulink block can be altered such that the coded equation for the heater pressure slope is used as the target heater pressure slope. The question becomes; *where exactly does this equation fit into the model?* To answer this, one must decide on how much of the analog control system physics shall be maintained, if any. Is this equation simply used to back out a new command ramp voltage, or does this equation get put into a PID controller entirely? The physics of the analog control system allows for more reflective, one-to-one modeling; however, the historical data indicates a loose agreement between the control law schematics and the theoretical control law. The decision is to maintain the analog control system physics. As such, the coded equation is used to compute the predicted heater pressure slope, a simple plug and compute equation with the given parameters of the run condition. Then the predicted heater pressure slope can be put into the control law equation and solved for the respective command ramp voltage. Or in other words, back out the effective command ramp voltage based on the predicted heater pressure slope. Finally, this command ramp voltage is substituted for the nominal command ramp voltage that is specified in standard condition run sheets. This method should in theory provide the most accurate results as the model will still reflect the schematical equation derived earlier.

Chapter 5: Simulink Model Architecture and Plots

Model Construction and Top View

The model is designed as a simple controller-plant design where the control system is separated from the facility. The overall process can be described by two loops: an inner loop and an outer loop. The inner loop is driven by the control law voltage (CL), valve position command (CMD) and the valve position feedback (FB). This loop satisfies that the valve position feedback matches the valve position command, which is handled by the servo amplifier card. The valve position feedback is located on the valve actuator within the plant block. The outer loop is driven by the heater pressure (PHE) and the nozzle supply pressure (PNO), where the output is the control law voltage that feeds to the servo amplifier card inner loop. This diagram can be seen below in Figure 20.

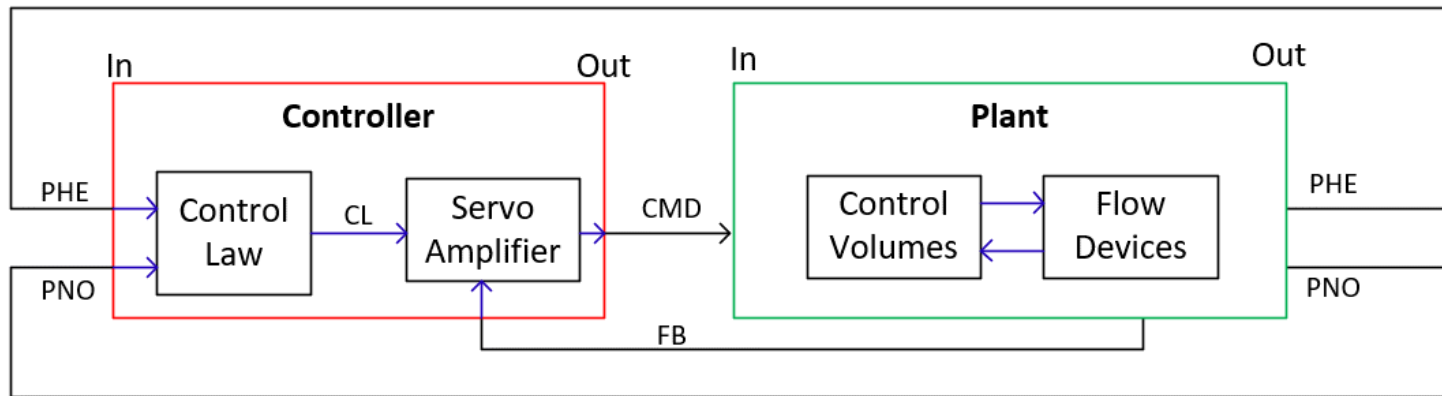


Figure 20: Simulink Model Top Level

In further modeling schematics, blocks transmit and receive signal through ‘mux’ and ‘demux’ blocks. The signal lines can be vectors of containing a variety of quantities, achieved by combining model quantities into a vector through a ‘mux’ block. In contrast, the signal can also be broken back down into each individual signal or into a subset vector by using the ‘demux’ block. For example, the control volume blocks input and output a vector signal of upwards of 20 values, where some are the respective values discussed above, and some are spare ports used to give more flexibility in modeling.

Controller

Control Law

The control law, shown in Figure 21, is created to be similar in schematic to the actual electrical schematics of the control law, where each function coupled with a gain operator represents an OpAmp. There are simple Boolean logic blocks coupled with delays to sequence the control law sequencer functions, as previously discussed.

Servo Amplifier Controller Card

The servo amplifier controller card is modeled as the intermediate block between control law voltage and the respective valve commanding signal, shown in Figure 22.

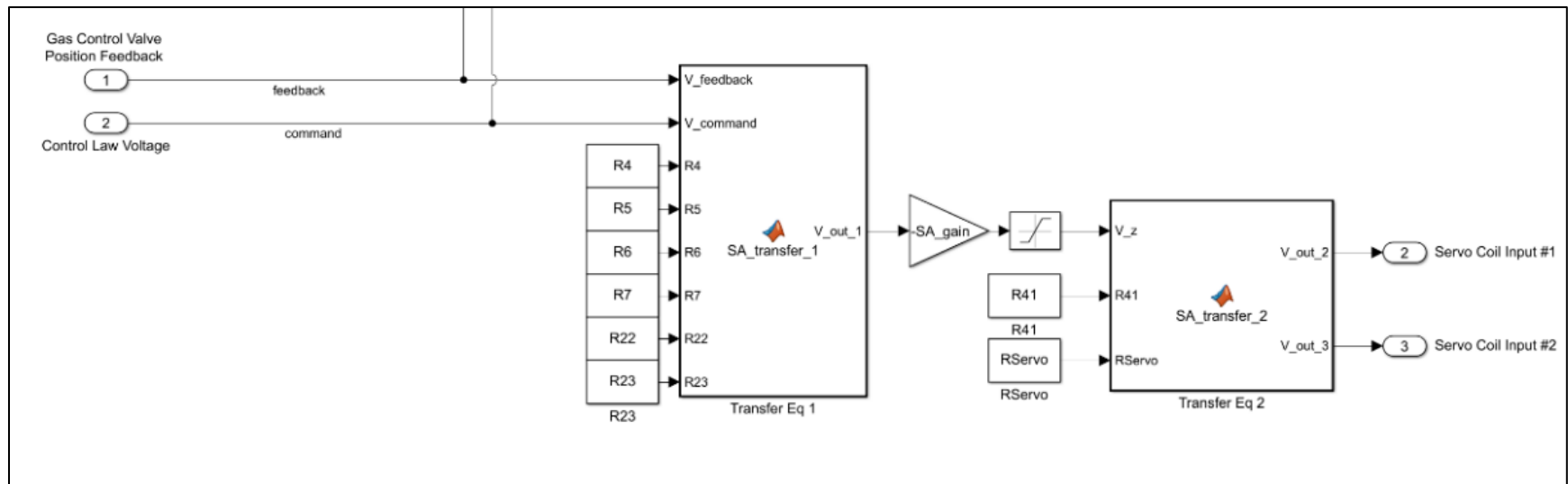


Figure 22: Servo Amplifier Controller Card Transfer Function Block Architecture

Plant

Within the plant, there are the four discussed control volumes: driver vessels, heater vessel, diaphragm area, and vacuum sphere. Coupled with each control volume is a flow device, either a valve or an orifice. The driver vessels output gas properties to the main gas control valves, which has a further substructure of servo valve and actuator physics. From the main gas control valves, the heater vessel follows. The heater vessel is both modeled as a singular volume and alternatively split into two separate volumes, branching the model into two configurations. The model results depict a stronger agreement to historical data by the singular volume heater. The ultimate reason for this was time; the model takes significantly more time to correctly implement such that the two-volume heater is accurate in modeling. With relevancy to the control law, the heater temperature is not relevant, and former attempts to attain a working two-volume heater model resulted in significantly different heater pressure plots; a value that in fact does have significant relevancy to the control law. For this reason, further development of the two-volume heater vessel is preliminarily discussed, however the discussion of model architecture and results will majority be constricted to the single volume heater model. After the heater vessel is the flow restrictor orifice block, the downstream diaphragm area and nozzle inlet control volume, nozzle throat orifice block, and lastly the vacuum sphere. The plant model architecture is shown in Figure 23 and Figure 24.

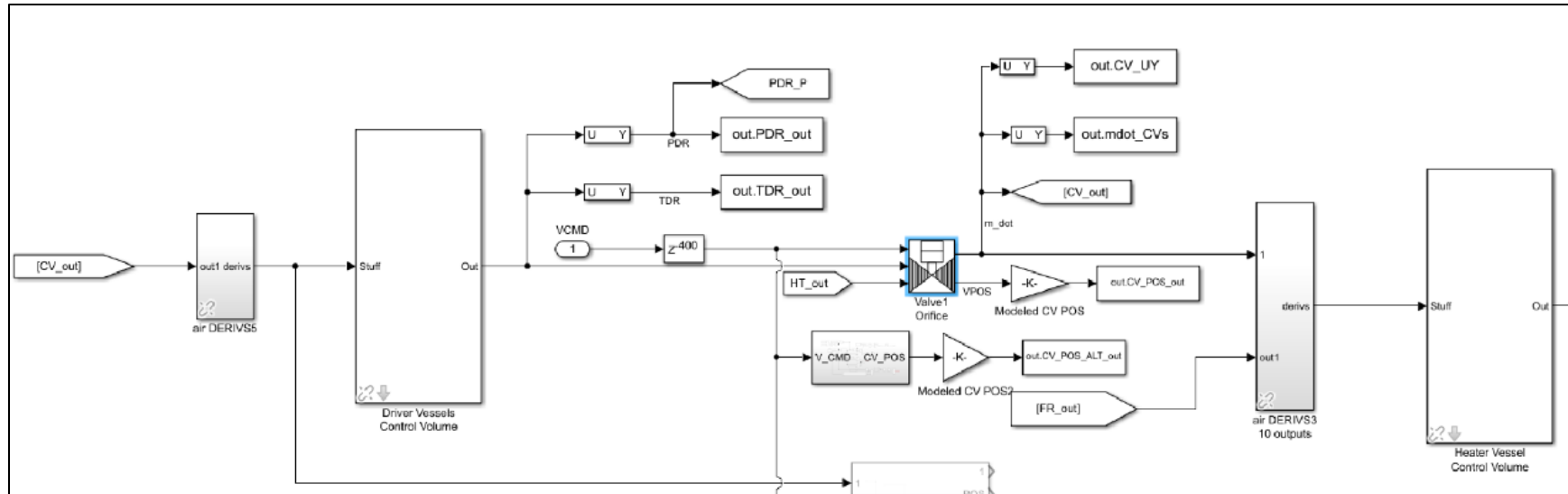


Figure 23: Single-Heater Model Plant – Block Architecture (Drivers to Heater)

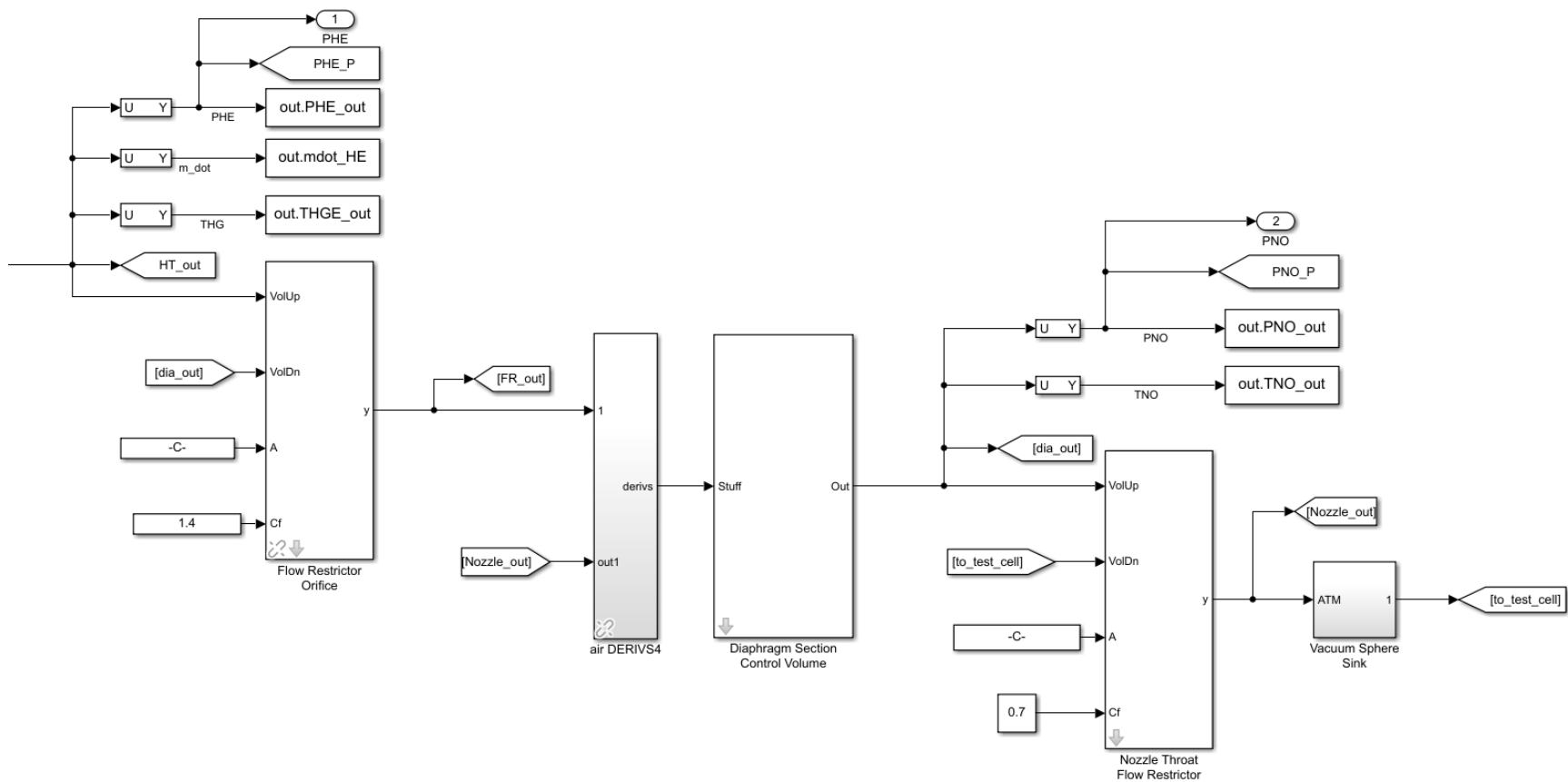


Figure 24: Single-Heater Model Plant – Block Architecture (FR to Vacuum)

There are probes and tags that are labeled accordingly. These probes are output to the workspace for plotting and model comparison to historical data. For example, the tag “out.PHE_out” is the variable assignment where the modeled heater pressure is output to the MATLAB workspace for plotting. It is noted that the typical ‘scoping’ method in Simulink is not used, and rather exporting to workspace and plotting the variables through traditional plotting is employed, allowing for higher degree of graphical settings.

Gas Control Valves

The gas control valves are modeled as a singular unit rather than multiplying for the identical number of control valves used in the tunnel. This is due to stability issues that result from excessive flow devices connecting control volumes. If there are too many flow devices, the mass flow rate calculation tends to oscillate and occasionally diverge, hence a singular, lumped flow device proves to solve the issue. In theory, the control valves should produce identical performance, further solidifying the effects that the flow device can lump valve areas. Within the valve block, the block diagram in Figure 25 is the high level architecture where further sub models are incorporated. The intermediate block performs the actuator physics portion where the incompressible fluid mechanics and kinematic force balance equations are computed. The resulting actuator position is transported to a valve area through a normalized vector and a respective gain to convert the valve area to correct units and scaled per the number of control valves used. This valve area is based on geometric calculations of the valve stem and seat. The downstream block is the typical flow device block that takes in the up and downstream control volumes, the upstream area calculation, and the flow coefficient. It should be noted the flow coefficient is 2.8 as this provided desirable results in the driver pressure and the heater pressure, later shown.

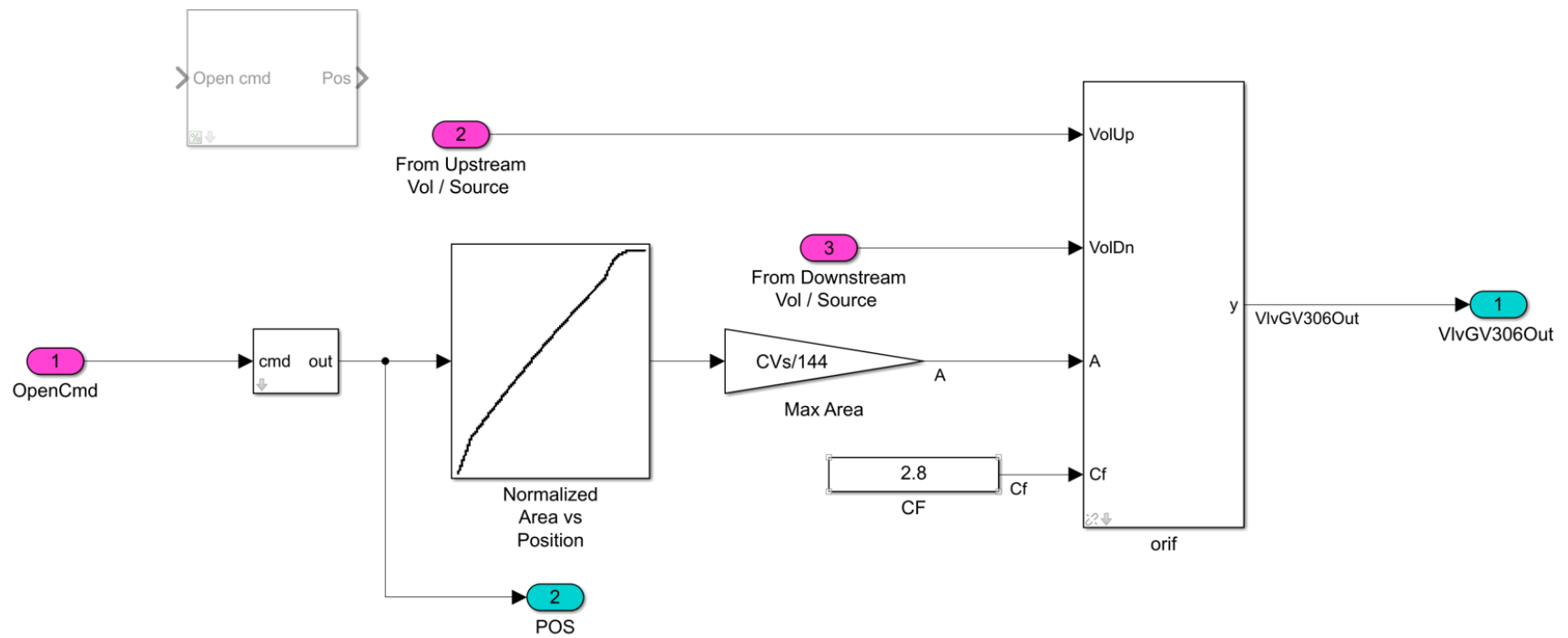


Figure 25: Control Valve Upper Level Block Architecture

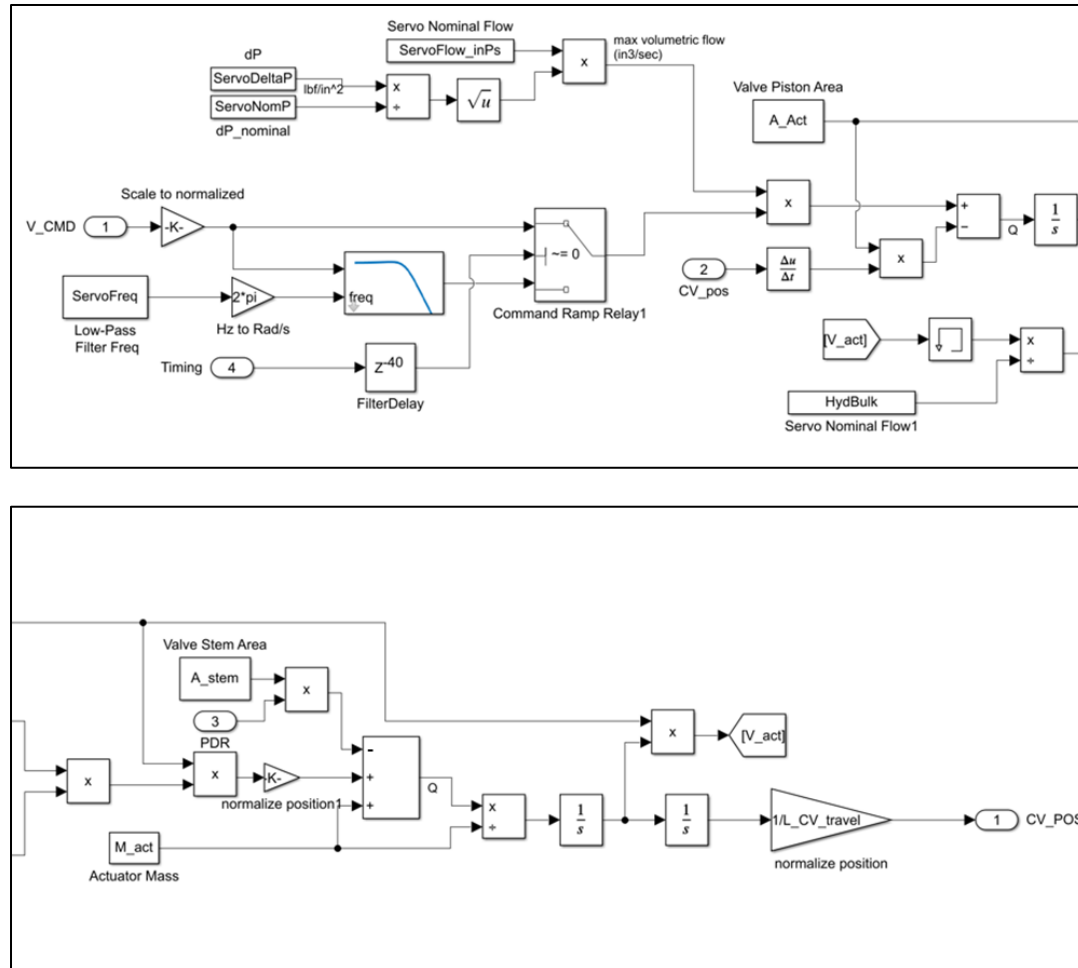


Figure 26: Servo Valve and Actuator Block Architecture

Heater vessel

As discussed, the heater vessel is a singular control volume, similar to the driver vessel control volumes. The block takes in the incoming muxed signal and outputs a muxed signal, both composed of the properties discussed in above sections (ie. mass flow rate, total and static pressures, etc.). In future work, the solution slated for design and mockup is a heater vessel where the model effectively is split into two separate systems, where the lower portion of the heater vessel is essentially zero volume, and the upper heater portion is the full heater volume with the bulk properties of hot gas. When the run starts, the lower control volume receives the flow from the gas control valves and the mass flow rate drives the effective volume of the heater vessel lower portion. On the opposing side, the heater vessel upper portion then expels its hot gas as a function of the flow restrictor and nozzle throat properties and its mass flow rate drives the volume down. What is important to note is that the mass flow rates may not be equal on either input or output from the heater vessel, which is expected, yet the pressures of each portion will be equal.

Flow Restrictor, Diaphragm Area, Nozzle Throat, and Vacuum

The downstream side of the facility is more rudimentary and simplistic in regard to the AEDC Simulink library, each control volume has an input of flow from the given source or flow device and an output that is directed to the downstream flow device or source. The flow devices have an input of the upstream and downstream control volumes as well as the flow area and the coefficient of flow, which allows for more custom modeling of facility components such as that of the flow restrictor. The sink of the nozzle throat is simply a terminal that ...

Results

The resulting plots show the comparison of the simulated metric versus the historical data metric (ie. Driver Pressure, PDR). For most cases, the y-axis units are omitted or normalized, and the x-axis is time, while the legend displays the respective series. The controller and plant work in parallel and react to one another, thus the controller and plant have to be considered equal in model validity. More broadly, the plant may appear to agree with historical plots, but in fact it could not be accurate if the controller is not accurate. The following plots show the output-to-workspace variables.

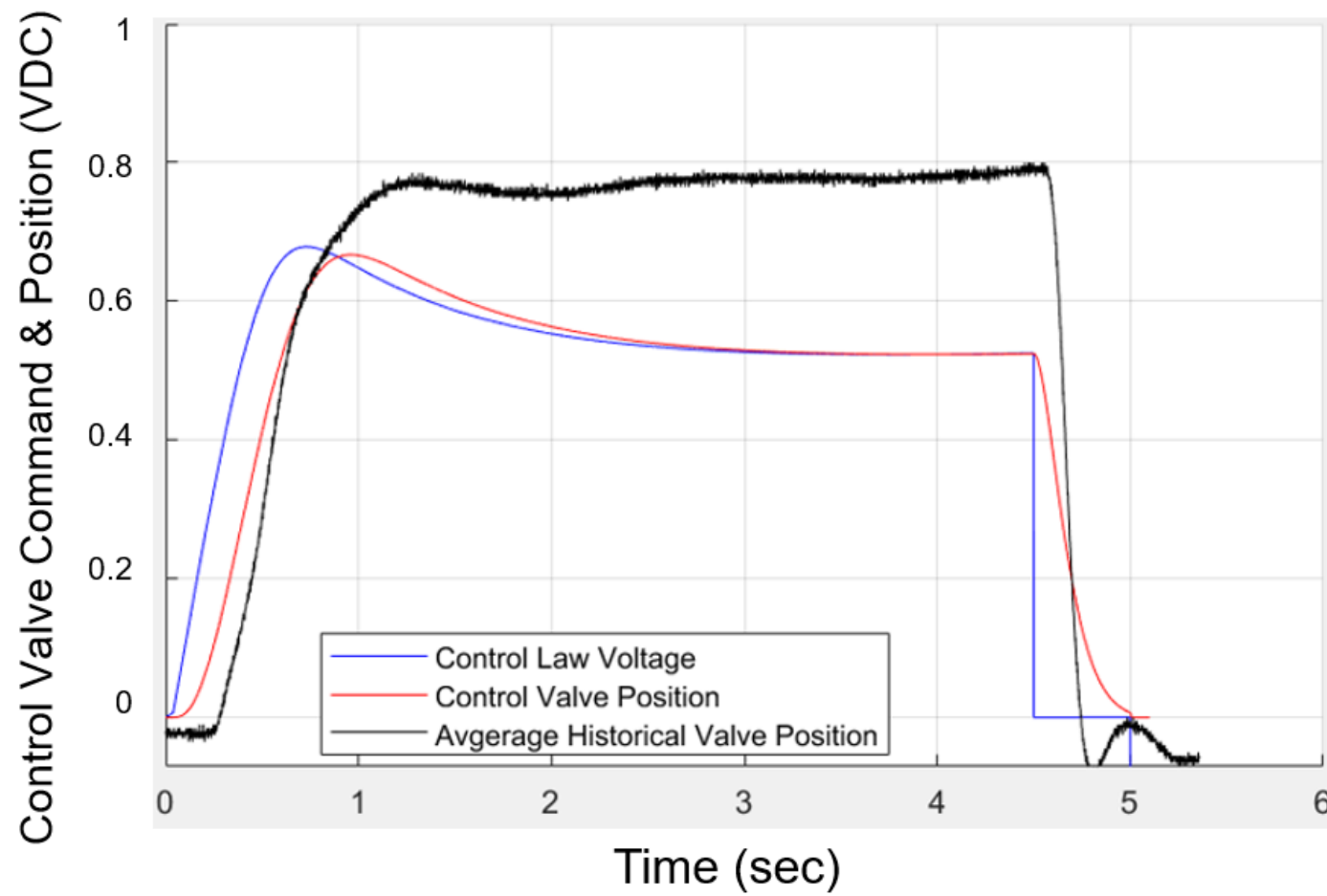


Figure 27: Control Valve Position vs Time

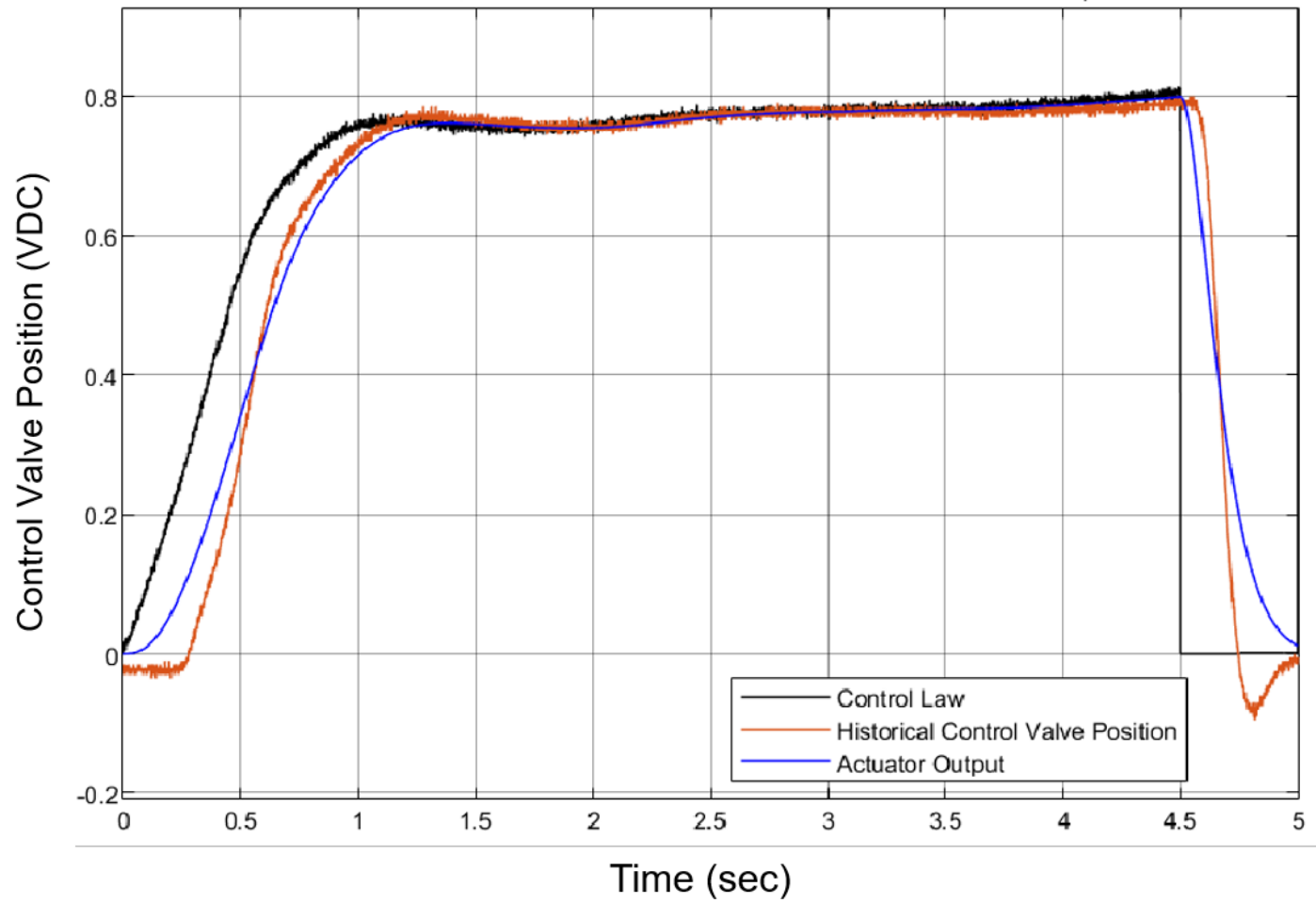


Figure 28: Stand Alone Control Law Voltage vs Time

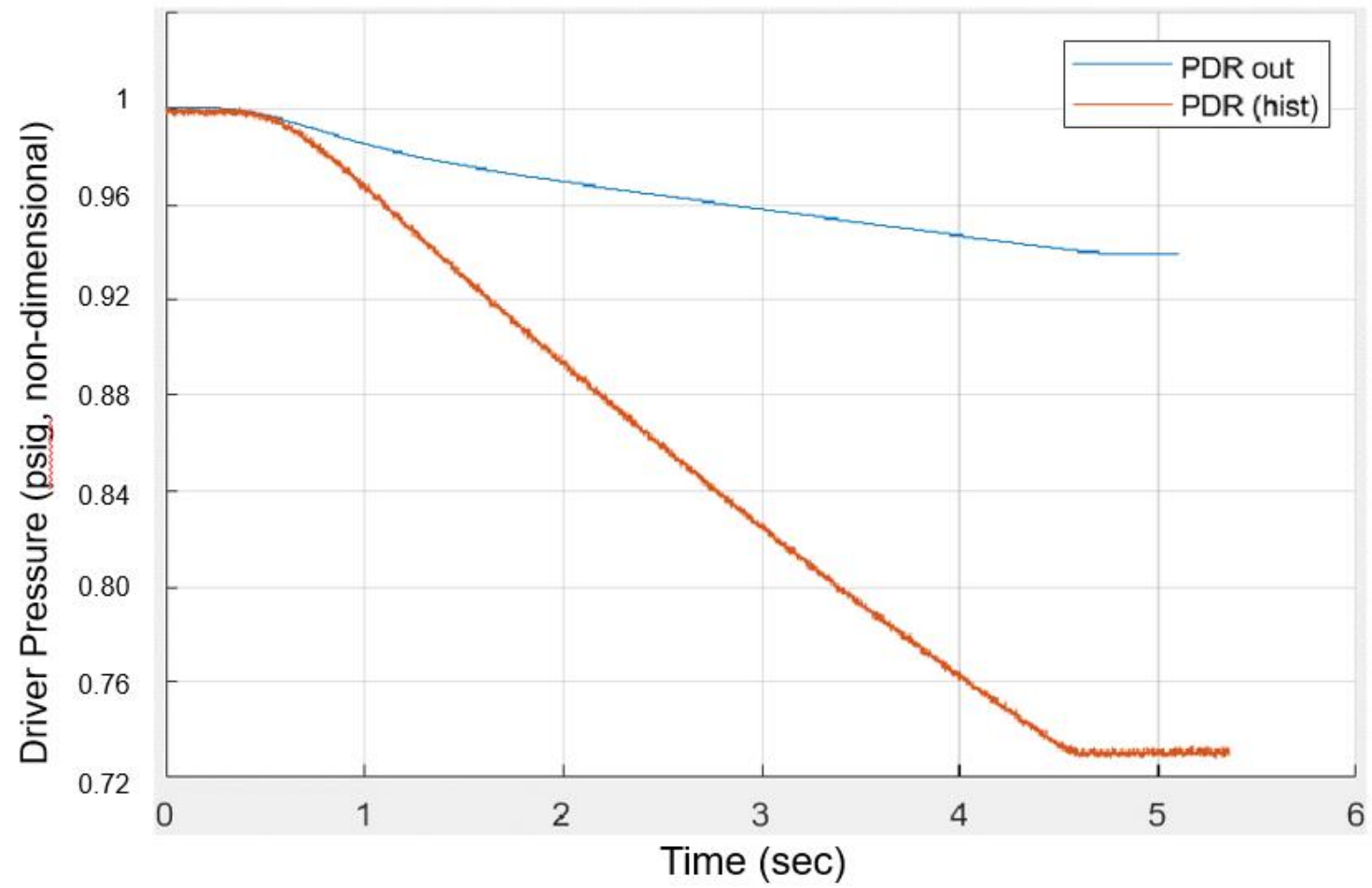


Figure 29: Driver Pressure vs Time

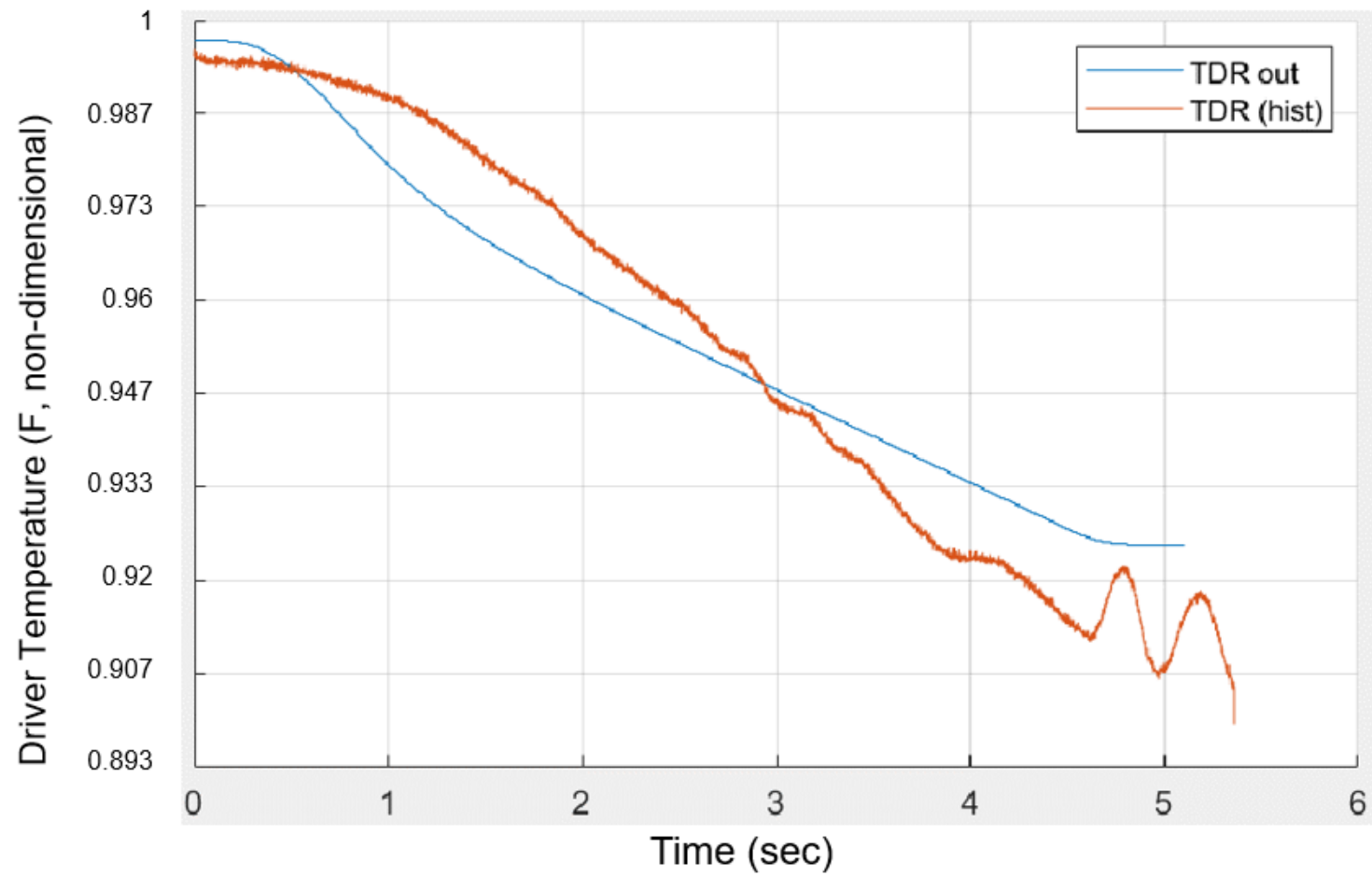


Figure 30: Driver Temperature vs Time

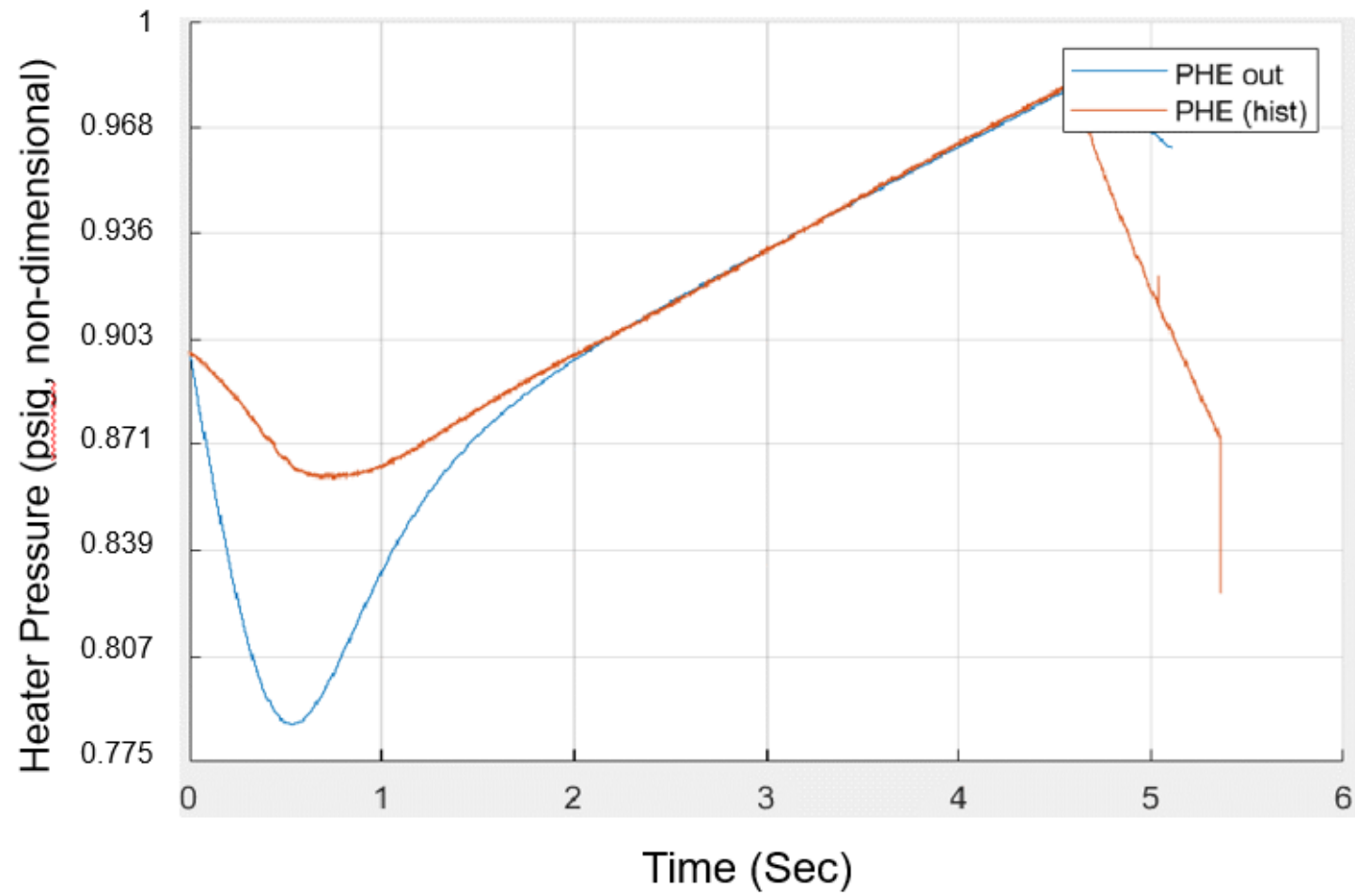


Figure 31: Heater Pressure (Single-Volume Heater Model) vs Time

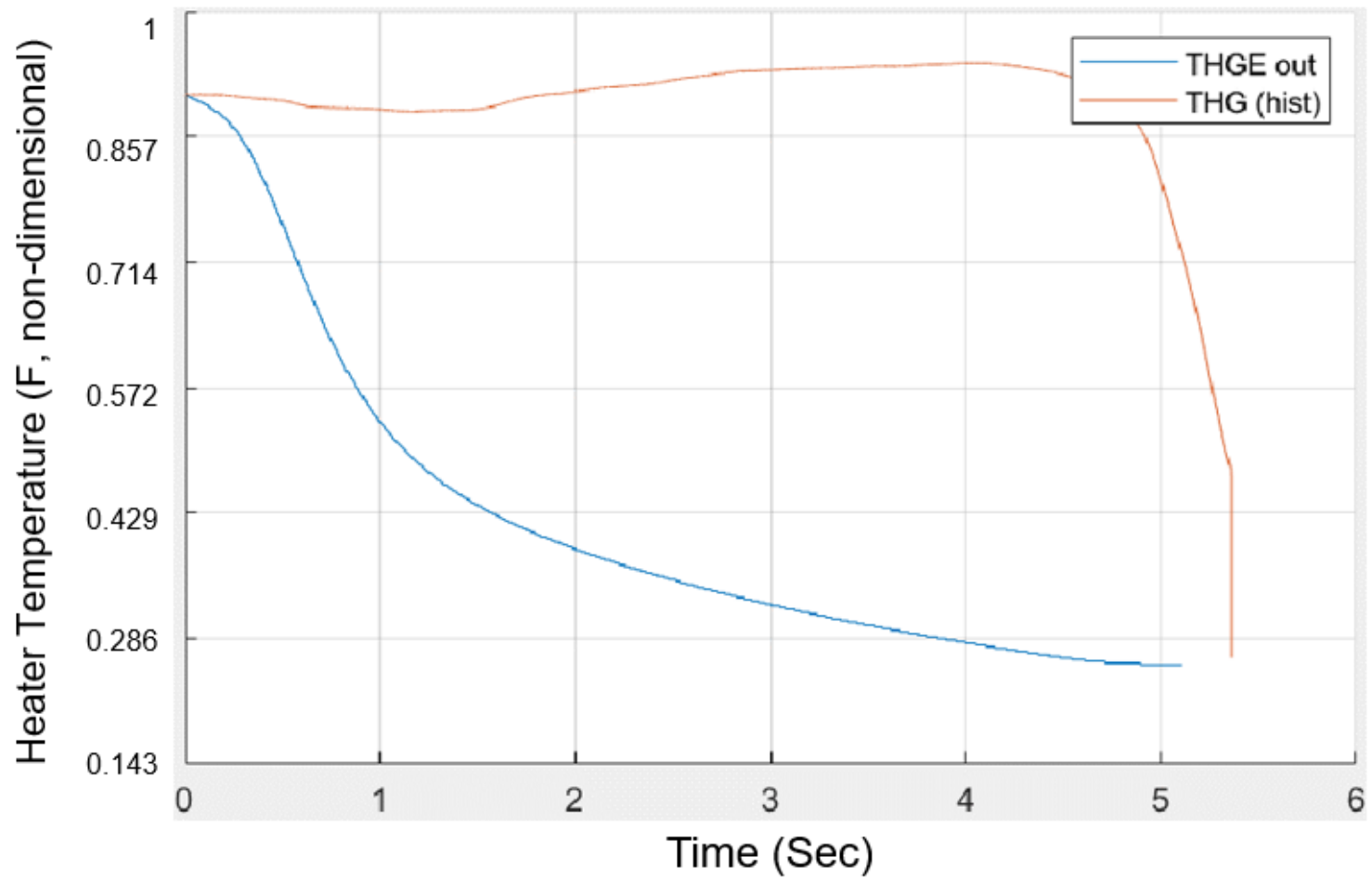


Figure 32: Heater Temperature (Single-Volume Heater Model) vs Time

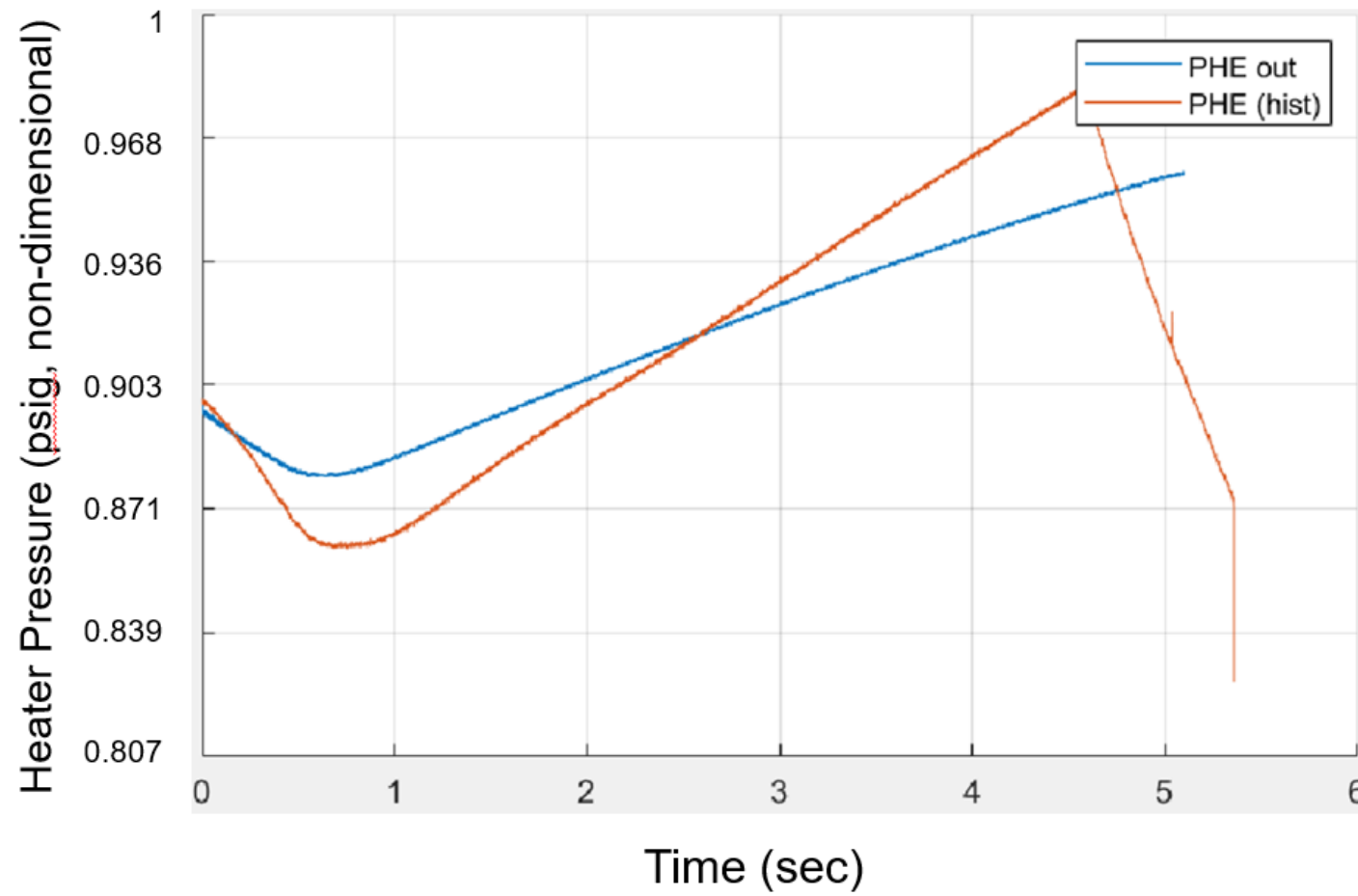


Figure 33: Heater Exit Pressure (Two-Volume Heater Model) vs Time

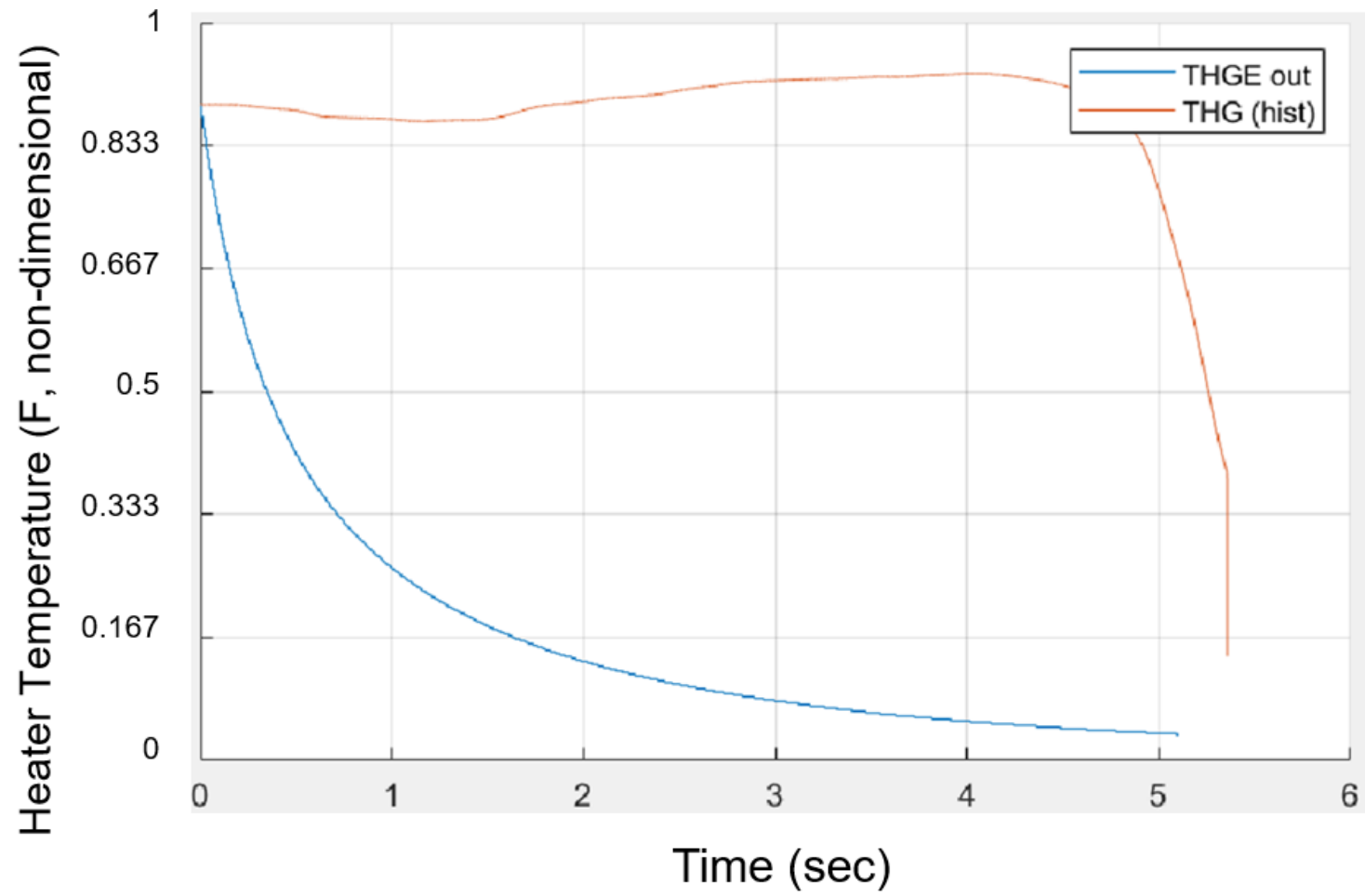


Figure 34: Heater Exit Temperature (Two-Volume Heater Model) vs Time

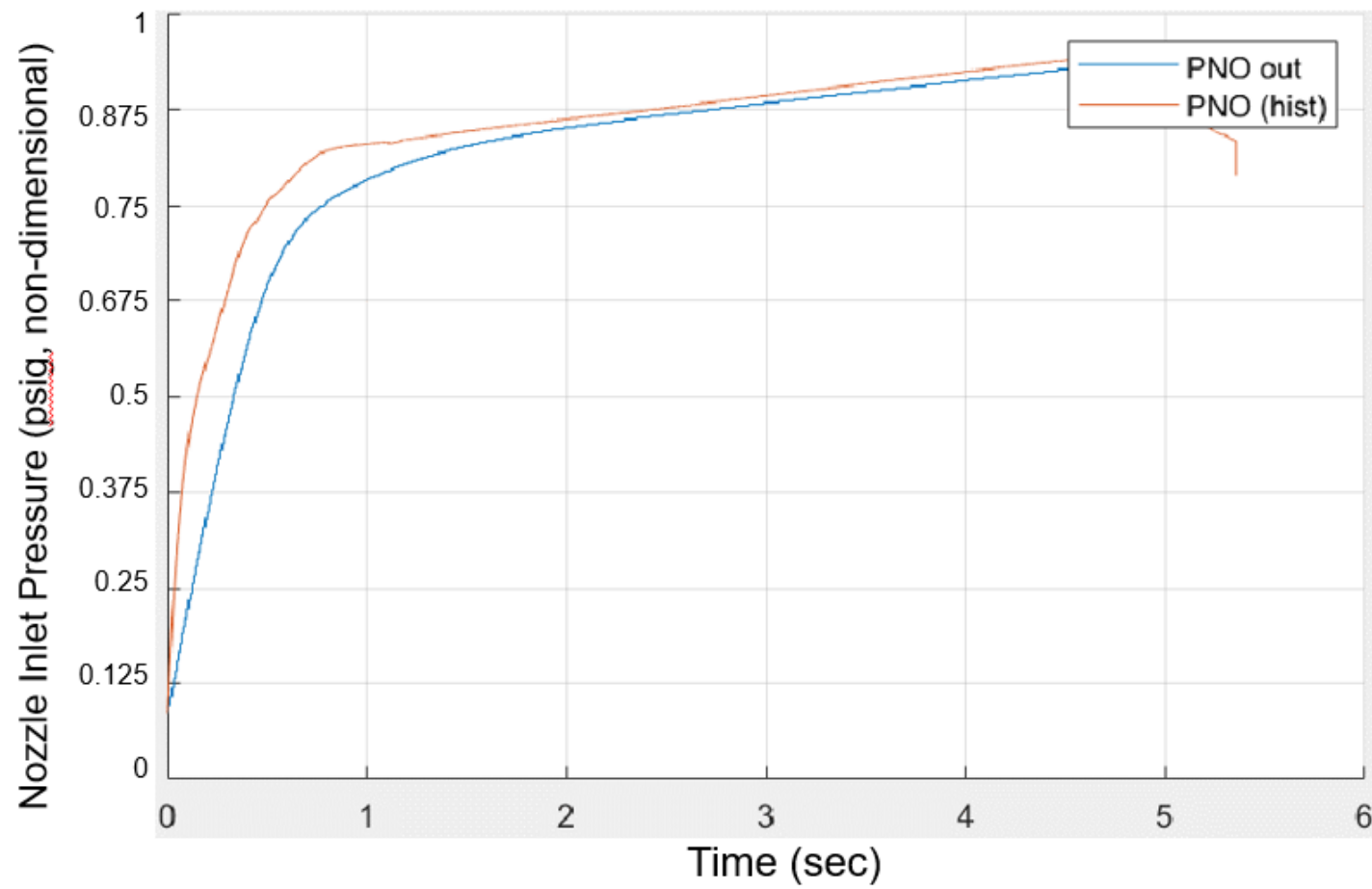


Figure 35: Nozzle Supply Pressure vs Time

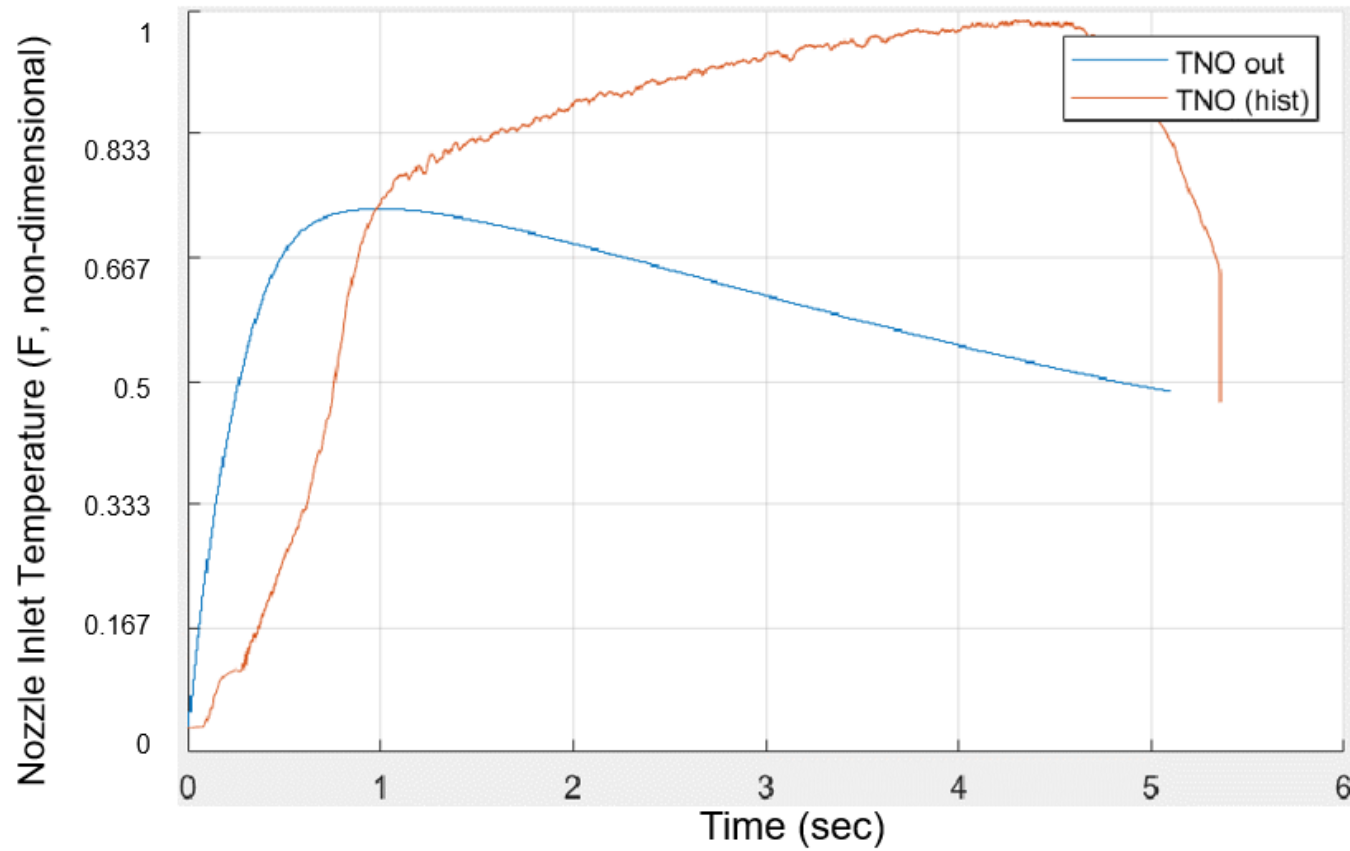


Figure 36: Nozzle Supply Temperature vs Time

Chapter 6: Conclusions and Recommendations for Future Research

Simulink Model Conclusions

The model shows promise in regard to the system pressures, however there are revisions and edits that certainly can be implemented to improve the model accuracy. To review the control law, the model performs well and the control valve behavior in Figure 27 is in line for the initial opening portion, however the transient portion is deviated from historical average. This is mainly attributed to the discrepancies in the heater pressure model, which is later shown. To validate that the controller works as intended, a separate model composing of the control law, servo amplifier card, and the actuator valve were only modeled with feed in signal from historical PHE data. The plant downstream of the actuator valve was removed from this model and the control law relied only on this historical average PHE signal. This model results are pictured in Figure 28. The key observation associated with this plot is the close agreement between the historical data and the modeled control law voltage in the non-transient portion. Transient effects such as slew rates, voltage offsets, biases, and delays are not captured identically in the control law voltage, and as such the control law voltage does not agree in the initial opening portion of the plot. After this initial period, both all three data series agree very well and show promising agreement. This can conclude the controller portion of the model is sufficient in accuracy for an initial pass through, as the time-influencing variables are not quite modeled properly.

To review the plant system metrics, the pressure plots all suggest a relatively favorable agreement, however the temperature plots are unfavorable. The driver pressure in tandem with the single-volume heater model pressure, Figure 29 and Figure 31, show loose agreement to the respective historical data, though the drop in pressure is significantly less than historical. Similarly, the nozzle supply pressure shown in Figure 35 also shows a favorable agreement to historical data with the exception that the initial pressure rise portion is slightly separated. This separation can be attributed to the control volume initial conditions, flow restrictor orifice block physics, or perhaps uncaptured real gas effects. To add, the two-volume heater exit pressure and temperature were plotted in Figure 33 and Figure 34, respectively, to emphasize the decision to omit this alternate model. The heater pressure shows a lower heater pressure slope but more importantly did not capture the intended effect of a more accurate heater exit temperature. Moving to the system temperatures, the model significantly lacks in this regard, majorly due to the heater vessel model assignment as a single volume. The driver temperature is observed to decrease much steeper than historical data indicates, shown in Figure 30. The mixing of gases inside the heater vessel can of course be seen in Figure 32, showing a large decrease in heater exit temperature. As a result, the nozzle supply temperature is also affected, showing a steep increase in temperature and then a steady fall off, observed in Figure 36.

Recommendations for Future Research and Modeling

There are several improvements that can be made to further develop the model and the methodology of simulating the model. The most apparent being the modeling of a two-part heater as this can potentially provide better results. The effects of the heater vessel assuming bulk, average temperature causes both upstream and downstream effects in temperature, pressure, and mass flow rate. Continued development to this idealized solution shall be

explored, and perhaps branched off to a different approach strategy that appropriately reflects the unmixed gas effect.

Another area of improvement that can be explored is the refinement to the control law. The DesignExpert analysis took in the nominal run conditions and the response heater exit pressure slope, where in reality, some run condition parameters should have no real effect on the observed heater exit pressure slope. Some of these unnecessary factors are handled by DesignExpert, assigning a miniscule coefficient to the coded equation, but others are in fact significant in their effect. One potential avenue is to manually restrict the analysis from considering these factors within the coded equation two-factor interaction analysis. This would most likely decrease the agreement of the prediction versus actual (ie. R^2 value), but nonetheless provide a more representative coded equation that reflects only feasible parameter effects. In addition to this change, the control law theoretical equation based on the electrical schematic contains a plethora of resistors, capacitors, and OpAmps, all of which can be independently factored into a higher degree-of-freedom DesignExpert analysis. This change could certainly provide even more accurate results, and potentially explain the discrepancy between the theoretical and actual heater pressure slopes. For instance, if several resistors prove to be mislabeled or misrepresented (ie. 200k Ω versus a 20k Ω resistor), the entire circuit is then invalid in terms of the theoretical voltage output. This methodology could aid in potentially diagnosing further issues within the control system, not only limited to the control law circuit. More importantly, this could solidify the model controller such that the plant can be further refined independently without sacrificing time to tweak the controller model.

It is the intention to continue this model such that Tunnel 9 system engineers and operators can fully use the model to provide accurate estimations of facility measurements. Secondly, the estimated facility results can influence consequential decisions with respect to

test cell conditions, facility component operating conditions, facility component safety limits, and facility sustainment.

Appendices

Appendix A: Control Valve Run Faults; Slew Rate Observations

Due to the nature that the tunnel 9 driver vessels are always under high pressure, it is rare to be able to test the limited and unlimited slew rates of the gas control valve assemblies. Recently, Tunnel 9 experienced a significant lack of operational gas control valves due to malfunction or fatigued pilot servo valves. The servo valves receive input from the control system and output a central spool position to direct hydraulic fluid to actuation ports. While it is undesired for the control valves to malfunction, two recent faulty runs have resulted in the ability to study the unique control valve behavior. In a recent tunnel run, *Run A*, there was a ~1 second delay in the control valve actuation, and as a result the heater pressure slope significantly dropped and lagged in ‘time-to-slope’ performance. That is, the heater pressure slope could not achieve the predetermined slope due to the delay in gas control valve actuation. The controller would consequently send a continuous signal to open the valve until the position was satisfied. The reason for the delay was unknown and further steps and tunnel runs were executed to verify the delay was in fact an anomaly.

In an alternative, but also recent run, *Run B*, the controller card had seemed to malfunction, sending an abnormally high magnitude signals to the servo valve when input a small signal by the control system, an unwanted excessive electrical gain. The result was a rapidly opening and closing gas control valve. Further diagnosis was completed to confirm the servo amplifier controller card was in fact faulty. These two runs allowed the study the slew rates under nominal controller operation and under seemingly no controller operation, limited and unlimited respectively.

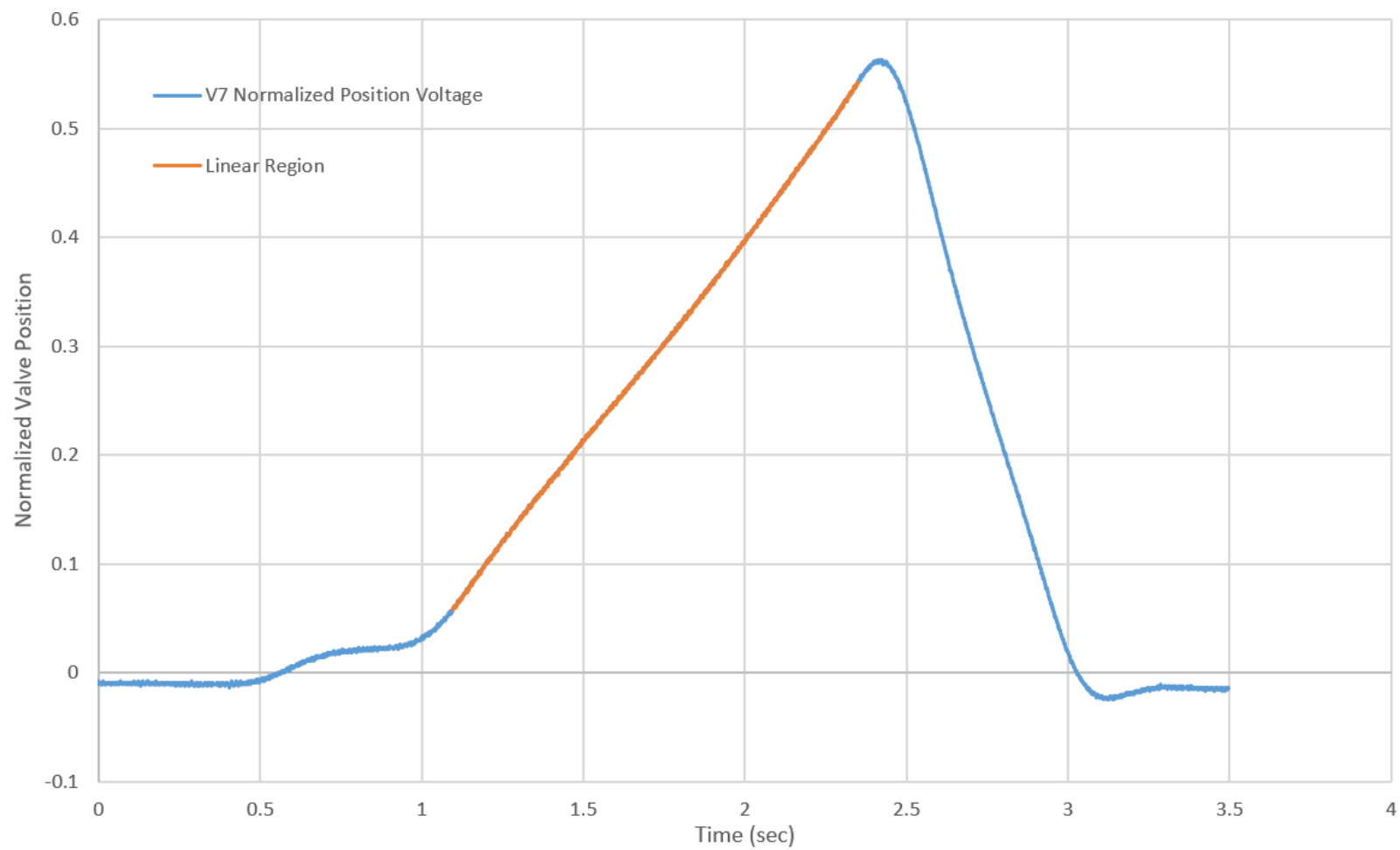


Figure 37: Normalized Control Valve Position vs Time, Run A

In this run, *Run A*, there is a clear delay of approximately one second where the valve does not respond appropriately. The valve seemingly stuttered and then resumed opening. As a result, the downstream effects caused a significantly lacking heater pressure and heater pressure slope. The control law dictates that the heater pressure slope is met by actuating the control valves, hence in this condition, the control valves were commanded to open as fast as possible, limited by the servo amplifier controller card and the control law gains. The exact slew rate will vary from condition to condition because the control law gains also change.

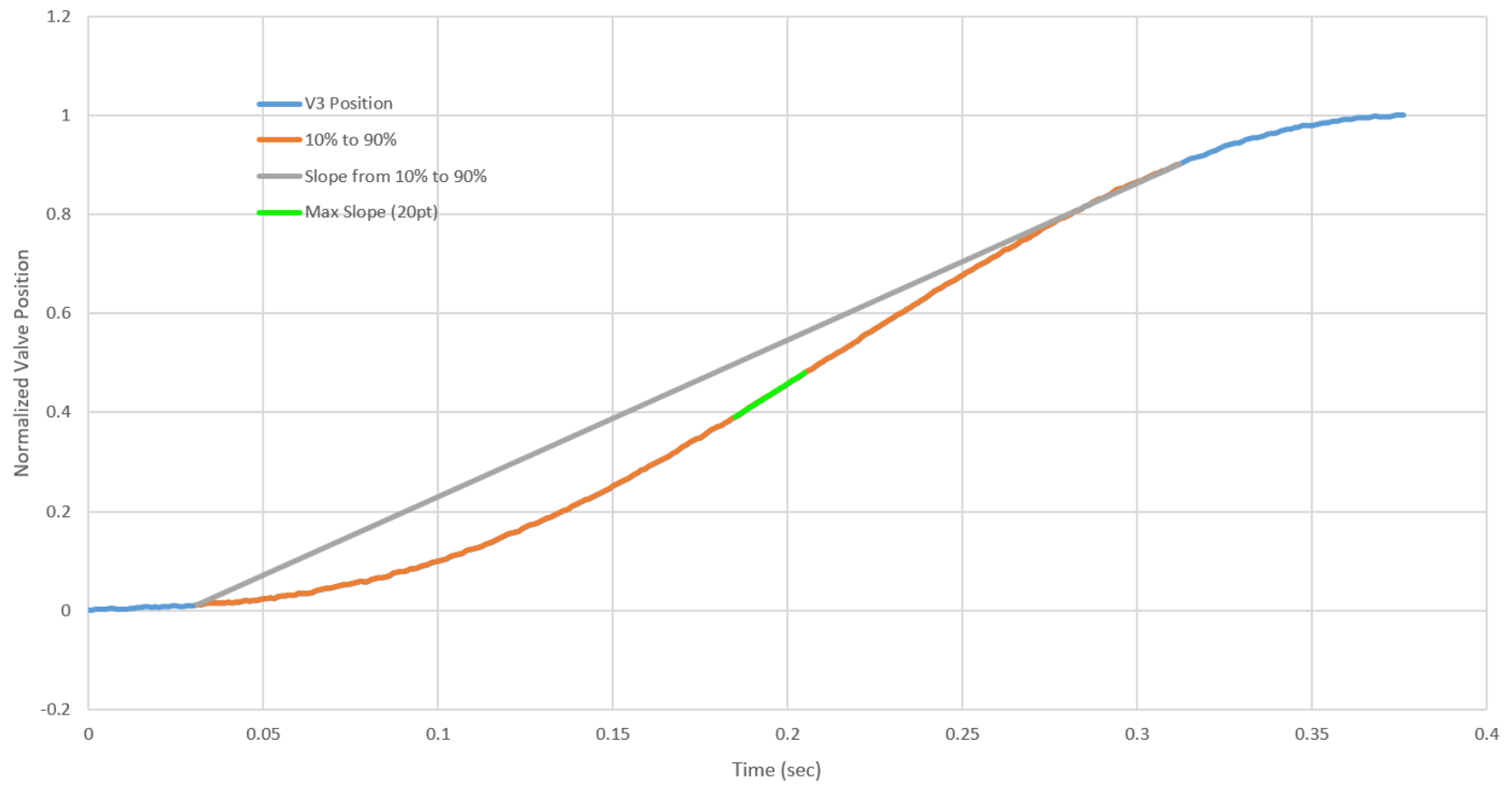


Figure 38: Normalized Control Valve Position vs Time, Run B

In the next run, *Run B*, the control valves received an erroneous signal due to a faulty controller, causing the control valves to receive essentially a step response from closed to 100% open. The control system records data at 1000 Hz and was able to capture a relatively high-resolution plot of the control valve behavior. The plot indicates a slew rate of ~ 2.6 [1/sec] with no impedance (ie. no controller saturation), though this is dangerous to have such high slew for purposes of preventing damage to the heater liner element. The plot also indicates a time from 10% to 90% of about 0.22 seconds, corresponding to a slew rate of ~ 3.12 [1/sec]. Lastly, a twenty-point moving window was scanned through the plot and determined a maximum slope between 0.185 and 0.205 seconds, where the control valve position shows a slew rate of ~ 4.43 [1/sec].

To take this a step further, the curve follows a definitive “S-shape” indicating there may be a relatively constant second derivative to the valve actuation which may provide an additional measure of valve opening rate limitation. This second-derivative can be extracted through a simple discrete-time second order differentiation. As discussed, the run rapidly opened and closed the valve, which may show a clear upper bound and lower bound second derivative to the data, and at the center of this “S-shape” is where the second-derivative alternates in direction (ie. positive or negative). This second order derivative upper and lower bound can be implemented into the model as a hard constraint saturation to the valve position plot. In theory, the servo valve specifications and characteristics, actuator valve kinematics, and controller-associated slew rates should be able to accurately reflect the control valve actuation delay, offset, and slew rate, but the additional constraint of this second-order slew rate may provide another layer of accuracy to the model.

Bibliography

- [1] "T9 Technical Communications," AEDC White Oak Technical Documentation.
- [2] W. J. Glowacki, E. L. Harris, R. K. Lobb and M. I. Schlesinger, "The NOL Hypervelocity Wind Tunnel," AIAA, Albuquerque, 1971.
- [3] J. Hill, "Initial operation of the NOL hypervelocity tunnel," AIAA 1974-608, Silver Spring, MD, July 1974.
- [4] A. R. Hambley, Electrical Engineering; Principals and Applications, 6th, New Saddle River, NJ: Pearson Education Inc., 2014.
- [5] W. J. Thayer, "Transfer Functions for MOOG Servo Valves," 1958.
- [6] Parker-Hannefin Corporation, "SE60 Series 4-Way Hydraulic Servo Valves," Parker, Elyria, 2019.
- [7] MOOG, "Electro-Hydraulic Servo Valves - A Technical Look," MOOG, Inc., 2016.
- [8] R. Span, E. W. Lemmon, R. T. Jacobsen, W. Wagner and A. Yokozeki, "A Reference Equation of State for the Thermodynamic Properties of Nitrogen for Temperatures from 63.151 K to 1000 K and Pressures to 2200 MPa," *Journal of Physical and Chemical Reference Data*, vol. Vol. 29, no. No. 6, 2000.
- [9] P. Gerhart, A. Gerhart and J. Hohenstain, Fundamentals of Fluid Mechanics - Eighth Edition, Wiley Publishing, 2016.
- [10] P. H. Oosthuizen and W. E. Carscallen, Introduction to Compressible Fluid Flow - Second Edition, CRC Press - Taylor and Francis Group, 2013.

